Exploration of simple analytical approaches for rapid detection of pathogenic bacteria

by

Salma Rahman

A dissertation submitted to the graduate faculty

in partial fulfillment of the requirements for the degree of

DOCTOR OF PHILOSOPHY

Major: Analytical Chemistry

Program of Study Committee:
Marc D. Porter, Major Professor
Robert S. Houk
Lee K. Woo
Nancy Cornick
Andrew C. Hillier

Iowa State University

Ames, Iowa

2005

Graduate College

Iowa State University

This is to certify that the doctoral dissertation of

Salma Rahman

has met the dissertation requirements of Iowa State University

Major Professor

For the Major Program

TABLE OF CONTENTS

ACKNOWLEDGMENTS

I would like to express my sincere appreciation and thanks to my major professor, Marc D. Porter. His guidance, support, patience and enthusiasm made this long journey possible. I express my utmost respect to him not only as a professor, but also as a person for his kindness, friendliness, broadminded attitude and for accommodating my personal extraordinary circumstances during the tenure of my graduate student life. Indeed, I have been very fortunate to have him as my supervisor and as a teacher for my graduate studies at the Iowa State University.

Sincere thanks are also extended to Professor Sam Houk, Denis Johnson, Keith Woo, Nancy Cornick, Susan Carpenter, and Andrew Hillier, who serve as committee members. The effort of their critical reading of this manuscript, interest and suggestions are greatly appreciated.

I owe a great deal to Bob Lipert for his extraordinary support in every step of my work in Porter's group. He has been always patient, always supporting and his door was always open for me. I would like to thank Bob Doyle for his support in answering and making me understanding about Biological questions. Also I like to thank Toshi Kawaguchi for his unselfish support in completing the "monolayer characterization" research project

I owe the past and present members of the Porter group (especially, Dave, Hye-Young, Nikola, April, Cherry, Rachel, Jeremy, Karen, and Adam) deep appreciation for their help in scientific discussions and also for the friendship (especially, the "Friday-Lunch Group" members) to they have extended to me during my stay at Iowa State University. I

especially want to thank Becky Staedtler for her enormous help in all respect. She has been always "Mushkil Ashan" for all the problems.

Finally, I like to remember my mother Badrunnesa Rahman and father Ahmed Rezaur Rahman, their contribution to my life is beyond my writing limit. Most importantly, I would like to remember my best friend and husband, Towhid, for his enormous devotion to this cause, taking life easy on Interstate 80 and for always supporting to this effort. I feel to my little angel, Naisha, that this whole graduate school time is "time away from her".

This work was performed at the Institute for Combinatiorial Discovery of the Iowa State University through the Roy J. Carver Laboratory for Ultra High Resolution Biological Microscopy and Ames Laboratory under Contract W-7405-Eng-82 with the U.S. Department of Energy. Funding for this work was provided by the United State Department of Agriculture Cooperative State Research, Education, and Extention Service (UDSA CSREES award number 20002-35201-12659) and the Roy J. Carver Charitable Trust through a University Exploratory Research Program. The United States government has assigned the DOE Report number IS-T 2458 to this thesis.

GENERAL INTRODUCTION

Dissertation Organization

Many of the current methods for pathogenic bacterial detection require long sample-preparation and analysis time, as well as complex instrumentation. This dissertation explores simple analytical approaches (e.g., flow cytometry and diffuse reflectance spectroscopy) that may be applied towards ideal requirements of a microbial detection system, through method and instrumentation development, and by the creation and characterization of immunosensing platforms.

This dissertation is organized into six sections. In the general Introduction section a literature review on several of the key aspects of this work is presented. First, different approaches for detection of pathogenic bacteria will be reviewed, with a comparison of the relative strengths and weaknesses of each approach. A general overview regarding diffuse reflectance spectroscopy is then presented. Next, the structure and function of self-assembled monolayers (SAMs) formed from organosulfur molecules at gold and micrometer and sub-micrometer patterning of biomolecules using SAMs will be discussed.

This section is followed by four research chapters, presented as separate manuscripts. Chapter 1 describes the efforts and challenges towards the creation of immunosensing platforms that exploit the flexibility and structural stability of SAMs of thiols at gold. 1H, 1H, 2H, 2H-perfluorodecyl-1-thiol SAM (PFDT) and dithio-bis(succinimidyl propionate)-(DSP)-derived SAMs were used to construct the platform. Chapter 2 describes the characterization of the PFDT- and DSP-derived SAMs, and the architectures formed when it is coupled to antibodies as well as target bacteria. These studies used infrared reflection

spectroscopy (IRS), X-ray photoelectron spectroscopy (XPS), and electrochemical quartz crystal microbalance (EQCM). Chapter 3 presents a new sensitive, and portable diffuse reflection based technique for the rapid identification and quantification of pathogenic bacteria. Chapter 4 reports research efforts in the construction and evaluation of a prototype flow cytometry based cell detector and enumerator. This final research chapter is followed by a general summation and future prospectus section that concludes this dissertation.

Literature Review

Bacterial contamination

Bacterial pathogens are widely distributed throughout nature, e.g., in soil, water, and the intestinal tracts of animals. Pathogens such as *Listeria monocytogenes*, *Clostridium botulinum*, and *Bacillus cereus* may be therefore be present in fresh produce. *Salmonella*, *Escherichia coli* O157:H7, *Campylobacter jejuni*, *Vibrio cholerae*, parasites, and viruses are more likely to contaminate fresh produce through improperly composted manure or contaminated water.[1] Bacterial contamination of food and water is a long standing problem around the globe.[2] The severity of the problem is evident in estimates from the Center for Disease Control, which indicates that there are approximately 76 million illnesses, 325000 hospitalizations, and 5000 deaths caused by microbial pathogens in the United States each year.[3] The breadth of the problem is further underscored by the concomitant loss of billions of dollars every year due to medical costs and low productivity.[4]

A major part of the problem rests with the challenges in developing cost-effective analytical methods that have the requisite capabilities for the rapid and reliable identification and enumeration of such pathogens. This limitation not only has an impact on the

implementation of regulatory control protocols,[5] but also on the technical ability to respond rapidly in the event of an outbreak by identifying the source of contamination and controlling its spread. In the past few years, a wide range of strategies have been explored in response to this critical problem.[2, 6-9] Only a few, however, show real promise.[10-12] Despite significant improvements, there is no single method that is completely satisfactory in determination of microbial content.

The ideal microbial detection system

Ideal requirements of a microbial detection system are as follows[13]: accurate, real time response, sensitive, reproducible, no sample pretreatment, no interference from culture or other enrichment conditions, large dynamic range, and wide applicability. The instrument should be easy to calibrate, portable, user friendly, robust, and low cost. The expense per sample analysis should also be low. These criteria are challenging to meet, and the work herein explores potential avenues toward these ends.

***E. coli* O157:H7 facts**

E. coli O157:H7, which is one of the food borne pathogenic bacteria that is of most concern today, was selected as a model microorganism for use in this thesis. Ingestion of as few as 10-100 organisms may be sufficient to cause infection.[14] *E. coli* O157:H7 was first recognized as a pathogenic bacterium in 1975.[15] *E. coli* O157:H7 produces potent toxins (verotoxins or shiga-like toxins: Stx1 and Stx2) that severly damage the lining of the intestine and may cause life-threatening complications-hemolytic uremic syndrome and hemorrhagic colitis (severe abdominal pain, bloody diarrhea, and occasionally vomiting or kidney failure)-

in humans through affecting vascular endothelial cells of kidneys, intestines, the central nervous system, and other organs.[1, 16, 17] The pathogenicity of *E. coli* O157:H7 is also associated with several other virulence factors, including intimin (encoded by the *eaeA* gene) and enterohemorrhagic *E. coli* hemolysin (EHEC *hlyA*).[18] Intimin facilitates adherence to intestinal villi, forming the attaching-and-effacing intestinal lesion.[16] The genes, *rfbE* encodes the *E. coli* O157 serotype and *fliC* encodes the *E. coli* flagellum H7 serotype.[18] The natural reservoirs of enterohemorrhagic *Escherichia coli* are cattle and other domestic animals.[19] *E. coli* O157:H7 can be transmitted to humans through the consumption of a wide range of foods including undercooked beef, unpasteurized milk, cheeses, raw vegetables, fermented meats, apple juice, and contaminated water.[20]

Methods for detection of pathogenic bacteria

Traditionally, the most widely methods used for detection of bacteria are plate-culture based. However, these approaches require approximately 48 h enrichment to allow the target organism to multiply, but may underestimate the contaminant level due to physiological factors (e.g., sublethal injury) that can impede culturability.[21, 22] These methods are also labor intensive and can be procedurally cumbersome.[3, 23, 24] Other common techniques employed for the identification and enumeration of bacteria are to count and analyze the cells by optical microscopy[25-33] or by flow cytometry. A brief discussion regarding flow cytometry-based detection will be presented in the later section. In addition, other methods include measurements of physical parameters by piezocrystals, impedimetry, redox reactions, optical methods, and calorimetry, and the detection of cellular components such as ATP (by bioluminescence), DNA, protein and lipid derivatives (by biochemical methods); radioactive

isotope monitoring by radiometry has also been employed.[2] The vast majority of research in this area has exploited the selectivity derived either from immunological- or DNA-based processes. In the former, antibodies targeted to a specific pathogen are selectively tagged with labels that can be coupled with radiochemical, optical, and electrochemical detection techniques. In the latter, selectivity is derived from the genetic characteristics of the pathogen by amplification of a specific sequence of DNA, using the polymerase chain reaction (PCR) and a fluorogenic assay.

(i) Immunoanalytical methods

Immunoanalytical methods are attractive because antibodies can be developed not only for recognizing proteins, but also for surface antigens of microorganisms and low-molecular-weight compounds. The antigenic targets of *E. coli* O157:H7 are somatic (O157) or flagellar (H7) antigens and the virulence-associated Shiga-like toxin (SLT) types I and II.[34] The specificity and high affinity of the antibody-analyte interaction significantly simplifies sample pretreatment.[6] Although it requires additional reagents and preparation steps, the incorporation of labels into immunodetection techniques often leads to an improvement in sensitivity. In fact, most of the immunoanalytical procedures, including immunosensor systems, are based on multistep procedures and deliver a signal after the introduction of the analyte and further workup.[6]

(i. a) Label-based methods

Immunoanalytical methods using labels (e.g., radioisotopes, fluorophores, and enzymes) are known as indirect systems. Radioisotopes are used as labels in

radioimmunoassay. The decay process of radioisotopes is not affected by the factors such as pH and ionic strength that may affect optical or enzyme-based detection methods. Moreover, due to negligible radioactive background in biological samples, high sensitivity is observed in such assays. However, health hazards and restrictive legislation constrain the use of this technology.[35] Fluoroimmunoassays have been studied for almost 20 years as alternatives to radioimmunoassay.[36] Fluorescence is more rapid and sensitive, has a lower cost, and is safer than radioisotopic methods. Identification of bacteria by fluorescent immunoassays (FIA) takes the advantage of high degree of specificity inherent in immunological reaction.[2] Many microbial assays are currently based on solid phase enzyme linked immunoassays (ELISA), which involve the use of enzymatic activity as a means of detecting the binding of an antibody-enzyme conjugate. The catalytic activity of the enzymes can also be used to amplify the response and lower the limit of detection. ELISA techniques have typical detection limits of ~10^5 cells/mL.[37, 38] Although ELISA techniques are sensitive and have high throughput, they require long incubation times, extensive sample manipulations, and tend to yield positive results that cannot be confirmed by culturing.[20, 24, 39]

Electrochemical techniques, based on measuring either a current or a potential of a reaction, have also been explored for use in bacterial detection.[11, 17, 40, 41] Impedimetric and conductimetric methods require lengthy incubation times to achieve a signal corresponding to microbial growth. The data analysis especially in the case of impedence measurements, can also be complex. Potentiometric techniques involve measurement of the potential when a species interacts with a selective surface and generates a potential difference. Potentiometric techniques are comparatively simple, sensitive, and less costly, but suffer from fouling of the selective surface or membrane material.[13] Amperometric systems

involve application of an external potential to drive the electrochemical reaction in a desired direction and the measured current is used to quantify the rate of the redox reaction. These techniques are sensitive, rapid, and inexpensive[42] and they also have a linear concentration dependence compared to a logarithmic relationship in potentiometric systems.[11, 43] However, the selectivity of amperometric measurements is governed by the redox potential of the electroactive species present. Thus, the measured current can include the contributions of several chemical species.[44] One of the other advantages of electrochemical techniques is that they can be operated in optically opaque media. However, the sample extraction is frequently required to prevent poisoning of the electrode surface.[35]

New classes of labels. Recently, bacterial detection methods based on new classes of labels (e.g., quantum dots (QDs) such as CdSe-ZnS core-shell nano crystals,[45, 46] fluorescent-bioconjugated silica nanoparticles where each nanoparticle encapsulates thousands of fluorescent dye molecules in a protective silica matrix,[47] immunoliposomes in which liposomes are tagged with antibody and encapsulate a fluorescent dye,[1, 48] and fluorescent protein-labeled bacteriophage[24, 49]) have appeared in the literatures. These new labels show promise in providing a highly amplified and reproducible signal. QDs have some advantages such as a narrow, symmetric emission band, which is independent of the excitation wavelength, long-term photostability, and a high quantum yield. Moreover, the emission wavelength of QDs is tunable by changing the material composition and size of the cores. QDs have found increasing applications in biological imaging and analyses including cell staining,[50, 51] DNA detection,[52] cell surface receptor targeting,[53] and imunoassays of protein

toxins and TNT.[54, 55] Some techniques have also developed for detection of multiple organisms, e.g., solid-phase capture-[56] and liquid array-based methods.[57]

(i. b) Label-free methods

Immunoanalytical methods not requiring a label are known as direct systems. These label-free detection methods involve determination of changes in physical characteristics due to the formation of an immunocomplex. Mass-sensitive detection methods for whole cells, with specific antibodies immobilized on the transducer surface, should therefore be ideal because they offer a real time output, simplicity of use, and cost effectiveness.[2, 58] The increase in mass loading can be directly monitored by a microbalance using acoustic sensors or indirectly by using an optical transducer to measure changes in the refractive index of waveguide systems. Acoustic sensors are of only limited reusability.[59] The performance of these sensors may also be compromised by the steric inaccessibility of the binding sites of the immobilized antibody.[6] Surface plasmon resonance (SPR) involves excitation of surface plasmons in metal layers by laser light. The angle of the light beam leading to SPR is the recorded measurement signal.[6] SPR has been utilized to detect bacteria, but its detection capability (5×10^7 CFU/mL) is fairly poor.[60] Moreover, a high degree of non-specific binding to the metal surface was observed when real sample matrices were used.[61]

(ii) <u>Nucleic acid-based methods</u>

DNA based analytical methods (e.g., detection of a specific DNA sequences by amplification of target DNA sequences using PCR or hybridization of PCR products to immobilized oligonucleotides (DNA chips)) are among the most sensitive of the approaches

for detecting microorganisms.[10, 18, 34, 62-74] Fluorogenic PCR assays eliminate the necessity of post-PCR analysis, which typically involves subjecting the PCR product to enzymatic treatment, hybridization capture, and/or electrophoretic separation.[75] However, DNA-based techniques require the extraction of DNA from the sample.[3, 6, 49] Moreover, the total process can be lengthy (> 8 h)[72] and may involve a pre-enrichment step for low level of detection.[16, 63, 73] As importantly, PCR techniques are challenged when analyzing environmental samples due to widespread presence of common genes (e.g., Shiga toxins 1 and 2) in bacteria.[24] This problem is particularly problematic with highly complex samples (e.g., ground beef).[73, 76]

Immunomagnetic separations (IMS)

In IMS, magnetic particles are labeled with an antibody specific to a target pathogen, which after binding to the target pathogen, are separated from the sample by application of a magnetic field. IMS has been employed to selectively isolate and concentrate target bacteria and shown to be a potentially powerful component of systems for the detection of bacteria in water, food, and feces.[77-79] The debris, color, and contaminants of an environmental sample can be removed during the IMS procedure.[80] After IMS, the immuno complexes can be detected by techniques such as flow cytometry, ELISA, PCR, and fluorescence.[15, 16, 38, 46, 76, 81-84]

Detection of low number of bacteria

Lower levels of bacterial detection (e.g., ~10^3 cells/mL) are generally achieved only with techniques such as PCR, fluorescence, ELISA, electrochemistry, and electrochemiluminesence, without a pre-enrichment step.[10, 33, 46, 48, 56, 85-88] Total workup

times of less than ~1h have been reported. However, pre-enrichment steps are required by most methods.[38, 49, 73, 76, 84, 89, 90] Normally, a selective agent such as novobiocin, cefmide, or tellurite is included in the enrichment broth to reduce the numbers of competing bacteria and favor enrichment of the target bacteria.[76] Even without pre-enrichment, some methods are lengthy (>6 h).[3, 15, 79] The next section will briefly present flow cytometry based bacterial detection methods.

Flow cytometry of bacteria

Cytometry refers to the measurement of physical and chemical characteristics of cells or biological particles. A variety of cytometric techniques can be employed to study microorganisms using fluorescent probes.[91] Confocal microscopy is capable of precise spatial localization of fluorescence and provides the highest resolution images, thus giving information about cell structure. Conventional fluorescence microscopy, scanning laser cytometry, and volumetric capillary cytometry are considered as lower resolution techniques; they provide relatively minimal information about structure but allow repeated observation of cells over a period of time.

Flow Cytometry is a process in which sheath and sample core solution carry the fluorescently tagged target cells through a flow cell, typically quartz, where hydrodynamic focusing results in single file cell flow through the detection region.[92, 93] Figure 1 presents the general concept of flow cytometry. Utilizing flow cytometry, single-cell enumeration and analysis can be performed, depending on several parameters (e.g., size, nucleic acid content, presence of antigens, membrane potential, internal pH, enzyme activity are considered as cellular parameters whereas absorption, light scattering, fluorescence are

considered as physical parameters).[91] The performance of flow cytometry continues to improve because of breakthroughs in detector sensitivity, electronics, laser light sources, and intense fluorescent labels.[38, 83, 94-101] Flow cytometry has the capability for rapid quantitative measurements of multiple parameters of each cell within a large number of cells. Thus, properties of component subpopulations of an overall population can be determined.[2] The main advantages of flow cytometry are high sample throughput and ease of automation, with the ability to analyze thousands of cells per second. Flow cytometric analyses are commonly performed at a flow rate of 10–100 μL min^{-1}, with the detection of ~10000 events s^{-1}.[9] Though conventional flow cytometry has the capability of analysis of tens of thousands of cells per second, it permits only one observation of each cell. As a read-out tool, flow cytometry can be considered a real-time technique since the analysis of a sample can be performed within a few minutes.[38]

Flow cytometry has recently been applied to microbial analysis by employing the specific binding of fluorescently labeled antibodies to bacteria.[38, 83, 102-105] Other applications of flow cytometry include bacterial discrimination from other particles on the basis of nucleic acid staining, determination of basic cell functions such as reproductive ability, metabolic activity, membrane integrity, or membrane potential.[106, 107] Multiparameter flow cytometry, using simultaneous staining with different fluorochromes, provides insight into heterogeneity of microbial population, viability, and variation in metabolic patterns.[106, 108-111]

Newly developed microfluidic flow cytometers may combine the best features of flow and static cytometers.[112] Ramsey et al. demonstrated flow cytometry of bacteria on a microfabricated fluidic device (microchip).[113] It incorporated electrokinetic (electroosmotic and electrophoretic) focusing to spatially confine fluids and particles. They also claim that

the devices have the potential to significantly reduce the size of flow cytometers and increase the throughput because many devices can be fabricated on a single substrate in parallel.

Limitation of flow cytometry

Although flow cytometry based commercial instrumentation has outstanding resolution and capacity for real time measurement,[99, 104, 108, 110, 113] the high cost of the instruments, the need for skilled personnel for sample preparation and operation, and adequate refrigeration systems for high-powered lasers limits field deployment.[9, 114]

We have constructed a novel prototype low cost flow cytometry-based bacteria counter utilizing co-localization concept for detection and enumeration of pathogenic bacteria as described in Chapter 4. In this Chapter, the instrument and some of its performance characteristics are described. Co-localization, a dual labeling concept, has been used by some researchers for other purposes like cell identity, cell viability, and assessment of physiological activities.[27, 28, 30, 115, 116] For more detailed discussions regarding flow cytometry, the reader is referred to some of these articles and recent reviews.[9, 91, 114, 117, 118]

Despite the significant improvements in various detection techniques that have been made in recent years, there is still no ideal technique for the detection of pathogenic bacteria. However, continued research and study hopefully facilitate substantial improvements to this challenging problem in the future.[13] For more detail discussion regarding bacterial detection the reader is referred to some of the articles and reviews.[2, 6, 13, 35, 44, 119] The next few paragraphs will introduce a spectroscopic technique, diffuse reflectance spectroscopy, that has been utilized previously for various other analytical applications but not for bacterial detection.

Diffuse reflectance spectroscopy (DRS)

When light is reflected from a solid phase, the reflected light can be separated into two components, a specular reflection and a diffuse reflection. Specular reflection occurs at smooth, mirror-like surfaces, whereas diffuse reflection occurs from textured or dull surfaces. In reality, light reflected from any surface (smooth or rough) contains both specular and diffuse components.[120-122]

Figure 2 illustrates some optical phenomena resulting in diffuse reflectance.[123] When electromagnetic radiation impinges on a textured sample, such as bacteria captured membrane used in Chapter 3, a small fraction of the radiation is reflected specularly, but a substantial portion penetrates into the sample interior. This penetrating radiation undergoes a combination of wavelength-dependent absorption and scattering (i.e., reflection, refraction, and diffraction) within the sample before a portion of the light is returned to the surface. Samples of interest for DRS are therefore simultaneous absorbers and scatterers of the electromagnetic radiation. At the surface, the radiation re-emerges from the sample traveling in all directions with equal intensity, and the surface appears uniformly light at all angles of observation. This re-emitted light constitutes diffuse reflection. Diffusely reflected light can be utilized to create a reflectance spectrum, which contains compositional information about a sample.

Diffuse reflection is typically described by two-constant theories: one constant characterizes the sample absorbance and other constant describes the scattering by the sample. The most generally accepted theory to describe and analyze diffuse reflection spectra is the Kubelka-Munk theory, which was developed for an infinitely thick opaque layer.[123, 124] This theory leads to conclusions that are qualitatively confirmed by experiment

and also enables diffuse reflectance spectra to be used for quantitative work in a manner similar to absorbance spectra. In diffuse reflectance spectroscopy, the reflectance of sample is defined as the ratio of intensities of the reflected to incident light, as presented in expression 1,

$$R_\infty = J/I_o \quad (1)$$

where R_∞ is the absolute sample reflectance (the ∞ subscript indicates that the sample is infinitely thick). J and I_o are the intensity of the reflected and incident light, respectively. Since it is not practical to measure the absolute reflectance of a sample, the relative reflectance, R'_∞, is typically measured, as shown in expression 2,

$$R'_\infty = R_{\infty\,\text{sample}}/R_{\infty\,\text{standard}} \quad (2)$$

where $R_{\infty\,\text{sample}}$ and $R_{\infty\,\text{standard}}$ represent reflectance of the sample and a standard, respectively.

The Kubelka-Munk function enables the relative reflectance to be linearly related to analyte concentration under constant experimental conditions, analogous to absorbance using Beer-Lambert's law, as presented in expression 3,

$$F(R) = (1- R'_\infty)^2/2R'_\infty = 2.303\varepsilon C/s \quad (3)$$

where ε is the absorptivity, s is the scattering coefficient, and C is analyte concentration.

The relative error in the Kubelka-Munk function increases very rapidly at larger and smaller reflectance values. The most favorable range for DRS measurement lies between 20 and 70% reflectance.[123] A straight-line relationship between $F(R)$ and C is observed in case of weakly absorbing substances, when s remains constant, and the size of the sample particles is relatively small (ideally ~1 μm in diameter).[125, 126] The presence of moisture tends to increase the Kubelka-Munk response of the sample. Kortum et al. ascribed this phenomenon

to the dependence of the scattering coefficient (s) on the ratio of refractive indices of the sample species and the surrounding medium.[127] In a wetted sample, the displacement of air by water reduces this ratio as well as the scattering coefficient (s). As can be observed from equation 3, a reduction of the value of s will result in a greater $F(R)$.

Distortion of the diffuse reflectance spectra is observed when specular and diffuse reflectance components are superimposed on one another. In this case, dilution of the sample (i.e., light-absorbing species) with a non- or low absorbing species is recommended. Furthermore, any significant departure from the "infinite thickness" of the sample, a key assumption of Kubelka-Munk theory results in background interference. Kortum[121] and Wendlandt and Hecht[122] provide more details about the technique and its fundamental underpinnings.

Diffuse reflectance UV-visible spectroscopy is mostly utilized in the applied sciences for the analysis of dyestuffs, paints, pigments, printing ink, ceramic, and paper.[123] It is also used for denture materials, tiles, cosmetics, and medicinal tablets for color matching/analysis. However, most of this work is proprietary and industrially driven, and therefore, a significant body of work with this technique remains unpublished. Schmidt et al. reviewed the use of this technique for chromophore research on wood fibers.[128] Diffuse reflectance UV-visible spectroscopy has been also employed for studies of metal oxidation and heterogeneous catalysis.[129] Our group has demonstrated and has been advancing the development of colorimetric solid-phase extraction (C-SPE) and diffuse reflection spectophotometry for use as an on-membrane readout technique to meet the design and operational requirements imposed by NASA for on-orbit biocide determinations in spacecraft water.[130-135] Chapter 3 of this dissertation describes a methodology for the rapid identification and quantification of

pathogenic bacteria utilizing diffuse reflectance spectroscopy. To our best knowledge, diffuse reflectance spectroscopy has been utilized for the first time for such type of application. The next section will introduce a technology, self assembled monolayers (SAMs) of organosulfur molecules at gold, that allows for the easy creation of immunosensor platforms suitable for different readout methods.

Self assembled monolayers (SAMs) of organosulfur molecules at gold

Self-assembled monolayers (SAMs) result from bond formation between a precursor molecule and a site on the surface of the substrate. SAMs formed from organosulfur molecules (thiols: $X(CH_2)_nSH$, sulfides: $X(CH_2)_nS(CH_2)_mY$, and disulfides: $X(CH_2)_nSS(CH_2)_mY$) at gold have been extensively characterized and widely explored for various applications in the past two decades.[136-143] The monolayers have been characterized by a number of analytical techniques, e.g., X-ray Photoelectron Spectroscopy (XPS),[144-148] Raman spectroscopy,[149] Laser Desorption Fourier Transform-Mass Spectrometry,[150] Temperature Programmed Desorption,[151] and electrochemistry.[152] Chapter 2 reports characterization of 1H, 1H, 2H, 2H-perfluorodecyl-1-thiol (PFDT) SAM and dithio-bis(succinimidyl propionate) (DSP)-derived SAM, and also when it is coupled to antibody as well as target bacteria. We have used infrared reflection spectroscopy (IRS), X-ray photoelectron spectroscopy (XPS), and electrochemical quartz crystal microbalance (EQCM) as principal characterization techniques.

There are a number of factors that attribute to the popularity of SAMs at gold relative to other substrate (e.g., silver, copper, platinum, mercury, iron, iron oxide nanoparticles, gallium arsenide or indium phosphide) or to other SAM systems (e.g., alkylchlorosilanes on

hydroxylated surfaces). Gold is a reasonably inert metal. Only few functional groups besides organosulfur molecules couple strongly to gold [140] Also, it does not readily oxidize at temperatures below its melting point or react with atmospheric oxygen or moist chemicals.[141, 153] In addition, gold is exceptionally easy to pattern by various lithographic techniques. Gold is compatible with cells; SAMs of thiolates on gold are stable for several weeks in contact with liquid media required for cell studies.[153] Thin films of gold are common substrates used for a number of analytical techniques such as electrochemistry, surface plasmon resonance (SPR) spectroscopy, ellipsometry, quartz crystal microbalances (QCM). Since organosulfur molecules are compatible with many functional groups, synthesis of a large number of chemical precursors from them are possible.[139] In addition, these SAMs possess a high degree of structural order and the ability to tailor surface chemical properties. Therefore, these films can be utilized to control interfacial properties as well as in adaptations in analytical sensor platforms.[141, 154, 155]

The driving force to form a SAM mainly comprises chemical bond formation between gold and sulfur, and intermolecular interactions (e.g., chain-chain interactions). In the case of a thiol precursor, the S-H bond cleaves,[149] and the adsorbed species is a thiolate. For disulfides, the relatively weak S-S bond cleaves, and each molecular fragment adsorbs as a thiolate. Figure 3 represents the ideal structure of these monolayers on gold that include a head group, spacer region, and terminal group. The head group rigidly anchors the molecules to the surface, with a bond energy ~44 kcal/mol.[140] The head group is usually linked to a polymethylene chain, which acts as a molecular spacer. The spacer region plays an important role in the stability to the monolayer through van der Waals interactions. The terminal group largely controls interfacial properties, as it can be tailored through the

appropriate synthesis of the precursor molecule. Varying the identity of the terminal groups, the properties of the monolayer such as friction, capacitance, and ion permeability etc. can be manipulated. The most common terminal groups are CH_3, CF_3, Cl, Br, OH, COOH, NH_2, CN, $COOCH_3$, and SO_3H. The surface free energy of the terminal group and variation in surface chemistry allow SAMs to act as model systems in investigation of many surface related phenomena such as film growth and ordering, heterogeneous catalysis, wetting, corrosion, electrochemistry, and interfacial behavior of biomolecular systems such as proteins and cells.[140, 143, 156-158] We studied different functional group terminated SAMs in Chapter 1 for the creation of an immunosensing platform for *E. coli* O157:H7. The following paragraphs will briefly discuss a specific system utilized in Chapter 1 and 2 that involves the formation of monolayers from *N*-hydroxysuccinimidyl-terminated molecules, e.g., dithio-bis(succinimidyl propionate) (DSP), a disulfide coupling agent that can be employed for the covalent attachment of molecules containing primary amines (e.g., proteins) to gold.

N-hydroxysuccinimidyl-terminated SAMs

Monolayers formed from succinimidyl group-terminated thiols, e.g., dithio-bis(succinimidyl undecanote) (DSU) or dithio-bis(succinimidyl propionate) (DSP) can be used as a coupling agent for covalently immobilizing biomolecules containing amine groups without any activation step. The acyl carbon of the succinimidyl ester group is strongly susceptible to nucleophilic attack by primary amine containing molecules like the lysine residues of proteins. As a result, a covalent amide linkage is formed between the monolayer

and protein.[159, 160] Figure 4 depicts the chemisorption of DSP at gold and subsequent binding of amine-containing molecules.

Both DSU and DSP have been utilized for immobilizing a number of biomolecules (e. g., enzymes,[161, 162]antibodies,[163-165] and DNA) in various applications including the imaging of biomolecules in physiological environments[160, 166] and the creation of impedence based biosensors.[162] Chapter 1 discusses the creation of a miniaturized immunosensing platform comprised of domains of anti-*E. coli* O157:H7. Anti-*E. coli* O157:H7 domains, i.e., the addresses, were formed by covalent coupling of the antibody to the DSP derived SAM. Discussion regarding characterization by various techniques of the DSP-derived SAM before and after its coupling to an antibody is presented in Chapter 2. Various surface patterning techniques that can be exploited for the construction of analytical sensor platforms are discussed in the following section.

Micrometer and sub-micrometer surface patterning

Currently, the developed methods for high resolution biomolecule patterning are microcontact printing, photolithography, ink-jet printing, microfluidic networks, and scanning probe lithography (SPL).

Microcontact printing (μCP). In μCP technique, a polydimethyl siloxane (PDMS) stamp is usually "inked" with a thiol or siloxane solution and placed into contact with a surface (e.g., gold, silver, or silicon) to transfer the ink.[167-169] This technique also allows the direct transfer of the biomaterials to a substrate using a master stamp.[170-173] Proteins have been inked directly onto polymer surfaces,[174, 175] glass,[176, 177] and silicon.[174, 178, 179] Whitesides et al. first demonstrated μCP SAMs using PDMS stamps.[180, 181] PDMS is biocompatible and can be

chemically modified using standard siloxane chemistry.[182] Though μCP allows rapid stamping of micrometer-sized features on a variety of substrates, current approaches are limited to making single addresses because of difficulties encountered in the precise alignment of PDMS stamps for repeated stamping. Defects in the transferred antibody coating were also sometimes observed.[183]

Photolithography. Photolithography involves the irradiation of a surface comprised of photolabile groups through a photomask, which chemically transforms the irradiated areas and forms a compositionally patterned surface. The ultraviolet (UV) irradiation of SAMs has been widely used for creating patterns.[165, 182, 184-186] The more popular photolithographic technique involves the photooxidation of alkanethiolate monolayers on gold.[185, 187] The technique involves UV radiation in the presence of oxygen that converts the gold bound thiolate to various oxygenated forms of sulfur (e.g., RSO_3^-).[188] The species responsible for the oxidation seems to be ozone, formed by UV photolysis of oxygen.[189, 190] The oxygenated forms of sulfur can be readily rinsed from the surface with many organic solvents, such as ethanol, tetrahydrofuran, or acetone. Typically, a mercury arc lamp is used as the UV source with an exposure time ~15-20 min (power density of ~ 5 W/cm^2 at the sample surface).[153] The mechanism for the photooxidation process has been studied by a number of techniques such as mass spectrometry, XPS, surface-enhanced Raman spectroscopy, SPR spectroscopy, and IR, but the elementary steps for this mechanism are not completely understood.[153] An excimer laser (193 nm) was also used to generate arrays of lines (100-nm widths) within 1 min using a phasemask.[191] Compositionally patterned alkanethiolate monolayers on gold created by UV photolithography, and the patterning of proteins and DNA have been performed in our research group.[165, 186, 192-196] Shadnam et al. utilized a laser beam (488 nm)

to write patterns (~20 μm) directly into SAM in ~0.1 s.[197] The laser does not oxidize the SAM, but rather induces thermal desorption of the monolayer by local heating. Chapter 1 describes the creation of micrometer-sized patterns of SAMs (DSP and PFDT) using both transmission electron microscopy (TEM) grids and chromium photomask by using UV radiation.

Techniques utilizing laser abalation[198] or ion beams[199] to remove materials from surfaces for protein binding have also been explored. Photolithographic approaches facilitate complex patterning, but the need for multiple alignment steps makes these techniques labor- and cost- intensive.[182]

Ink-jet printing. This method involves the use of conventional ink-jet printers or specialized high precision robots equipped with narrow capillary arrays to directly deposit biomolecules onto polymer surfaces[200-202] or activated glass.[203-205] The technique allows for the parallel-patterning of multiple addresses, but has limited resolution (300-75 μm), and poor reproducibility with respect to feature size.[200] Multilayered structures were also observed.[202]

Microfluidic networks. Fluid conduits are constructed with micrometer channel widths using PDMS stamps for patterned fluid delivery to surfaces.[206-208] However, microfluidic networks only allow fabrication of linear structures.

Scanning probe lithography (SPL). The patterning of biomolecules using scanning probe lithography is still in an early stage of development.[186, 209-212] Most of the studies included the use of a surface tunneling microscopy (STM) or scanning force microscopy (SFM) tip to locally modify a surface. SPL can be divided into three basic types: optical modification, mechanical modification (scratching), electrical modification. Though SPL methods offer superior resolution, issues in terms of throughput need to be resolved.[182]

Cell and bacteria patterning

Cells and bacteria have been patterned either bio-specifically or non-specifically by various techniques. Cell patterning has been accomplished by patterning the deposition of metals[213] and self-assembled monolayers (SAMs) of alkylsiloxane on silica/glass by optical,[214, 215] UV,[216, 217] and plasma lithography.[218] Though these methods are useful, they offer limited control over surface chemistry and generate regions differentiated mainly by hydrophilicity.[219] On the other hand, SAMs of alkanethiolates on gold provide more convenient patterning methods (lithographic or nonlithographic). μCP of alkanethiolates on gold or silver, using PDMS stamps for engineering cell shape and function, has been performed.[196, 220, 221] Nonselective patterning of bacteria within three dimensional heperbranched polymer film templates was performed by Crooks et al.[222] However, little work has been done to selectively capture bacteria using an immobilized antibody into specific addresses (e.g., capturing bacteria on bioplastic film (polyurethane)[223]or on array biosensors)[183, 224-226] To our knowledge, no work has been done for patterning bacteria specifically into less than 10 μm addresses. In Chapter 1, we focused on construction of such platform comprised of domains of defined shape and size to capture target cells (e.g., *E. coli* O157:H7). Because of the presence of a large number of addresses (>50000) in single platform and exposure of all the addresses to the sample solution at the same time, selective capturing of a very low number of microorganisms from the solution is possible. Moreover, nonspecific binding continues to be a major concern for all biomolecule patterning technologies. We also discussed this issue in terms of minimizing nonspecific binding of antibody and *E. coli* O157:H7 in Chapter 1. A miniaturized immunosensing platform

comprised of arrays of tens to thousands of antibody-modified addresses on the surface of a single chip can provide some useful features including high throughput, reduction of sample volume, and low level of detection.

Dissertation Overview

Centered on the main themes presented above, the body of this dissertation is divided into four data chapters. Each chapter is presented as a separate manuscript.

In Chapter 1, I discuss the construction of a miniaturized immunosensing platform comprised of defined shape and sized domains (<10 x 10 μm) of anti-*E. coli* O157:H7 surrounded by a fluorine terminated monolayer that resists the nonspecific adhesion of both antibody and *E. coli* O157:H7. Anti-*E. coli* O157:H7domains, i.e., the addresses, were formed by covalent coupling of the antibody to the succinimidyl group terminated SAM. This relatively robust platform can potentially be utilized for the low level detection of specific bacteria as there are many addresses (>50000) in single platform and exposure of all the addresses to small volume of sample solution at the same time.

Chapter 2 describes characterization of PFDT SAM and DSP derived SAM, and also when it is coupled to antibody as well as target bacteria that have been used to create the immunosensing platform. As principal characterization techniques, IRS, EQCM, and XPS have been employed.

Chapter 3 presents a new methodology for the rapid identification and quantification of pathogenic bacteria. It combines the selectivity of dye-labeled antibodies with the sample concentration capability of solid phase extraction, and the facile readout of the extracted, dye-labeled microorganisms by diffuse reflectance spectroscopy. The amount of captured

bacteria is then directly determined in only 2 s by comparing the signal with a calibration curve based on the Kubelka-Munk function.

Chapter 4 reports the research efforts and preliminary work to construct and evaluate a prototype flow cytometry based cell detector and enumerator that can simultaneously detect one global label (e.g., nucleic acid stain such as SYTO 61™) and one antibody label (fluorescent labeled antibody for target cell such as Cy5™-anti-*E. coli* O157:H7). Fluorescence is collected and imaged on a multichannel detector. A positive count has been recorded only when there was coincidence-detection of both dyes for the target bacteria cell. This chapter presents a proof of concept study demonstrating the ability of the co-localization of two dyes on an organism to provide a high level of confidence in identification of the pathogen.

The dissertation is concluded with a brief look at what insights have been gained throughout this work and speculation on its extension.

References

(1) Ho, J. A. A.; Hsu, H. W. *Anal. Chem.* **2003**, *75*, 4330-4334.

(2) Ivnitski, D.; Abdel-Hamid, I.; Atanasov, P.; Wilkins, E. *Biosens. Bioelectron.* **1999**, *14*, 599-624.

(3) Kourkine, I. V.; Ristic-Petrovic, M.; Davis, E.; Ruffolo, C. G.; Kapsalis, A.; Barron, A. E. *Electrophoresis* **2003**, *24*, 655-661.

(4) Golan, E. H.; Vogel, S. J.; Frenzen, P. D.; Ralston, K. L., "Tracing the Costs and Benefits of Improvements in Food Safety," Agricultural Economic Report No. 791, U.S. Department of Agriculture, **2000**.

(5) U.S. Department of Agriculture, F. S. a. I. S., "Pathogen Reduction; Hazard Analysis, and Critical Control Points (HACCP) Systems: Final Rule," Supplement-Final Regulatory Impact Assessment for Docket No. 93-016F, **1996**.

(6) Bilitewski, U. *Analytical Chemistry* **2000**, *72*, 692A-701A.

(7) Hage, D. S. *Anal. Chem.* **1999**, *71*, 294 R-304 R.

(8) Hennion, M.-C.; Barcelo, D. *Anal. Chim. Acta* **1998**, *362*, 3-34.

(9) Vives-Rego, J.; Lebaron, P.; Nebe-von Caron, G. *FEMS Microbiol. Rev.* **2000**, *24*, 429-448.

(10) Belgrader, P.; Benett, W.; Hadley, D.; Richards, J.; Stratton, P.; Mariella, R., Jr.; Milanovich, F. *Science* **1999**, *284*, 449-450.

(11) Brewster, J. D.; Gehring, A. G.; Mazenko, R. S.; Van Houten, L. J.; Crawford, C. J. *Anal. Chem.* **1996**, *68*, 4153-4159.

(12) Wadkins, R. M.; Golden, J. P.; Pritsiolas, L. M.; Ligler, F. S. *Biosens. Bioelectron.* **1998**, *13*, 407-415.

(13) Hobson, N. S.; Tothill, I.; Turner, A. P. F. *Biosens. Bioelectron.* **1996**, *11*, 455-477.

(14) Willshaw, G. A.; Thirlwell, J.; Jones, A. P.; Parry, S.; Salmon, R. L.; Hickey, M. *Lett. Appl. Microbiol.* **1994**, *19*, 304-307.

(15) DeCory, T. R.; Durst, R. A.; Zimmerman, S. J.; Garringer, L. A.; Paluca, G.; DeCory, H. H.; Montagna, R. A. *Appl. Environ. Microbiol.* **2005**, *71*, 1856-1864.

(16) Fu, Z.; Rogelj, S.; Kieft, T. L. *Intl. J. Food Microbiol.* **2005**, *99*, 47-57.

(17) Yang, L. J.; Li, Y. B.; Erf, G. F. *Anal. Chem.* **2004**, *76*, 1107-1113.

(18) Wang, G. H.; Clark, C. G.; Rodgers, F. G. *J. Clin. Microbiol.* **2002**, *40*, 3613-3619.

(19) Vuddhakul, V.; Patararungrong, N.; Pungrasamee, P.; Jitsurong, S.; Morigaki, T.; Asai, N.; Nishibuchi, M. *FEMS Microbiol. Lett.* **2000**, *182*, 343-347.

(20) Blackburn, C. D.; McCarthy, J. D. *Intl. J. Food Microbiol.* **2000**, *55*, 285-290.

(21) Mossell, D. A. A.; Corry, J. E. L.; Struikj, C. B.; Baird, R. M. In *Essentials of the Microbiology of Foods: A Textbook for Advanced Studies*; John Wiley & Sons: Chichester, 1995, pp 96-106.

(22) Smith, J. J.; Howington, J. P.; McFeters, G. A. *Appl. Environ. Microbiol.* **1994**, *60*, 2977-2984.

(23) Dey, B. P., Lattuuada, C. P. *Microbiology laboratory guidebook, U. S. Department of Agriculture*, 3rd ed.: Washington, D. C., 1998.

(24) Oda, M.; Morita, M.; Unno, H.; Tanji, Y. *Appl. Environ. Microbiol.* **2004**, *70*, 527-534.

(25) Heldal, M.; Norland, S.; Bratbak, G.; Riemann, B. *J. Microbiol. Methods* **1994**, *20*, 255-263.

(26) Hobbie, J. E.; Daley, R. J.; Jasper, S. *Appl. Environ. Microbiol.* **1977**, *33*, 1225-1228.

(27) Hoff, K. A. *Appl. Environ. Microbiol.* **1988**, *54*, 2949-2952.

(28) Mcfeters, G. A.; Singh, A.; Byun, S.; Callis, P. R.; Williams, S. *J. Microbiol. Methods* **1991**, *13*, 87-97.

(29) Pettipher, G. L.; Rodrigues, U. M. *Appl. Environ. Microbiol.* **1982**, *44*, 809-813.

(30) Pyle, B. H.; Broadaway, S. C.; Mcfeters, G. A. *Appl. Environ. Microbiol.* **1995**, *61*, 2614-2619.

(31) Singh, A.; Pyle, B. H.; Mcfeters, G. A. *J. Microbiol. Methods* **1989**, *10*, 91-101.

(32) Singh, A.; Yu, F. P.; Mcfeters, G. A. *Appl. Environ. Microbiol.* **1990**, *56*, 389-394.

(33) Tortorello, M. L.; Stewart, D. S. *Appl. Environ. Microbiol.* **1994**, *60*, 3553-3559.

(34) Oberst, R. D.; Hays, M. P.; Bohra, L. K.; Phebus, R. K.; Yamashiro, C. T.; Paszko-Kolva, C.; Flood, S. J. A.; Sargeant, J. M.; Gillespie, J. R. *Appl. Environ. Microbiol.* **1998**, *64*, 3389-3396.

(35) Cruz, H. J.; Rosa, C. C.; Oliva, A. G. *Parasitol. Res.* **2002**, *88*, S4-S7.

(36) Hemmila, I. *Clin. Chem.* **1985**, *31*, 359-370.

(37) Acheson, D. W. K.; Lincicome, L. L.; DeBreucker, S.; Keusch, G. T. *J. Food Prot.* **1996**, *59*, 344-349.

(38) Seo, K. H.; Brackett, R. E.; Frank, J. F. *Intl. J. Food Microbiol.* **1998**, *44*, 115-123.

(39) Chapman, P. A.; Malo, A. T. C.; Siddons, C. A.; Harkin, M. *Appl. Environ. Microbiol.* **1997**, *63*, 2549-2553.

(40) Gehring, A. G.; Crawford, C. G.; Mazenko, R. S.; VanHouten, L. J.; Brewster, J. D. *J. Immunol. Methods* **1996**, *195*, 15-25.

(41) Perez, F. G.; Mascini, M.; Tothill, I. E.; Turner, A. P. F. *Anal. Chem.* **1998**, *70*, 2380-2386.

(42) Ghindilis, A. L.; Atanasov, P.; Wilkins, M.; Wilkins, E. *Biosens. Bioelectron.* **1998**, *13*, 113-131.

(43) Rishpon, J.; Ivnitski, D. *Biosens. Bioelectron.* **1997**, *12*, 195-204.

(44) Mello, L. D.; Kubota, L. T. *Food Chem.* **2002**, *77*, 237-256.

(45) Hahn, M. A.; Tabb, J. S.; Krauss, T. D. *Anal. Chem.* **2005**, *77*, 4861-4869.

(46) Su, X. L.; Li, Y. B. *Anal. Chem.* **2004**, *76*, 4806-4810.

(47) Zhao, X. J.; Hilliard, L. R.; Mechery, S. J.; Wang, Y. P.; Bagwe, R. P.; Jin, S. G.; Tan, W. H. *PNAS* **2004**, *101*, 15027-15032.

(48) Ho, J. A. A.; Hsu, H. W.; Huang, M. R. *Anal. Biochem.* **2004**, *330*, 342-349.

(49) Goodridge, L.; Chen, J. R.; Griffiths, M. *Appl. Environ. Microbiol.* **1999**, *65*, 1397-1404.

(50) Watson, A.; Wu, X. Y.; Bruchez, M. *Biotechniques* **2003**, *34*, 296.

(51) Wu, X. Y.; Liu, H. J.; Liu, J. Q.; Haley, K. N.; Treadway, J. A.; Larson, J. P.; Ge, N. F.; Peale, F.; Bruchez, M. P. *Nat. Biotechnol.* **2003**, *21*, 41-46.

(52) Parak, W. J.; Gerion, D.; Zanchet, D.; Woerz, A. S.; Pellegrino, T.; Micheel, C.; Williams, S. C.; Seitz, M.; Bruehl, R. E.; Bryant, Z.; Bustamante, C.; Bertozzi, C. R.; Alivisatos, A. P. *Chem. Mater.* **2002**, *14*, 2113-2119.

(53) Rosenthal, S. J.; Tomlinson, A.; Adkins, E. M.; Schroeter, S.; Adams, S.; Swafford, L.; McBride, J.; Wang, Y. Q.; DeFelice, L. J.; Blakely, R. D. *J. Am. Chem. Soc.* **2002**, *124*, 4586-4594.

(54) Goldman, E. R.; Anderson, G. P.; Tran, P. T.; Mattoussi, H.; Charles, P. T.; Mauro, J. M. *Anal. Chem.* **2002**, *74*, 841-847.

(55) Goldman, E. R.; Balighian, E. D.; Mattoussi, H.; Kuno, M. K.; Mauro, J. M.; Tran, P. T.; Anderson, G. P. *J. Am. Chem. Soc.* **2002**, *124*, 6378-6382.

(56) Weimer, B. C.; Walsh, M. K.; Beer, C.; Koka, R.; Wang, X. *Appl. Environ. Microbiol.* **2001**, *67*, 1300-1307.

(57) McBride, M. T.; Gammon, S.; Pitesky, M.; O'Brien, T. W.; Smith, T.; Aldrich, J.; Langlois, R. G.; Colston, B.; Venkateswaran, K. S. *Anal. Chem.* **2003**, *75*, 1924-1930.

(58) Fung, Y. S.; Wong, Y. Y. *Anal. Chem.* **2001**, *73*, 5302-5309.

(59) Guilbault, G. G.; Luong, J. H. T. In *Food Sci. Technol.*, 1994; Vol. 60, pp 151-172.

(60) Fratamico, P. M.; Strobaugh, T. P. In *J. Ind. Microbiol. Biotechnol.*, 1998; Vol. 21, pp 92-98.

(61) Cullen, D. C.; Lowe, C. R. *Sens. Actuators, B* **1990**, *1*, 576-579.

(62) Bopp, D. J.; Sauders, B. D.; Waring, A. L.; Ackelsberg, J.; Dumas, N.; Braun-Howland, E.; Dziewulski, D.; Wallace, B. J.; Kelly, M.; Halse, T.; Musser, K. A.; Smith, P. F.; Morse, D. L.; Limberger, R. J. *J. Clin. Microbiol.* **2003**, *41*, 174-180.

(63) Campbell, G. R.; Prosser, J.; Glover, A.; Killham, K. *J. Appl. Microbiol.* **2001**, *91*, 1004-1010.

(64) Fortin, N. Y.; Mulchandani, A.; Chen, W. *Anal. Biochem.* **2001**, *289*, 281-288.

(65) Grant, M. A. *J. Food Prot.* **2003**, *66*, 18-24.

(66) Heller, L. C.; Davis, C. R.; Peak, K. K.; Wingfield, D.; Cannons, A. C.; Amuso, P. T.; Cattani, J. *Appl. Environ. Microbiol.* **2003**, *69*, 1844-1846.

(67) Ibekwe, A. M.; Grieve, C. M. *J. Appl. Microbiol.* **2003**, *94*, 421-431.

(68) Imamura, O.; Arakawa, H.; Maeda, M. *Luminescence* **2003**, *18*, 107-112.

(69) Kimura, R.; Mandrell, R. E.; Galland, J. C.; Hyatt, D.; Riley, L. W. *Appl. Environ. Microbiol.* **2000**, *66*, 2513-2519.

(70) Louie, M.; Read, S.; Simor, A. E.; Holland, J.; Louie, L.; Ziebell, K.; Brunton, J.; Hii, J. *J. Clin. Microbiol.* **1998**, *36*, 3375-3377.

(71) McKillip, J. L.; Jaykus, L. A.; Drake, M. *J. Food Prot.* **2002**, *65*, 1775-1779.

(72) Sharma, V. K.; Dean-Nystrom, E. A.; Casey, T. A. *Mol. Cell. Probe.* **1999**, *13*, 291-302.

(73) Tims, T. B.; Lim, D. V. *J. Microbiol. Methods* **2003**, *55*, 141-147.

(74) Wang, L.; Rothemund, D.; Curd, H.; Reeves, P. R. *J. Clin. Microbiol.* **2000**, *38*, 1786-1790.

(75) Belgrader, P.; Benett, W.; Hadley, D.; Long, G.; Mariella, R.; Milanovich, F.; Nasarabadi, S.; Nelson, W.; Richards, J.; Stratton, P. *Clin. Chem.* **1998**, *44*, 2191-2194.

(76) Gooding, C. M.; Choudary, P. V. *J. Dairy Res.* **1997**, *64*, 87-93.

(77) Karch, H.; JanetzkiMittmann, C.; Aleksic, S.; Datz, M. *J. Clin. Microbiol.* **1996**, *34*, 516-519.

(78) Muller, E. E.; Grabow, W. O. K.; Ehlers, M. M. *Water Safety* **2003**, *29*, 427-432.

(79) Pyle, B. H.; Broadaway, S. C.; McFeters, G. A. *Appl. Environ. Microbiol.* **1999**, *65*, 1966-1972.

(80) Yu, H. *Anal. Chim. Acta* **1998**, *376*, 77-81.

(81) Nakamura, N.; Burgess, J. G.; Yagiuda, K.; Kudo, S.; Sakaguchi, T.; Matsunaga, T. *Anal. Chem.* **1993**, *65*, 2036-2039.

(82) Restaino, L.; Frampton, E. W.; Irbe, R. M.; Allison, D. R. K. *Lett. Appl. Microbiol.* **1997**, *24*, 401-404.

(83) Seo, K. H.; Brackett, R. E.; Frank, J. F.; Hilliard, S. *J. Food Prot.* **1998**, *61*, 812-816.

(84) Tu, S. I.; Patterson, D.; Briggs, C.; Irwin, P.; Yu, L. *J. Ind. Microbiol. Biotechnol.* **2001**, *26*, 345-349.

(85) Abdel-Hamid, I.; Ivnitski, D.; Atanasov, P.; Wilkins, E. *Biosens. Bioelectron.* **1999**, *14*, 309-316.

(86) Gehring, A. G.; Patterson, D. L.; Tu, S. I. *Anal. Biochem.* **1998**, *258*, 293-298.

(87) Yu, H.; Bruno, J. G. *Appl. Environ. Microbiol.* **1996**, *62*, 587-592.

(88) Brewster, J. D.; Mazenko, R. S. *J. Immunol. Methods* **1998**, *211*, 1-8.

(89) Bukhari, Z.; Weihe, J.; LeChevallier, M. *Water Sci. Technol.* **2004**, *50*, 233-237.

(90) Yu, L. S. L.; Reed, S. A.; Golden, M. H. *J. Microbiol. Methods* **2002**, *49*, 63-68.

(91) Shapiro, H. M. *J. Microbiol. Methods* **2000**, *42*, 3-16.

(92) Shapiro, H. M. *Practical Flow Cytometry*, 3rd ed.; John Wiley and Sons, Inc.: New York.

(93) Shapiro, H. M. *Practical Flow Cytometry*; Wiley- Liss: New York, 1995.

(94) Barnett, J. M.; Cuchens, M. A.; Buchanan, W. *J. Dent. Res.* **1984**, *63*, 1040-1042.

(95) Boye, E.; Steen, H. B.; Skarstad, K. *J. Gen. Microbiol.* **1983**, *129*, 973-980.

(96) Donnelly, C. W.; Baigent, G. J. *Appl. Environ. Microbiol.* **1986**, *52*, 689-695.

(97) Hutter, K. J.; Eipel, H. E. *J. Gen. Microbiol.* **1979**, *113*, 369-375.

(98) Kim, Y.; Jett, J. H.; Larson, E. J.; Penttila, J. R.; Marrone, B. L.; Keller, R. A. *Cytometry* **1999**, *36*, 324-332.

(99) Pinder, A. C.; Purdy, P. W.; Poulter, S. A. G.; Clark, D. C. *J. Appl. Bacteriol.* **1990**, *69*, 92-100.

(100) Steen, H. B. *Histochem. J.* **1983**, *15*, 147-160.

(101) Van Dilla, M. A.; Langlois, R. G.; Pinkel, D.; Yajko, D.; Hadley, W. K. *Science* **1983**, *220*, 620-622.

(102) Chapman, P. A.; Wright, D. J.; Siddons, C. A. *J. Med. Microbiol.* **1994**, *40*, 424-427.

(103) DeLeo, P. C.; Baveye, P. *Appl. Environ. Microbiol.* **1996**, *62*, 4580-4586.

(104) Mcclelland, R. G.; Pinder, A. C. *J. Appl. Bacteriol.* **1994**, *77*, 440-447.

(105) Wright, D. J.; Chapman, P. A.; Siddons, C. A. *Epidemiology and Infection* **1994**, *113*, 31-39.

(106) Nebe-von-Caron, G.; Stephens, P. J.; Hewitt, C. J.; Powell, J. R.; Badley, R. A. *J. Microbiol. Methods* **2000**, *42*, 97-114.

(107) Shapiro, H. M. *Methods* **2000**, *21*, 271-279.

(108) Gunasekera, T. S.; Veal, D. A.; Attfield, P. V. *Intl. J. Food Microbiol.* **2003**, *85*, 269-279.

(109) Novo, D. J.; Perlmutter, N. G.; Hunt, R. H.; Shapiro, H. M. *Antimicrob. Agents. Chemother.* **2000**, *44*, 827-834.

(110) Shapiro, H. M. *Cytometry* **2001**, *43*, 223-226.

(111) Barbesti, S.; Citterio, S.; Labra, M.; Baroni, M. D.; Neri, M. G.; Sgorbati, S. *Cytometry* **2000**, *40*, 214-218.

(112) Fu, A. Y.; Spence, C.; Scherer, A.; Arnold, F. H.; Quake, S. R. *Nat. Biotechnol.* **1999**, *17*, 1109-1111.

(113) McClain, M. A.; Culbertson, C. T.; Jacobson, S. C.; Ramsey, J. M. *Anal. Chem.* **2001**, *73*, 5334-5338.

(114) Rieseberg, M.; Kasper, C.; Reardon, K. F.; Scheper, T. *Appl. Microbiol. Biotechnol.* **2001**, *56*, 350-360.

(115) Tyndall, R. L.; Hand, R. E., Jr.; Mann, R. C.; Evans, C.; Jernigan, R. *Appl. Environ. Microbiol.* **1985**, *49*, 852-857.

(116) Yu, F. P.; Mcfeters, G. A. *J. Microbiol. Methods* **1994**, *20*, 1-10.

(117) Steen, H. B. *J. Microbiol. Methods* **2000**, *42*, 65-74.

(118) Wood, J. C. S. *Cytometry* **1998**, *33*, 260-266.

(119) Philips, R. J., "Real Time Monitoring of Foodborne Pathogens: *State-of-the-Art Report*," Food Manufacturing Coalition, **1997**.

(120) Ingle, J. D., Jr.; Crouch, S. R. *Spectrochemical Analysis*; Prentice Hall: Upper Saddle River: New Jersey, 1988.

(121) Kortum, G.; Springer-Verlag: New York: New York, 1969.

(122) Wendlandt, W. W.; Hecht, H. G.; Inter-science: New York: New York, 1966.

(123) Blitz, J. P. *Modern Techniques in Applied Molecular Spectroscopy*; John Wiley & Sons: New York, 1998.

(124) Kubelka, P. *J. Opt. Soc. Am.* **1948**, *38*, 448-457.

(125) Kortum, G. *T. Faraday Soc.* **1962**, *58*, 1624-&.

(126) Kortum, G. *Spectrochim. Acta* **1957**, *11*, 534-541.

(127) Kortum, G. B., W.; Herzog, G. *Angewandte Chemie, International Edition* **1963**, *2*, 333.

(128) Schmidt, J. A.; Heitner, C. *Tappi J.* **1993**, *76*, 117-123.

(129) Zou, W. Q.; Gonzalez, R. D. *J. Catal.* **1992**, *133*, 202-219.

(130) Arena, M. P.; Porter, M. D.; Fritz, J. S. *Anal. Chim. Acta* **2003**, *482*, 197-207.

(131) Arena, M. P.; Porter, M. D.; Fritz, J. S. *Anal. Chem.* **2002**, *74*, 185-190.

(132) Fritz, J. S.; Arena, M. P.; Steiner, S. A.; Porter, M. D. *J. Chromatogr., A* **2003**, *997*, 41-50.

(133) Gazda, D. B.; Fritz, J. S.; Porter, M. D. *Anal. Chim. Acta* **2004**, *508*, 53-59.

(134) Gazda, D. B.; Fritz, J. S.; Porter, M. D. *Anal. Chem.* **2004**, *76*, 4881-4887.

(135) Gazda, D. B.; Lipert, R. J.; Fritz, J. S.; Porter, M. D. *Anal. Chim. Acta* **2004**, *510*, 241-247.

(136) Porter, M. D.; Bright, T. B.; Allara, D. L.; Chidsey, C. E. D. *J. Am. Chem. Soc.* **1987**, *109*, 3559-3568.

(137) Weisshaar, D. E.; Lamp, B. D.; Porter, M. D. *J. Am. Chem. Soc.* **1992**, *114*, 5860-5862.

(138) Troughton, E. B.; Bain, C. D.; Whitesides, G. M.; Nuzzo, R. G.; Allara, D. L.; Porter, M. D. *Langmuir* **1988**, *4*, 365-385.

(139) Delamarche, E.; Michel, B.; Biebuyck, H. A.; Gerber, C. *Adv. Mater.* **1996**, *8*, 719-&.

(140) Dubois, L. H.; Nuzzo, R. G. *Annu. Rev. Phys. Chem.* **1992**, *43*, 437-463.

(141) Gooding, J. J.; Hibbert, D. B. *Trac-Trends Anal. Chem.* **1999**, *18*, 525-533.

(142) Ulman, A. *Chem. Rev.* **1996**, *96*, 1533-1554.

(143) Ulman, A. *An Introduction to Ultrathin Organic Films from Langmuir-Blodgett to Self-Assembly*; Academic Press: New York, 1991.

(144) Bain, C. D.; Biebuyck, H. A.; Whitesides, G. M. *Langmuir* **1989**, *5*, 723-727.

(145) Castner, D. G.; Hinds, K.; Grainger, D. W. *Langmuir* **1996**, *12*, 5083-5086.

(146) Evans, S. D.; Goppertberarducci, K. E.; Urankar, E.; Gerenser, L. J.; Ulman, A. *Langmuir* **1991**, *7*, 2700-2709.

(147) Walczak, M. M.; Alves, C. A.; Lamp, B. D.; Porter, M. D. *J. Electroanal. Chem.* **1995**, *396*, 103-114.

(148) Zhong, C.-J.; Brush, R. C.; Anderegg, J.; Porter, M. D. *Langmuir* **1999**, *15*, 518-525.

(149) Bryant, M. A.; Pemberton, J. E. *J. Am. Chem. Soc.* **1991**, *113*, 8284-8293.

(150) Li, Y.; Huang, J.; Robert T. McIver, J.; Hemminger, J. C. *J. Am. Chem. Soc.* **1992**, *114*, 2482-2432.

(151) Nuzzo, R. G.; Dubois, L. H.; Allara, D. L. *J. Am. Chem. Soc.* **1990**, *112*, 558-569.

(152) Widrig, C. A.; Chung, C.; Porter, M. D. *J. Electroanal. Chem.* **1991**, *310*, 335-359.

(153) Love, J. C.; Estroff, L. A.; Kriebel, J. K.; Nuzzo, R. G.; Whitesides, G. M. *Chem. Rev.* **2005**, *105*, 1103-1169.

(154) Everhart, D. S. *Chemtech* **1999**, *29*, 30-37.

(155) Kaifer, A. E. *Isr. J. Chem.* **1996**, *36*, 389-397.

(156) Bain, C. D.; Troughton, E. B.; Tao, Y.-T.; Evall, J.; Whitesides, G. M.; Nuzzo, R. G. *J. Am. Chem. Soc.* **1989**, *111*, 321-335.

(157) Green, J.-B. D.; McDermott, M. T.; Porter, M. D.; Siperko, L. M. *J. Phys. Chem.* **1995**, *99*, 10960-10965.

(158) Kane, R. S.; Takayama, S.; Ostuni, E.; Ingber, D. E.; Whitesides, G. M. *Biomaterials* **1999**, *20*, 2363-2376.

(159) Frey, B. L.; Corn, R. M. *Anal. Chem.* **1996**, *68*, 3187-3193.

(160) Wagner, P.; Hegner, M.; Kernen, P.; Zaugg, F.; Semenza, G. *Biophys. J.* **1996**, *70*, 2052-2066.

(161) Cabrita, J. F.; Abrantes, L. M.; Viana, A. S. *Electrochim. Acta* **2005**, *50*, 2117-2124.

(162) Nakano, K.; Taira, H.; Maeda, M.; Takagi, M. *Anal. Sci.* **1993**, *9*, 133-136.

(163) Dammer, U.; Hegner, M.; Anselmetti, D.; Wagner, P.; Dreier, M.; Huber, W.; Guntherodt, H. J. *Biophys. J.* **1996**, *70*, 2437-2441.

(164) Grubisha, D. S.; Lipert, R. J.; Park, H. Y.; Driskell, J.; Porter, M. D. *Anal. Chem.* **2003**, *75*, 5936-5943.

(165) Jones, V. W.; Kenseth, J. R.; Porter, M. D.; Mosher, C. L.; Henderson, E. *Anal. Chem.* **1998**, *70*, 1233-1241.

(166) Wagner, P.; Zaugg, F.; Kernen, P.; Hegner, M.; Semenza, G. *J Vac Sci Technol B* **1996**, *14*, 1466-1471.

(167) Pompe, T.; Fery, A.; Herminghaus, S.; Kriele, A.; Lorenz, H.; Kotthaus, J. P. *Langmuir* **1999**, *15*, 2398-2401.

(168) St John, P. M.; Davis, R.; Cady, N.; Czajka, J.; Batt, C. A.; Craighead, H. G. *Anal. Chem.* **1998**, *70*, 1108-1111.

(169) Zaugg, F. G.; Spencer, N. D.; Wagner, P.; Kernen, P.; Vinckier, A.; Groscurth, P.; Semenza, G. *J. Mater. Sci.-Mater. Med.* **1999**, *10*, 255-263.

(170) Craighead, H. G.; James, C. D.; Turner, A. M. P. *Curr. Opin. Solid State Mater. Sci.* **2001**, *5*, 177-184.

(171) Mrksich, M. *Chem. Soc. Rev.* **2000**, *29*, 267-273.

(172) Mrksich, M.; Whitesides, G. M. *Trends Biotechnol.* **1995**, *13*, 228-235.

(173) Tan, J. L.; Tien, J.; Chen, C. S. *Langmuir* **2002**, *18*, 519-523.

(174) Bernard, A.; Delamarche, E.; Schmid, H.; Michel, B.; Bosshard, H. R.; Biebuyck, H. *Langmuir* **1998**, *14*, 2225-2229.

(175) Patel, N.; Bhandari, R.; Shakesheff, K. M.; Cannizzaro, S. M.; Davies, M. C.; Langer, R.; Roberts, C. J.; Tendler, S. J. B.; Williams, P. M. *J. Biomat. Sci., Polym. Ed.* **2000**, *11*, 319-331.

(176) Geissler, M.; Bernard, A.; Bietsch, A.; Schmid, H.; Michel, B.; Delamarche, E. *J. Am. Chem. Soc.* **2000**, *122*, 6303-6304.

(177) James, C. D.; Davis, R. C.; Kam, L.; Craighead, H. G.; Isaacson, M.; Turner, J. N.; Shain, W. *Langmuir* **1998**, *14*, 741-744.

(178) Martin, B. D.; Gaber, B. P.; Patterson, C. H.; Turner, D. C. *Langmuir* **1998**, *14*, 3971-3975.

(179) StJohn, P. M.; Craighead, H. G. *Appl. Phys. Lett.* **1996**, *68*, 1022-1024.

(180) Kumar, A.; Whitesides, G. M. *Appl. Phys. Lett.* **1993**, *63*, 2002-2004.

(181) Tien, J. X., Y.; Whitesides, G. M. *Thin Solid Flims* **1998**, *24*, 227-254.

(182) Kenseth, J. R. Ph. D. thesis, Iowa State University, Ames, 2000.

(183) Howell, S. W.; Inerowicz, H. D.; Regnier, F. E.; Reifenberger, R. *Langmuir* **2003**, *19*, 436-439.

(184) Bhatia, S. K.; Teixeira, J. L.; Anderson, M.; Shriverlake, L. C.; Calvert, J. M.; Georger, J. H.; Hickman, J. J.; Dulcey, C. S.; Schoen, P. E.; Ligler, F. S. *Anal. Biochem.* **1993**, *208*, 197-205.

(185) Tarlov, M. J.; Burgess, D. R. F.; Gillen, G. *J. Am. Chem. Soc.* **1993**, *115*, 5305-5306.

(186) Kenseth, J. R.; Harnisch, J. A.; Jones, V. W.; Porter, M. D. *Langmuir* **2001**, *17*, 4105-4112.

(187) Lewis, M.; Tarlov, M.; Carron, K. *J. Am. Chem. Soc.* **1995**, *117*, 9574-9575.

(188) Zhang, Y. M.; Terrill, R. H.; Tanzer, T. A.; Bohn, P. W. *J. Am. Chem. Soc.* **1998**, *120*, 2654-2655.

(189) Norrod, K. L.; Rowlen, K. L. *J. Am. Chem. Soc.* **1998**, *120*, 2656-2657.

(190) Zhang, Y.; Terrill, R. H.; Bohn, P. W. *Chem. Mater.* **1999**, *11*, 2191-2198.

(191) Friebel, S.; Aizenberg, J.; Abad, S.; Wiltzius, P. *Appl. Phys. Lett.* **2000**, *77*, 2406-2408.

(192) Duhachek, S. D.; Kenseth, J. R.; Casale, G. P.; Small, G. J.; Porter, M. D.; Jankowiak, R. *Anal. Chem.* **2000**, *72*, 3709-3716.

(193) O'Brien, J. C.; Jones, V. W.; Porter, M. D.; Mosher, C. L.; Henderson, E. *Anal. Chem.* **2000**, *72*, 703-710.

(194) O'Brien, J. C.; Stickney, J. T.; Porter, M. D. *Langmuir* **2000**, *16*, 9559-9567.

(195) O'Brien, J. C.; Stickney, J. T.; Porter, M. D. *J. Am. Chem. Soc.* **2000**, *122*, 5004-5005.

(196) Takano, H.; Sul, J. Y.; Mazzanti, M. L.; Doyle, R. T.; Haydon, P. G.; Porter, M. D. *Anal. Chem.* **2002**, *74*, 4640-4646.

(197) Shadnam, M. R.; Kirkwood, S. E.; Fedosejevs, R.; Amirfazli, A. *Langmuir* **2004**, *20*, 2667-2676.

(198) Vaidya, R.; Tender, L. M.; Bradley, G.; O'Brien, M. J.; Cone, M.; Lopez, G. P. *Biotechnol. Progr.* **1998**, *14*, 371-377.

(199) Brizzolara, R. A. *Biosens. Bioelectron.* **2000**, *15*, 63-68.

(200) Kido, H.; Maquieira, A.; Hammock, B. D. *Anal. Chim. Acta* **2000**, *411*, 1-11.

(201) Lueking, A.; Horn, M.; Eickhoff, H.; Bussow, K.; Lehrach, H.; Walter, G. *Anal. Biochem.* **1999**, *270*, 103-111.

(202) Silzel, J. W.; Cercek, B.; Dodson, C.; Tsay, T.; Obremski, R. J. *Clin. Chem.* **1998**, *44*, 2036-2043.

(203) Joos, T. O.; Schrenk, M.; Hopfl, P.; Kroger, K.; Chowdhury, U.; Stoll, D.; Schorner, D.; Durr, M.; Herick, K.; Rupp, S.; Sohn, K.; Hammerle, H. *Electrophoresis* **2000**, *21*, 2641-2650.

(204) MacBeath, G.; Schreiber, S. L. *Science* **2000**, *289*, 1760-1763.

(205) Mendoza, L. G.; McQuary, P.; Mongan, A.; Gangadharan, R.; Brignac, S.; Eggers, M. *Biotechniques* **1999**, *27*, 778.

(206) Delamarche, E.; Bernard, A.; Schmid, H.; Michel, B.; Biebuyck, H. *Science* **1997**, *276*, 779-781.

(207) Kim, E.; Xia, Y. N.; Whitesides, G. M. *Nature* **1995**, *376*, 581-584.

(208) Pekas, N.; Granger, M.; Tondra, M.; Popple, A.; Porter, M. D. *J. Magn. Magn. Mater.* **2005**, *293*, 584-588.

(209) Nowall, W. B.; Wipf, D. O.; Kuhr, W. G. *Anal. Chem.* **1998**, *70*, 2601-2606.

(210) Wadu-Mesthrige, K.; Xu, S.; Amro, N. A.; Liu, G. Y. *Langmuir* **1999**, *15*, 8580-8583.

(211) Wittstock, G.; Hesse, R.; Schuhmann, W. *Electroanalysis* **1997**, *9*, 746-750.

(212) Xu, S.; Liu, G. Y. *Langmuir* **1997**, *13*, 127-129.

(213) Shay, J. W.; Porter, K. R.; Krueger, T. C. *Exp. Cell Res.* **1977**, *105*, 1-8.

(214) Britland, S.; Clark, P.; Connolly, P.; Moores, G. *Exp. Cell Res.* **1992**, *198*, 124-129.

(215) Kleinfeld, D.; Kahler, K. H.; Hockberger, P. E. *J. Neurosci.* **1988**, *8*, 4098-4120.

(216) Mooney, J. F.; Hunt, A. J.; McIntosh, J. R.; Liberko, C. A.; Walba, D. M.; Rogers, C. T. *PNAS* **1996**, *93*, 12287-12291.

(217) Stenger, D. A.; Georger, J. H.; Dulcey, C. S.; Hickman, J. J.; Rudolph, A. S.; Nielsen, T. B.; Mccort, S. M.; Calvert, J. M. *J. Am. Chem. Soc.* **1992**, *114*, 8435-8442.

(218) Vargo, T. G.; Thompson, P. M.; Gerenser, L. J.; Valentini, R. F.; Aebischer, P.; Hook, D. J.; Gardella, J. A. *Langmuir* **1992**, *8*, 130-134.

(219) Lopez, G. P.; Albers, M. W.; Schreiber, S. L.; Carroll, R.; Peralta, E.; Whitesides, G. M. *J. Am. Chem. Soc.* **1993**, *115*, 5877-5878.

(220) Mrksich, M.; Dike, L. E.; Tien, J.; Ingber, D. E.; Whitesides, G. M. *Exp. Cell Res.* **1997**, *235*, 305-313.

(221) Singhvi, R.; Kumar, A.; Lopez, G. P.; Stephanopoulos, G. N.; Wang, D. I. C.; Whitesides, G. M.; Ingber, D. E. *Science* **1994**, *264*, 696-698.

(222) Rowan, B.; Wheeler, M. A.; Crooks, R. M. *Langmuir* **2002**, *18*, 9914-9917.

(223) Koepsel, R. R.; Russell, A. J. *Biomacromolecules* **2003**, *4*, 850-855.

(224) Morhard, F.; Pipper, J.; Dahint, R.; Grunze, M. *Sens. Actuators, B* **2000**, *70*, 232-242.

(225) Rowe, C. A.; Tender, L. M.; Feldstein, M. J.; Golden, J. P.; Scruggs, S. B.; MacCraith, B. D.; Cras, J. J.; Ligler, F. S. *Anal. Chem.* **1999**, *71*, 3846-3852.

(226) Sapsford, K. E.; Rasooly, A.; Taitt, C. R.; Ligler, F. S. *Anal. Chem.* **2004**, *76*, 433-440.

Figure captions

Figure 1. General concept of flow cytometry technique.

Figure 2. Optical phenomena involved in diffuse reflectance.[123]

Figure 3. Idealized self-assembled monolayer (SAM) on gold.

Figure 4. Mechanism for covalent attachment of amine containing molecules (e.g., proteins) to dithio-bis(succinimidyl propionate) (DSP) derived SAM.

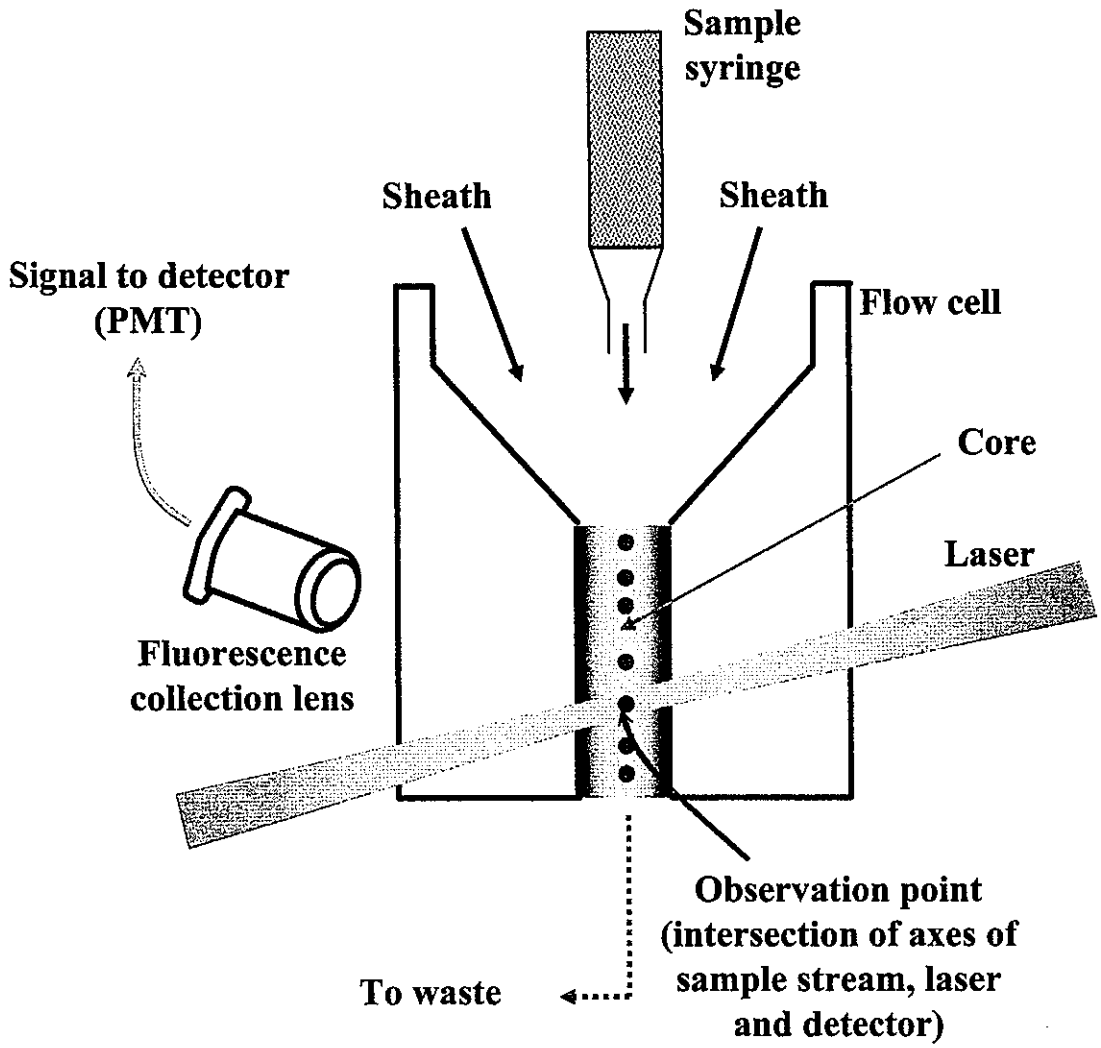
Sample syringe
Sheath
Sheath
Signal to detector (PMT)
Flow cell
Core
Laser
Fluorescence collection lens
Observation point (intersection of axes of sample stream, laser and detector)
To waste

Figure 1

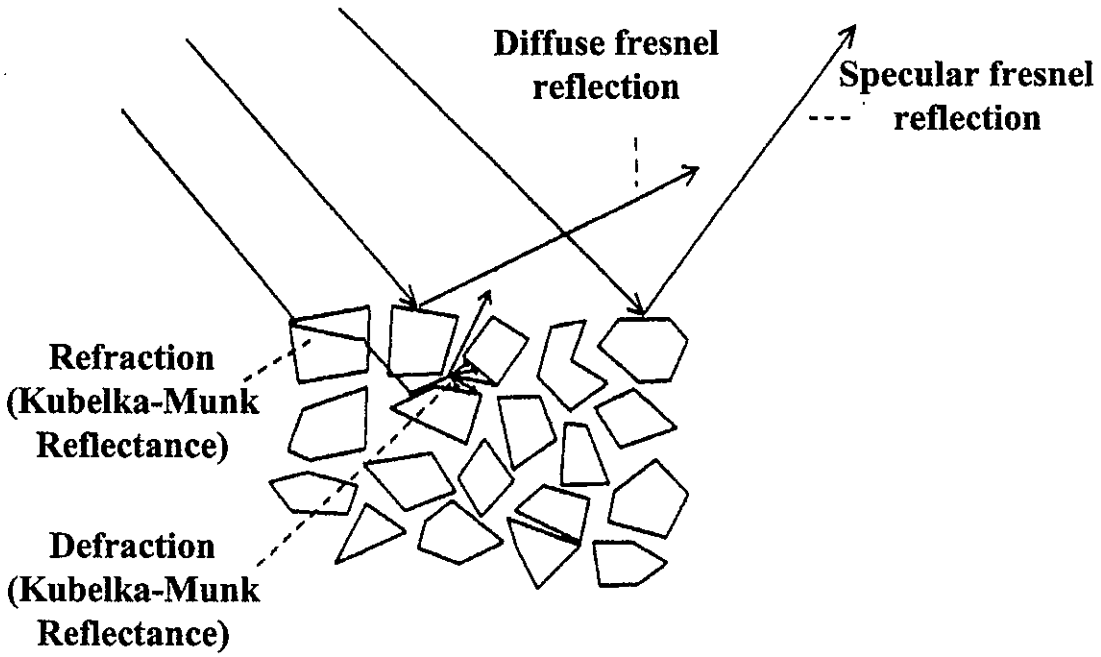
Diffuse fresnel reflection
Specular fresnel reflection
Refraction (Kubelka-Munk Reflectance)
Defraction (Kubelka-Munk Reflectance)

Figure 2

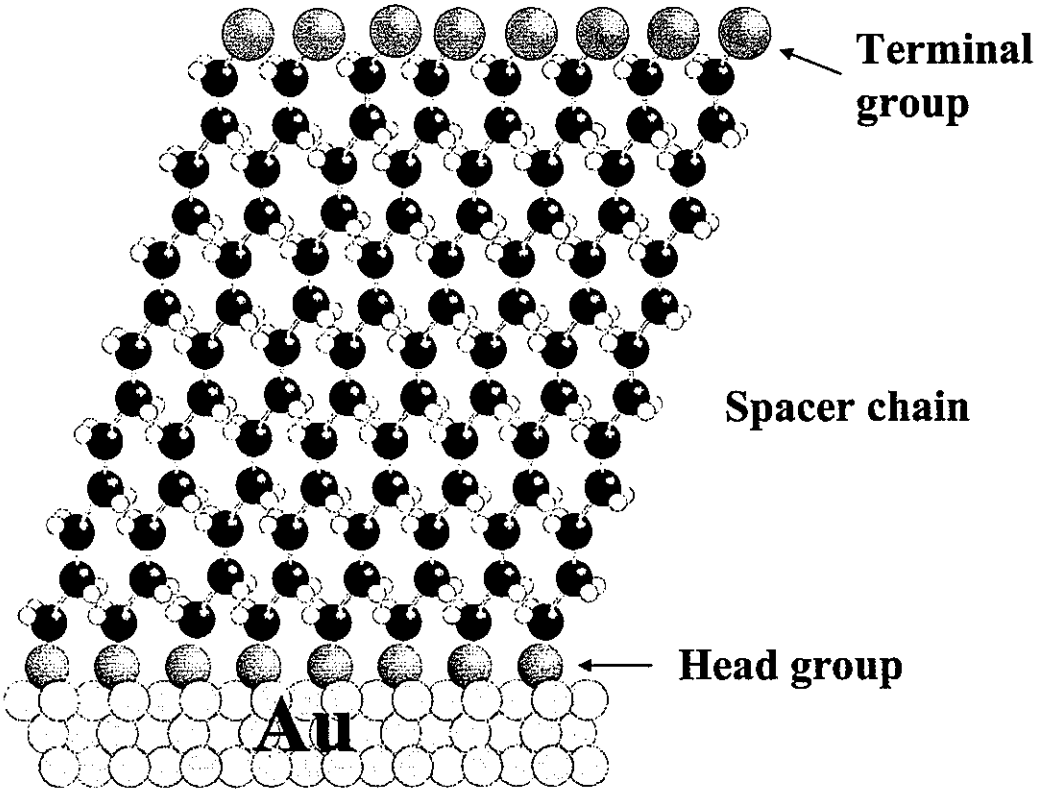

Figure 3

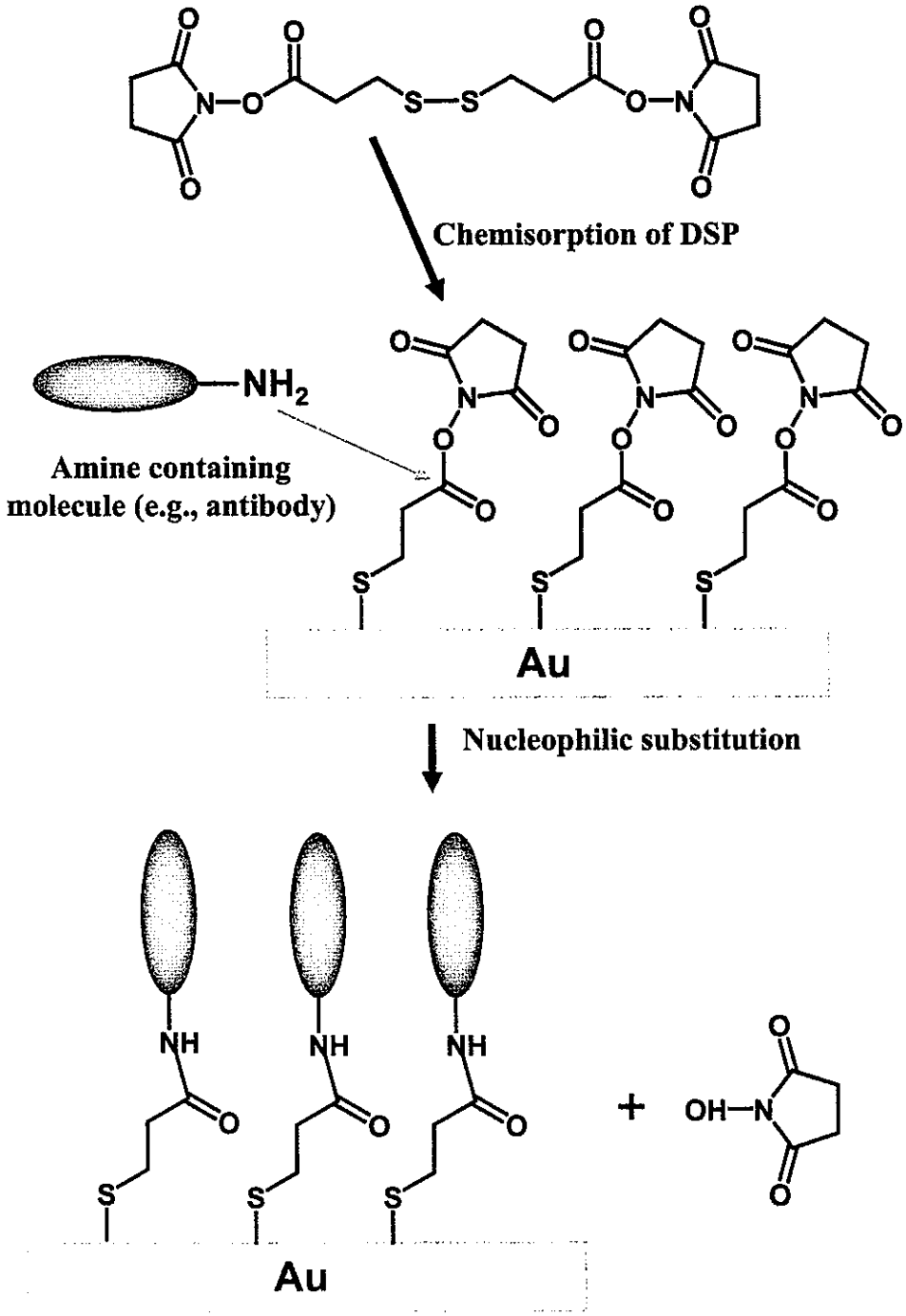
Chemisorption of DSP
NH2
Amine containing
molecule (e.g., antibody)
Au
Nucleophilic substitution
NH
NH
NH
OH
Au

Figure 4

CHAPTER 1: MICROMINIATURIZED IMMUNOSENSING PLATFORM PREPARED BY PATTERNING SPECIFIC CAPTURE ADDRESSES

A paper in preparation for submission to *Bioanalytical Chemistry*

Salma Rahman, Robert J. Lipert, and Marc D. Porter *

Institute of Combinatorial Discovery, Ames laboratory-USDOE, and Department of Chemistry and of Chemical and Biological Engineering, Iowa State University, Ames, IA 50011 USA

Abstract

A simple technique for fabrication of antibody addresses (microarrays) capable of capturing bacteria selectively in predetermined locations is described. The miniaturized platform is comprised of micrometer-sized addresses of anti-*E. coli* O157:H7 formed by its covalent coupling to a dithio-bis(succinimidyl propionate) (DSP)-derived self-assembled monolayer (SAM). Each address is also separated by micrometer-sized spacers composed of a monolayer formed from 1H, 1H, 2H, 2H-perfluorodecyl-1-thiol (PFDT), which minimizes nonspecific adsorption of both the capture antibody and target bacteria (i.e., *E. coli* O157:H7). Details of the substrate preparation, and results from investigations of the effect of pH, incubation time, and temperature on the binding of *E. coli* O157:H7 to the anti-*E. coli* O157:H7 are discussed. Various detection techniques can be employed to "digitally" enumerate the captured bacteria on this type of platform. Thousands of antibody-modified addresses on the surface of a single chip may provide some useful features including high throughput, reduction of sample volume as well as low level of detection.

* Corresponding Author

Introduction

Concern due to microbial contamination is growing around the world. Despite significant improvements, there is no single method that is completely satisfactory for detection of specific bacteria,[1] especially, when the concentration of the target organism is quite low, e.g., infectious dose of *E. coli* O157:H7 is only 10-100 cells.[2] Moreover, many current analytical methods require long analysis times, as well as complex instrumentation. Only a few of the techniques have achieved lower levels of detection (e.g., ~10^3 cells/mL) without a pre-enrichment step.[2-9] Most of the methods require pre-enrichment steps to allow the target organism to multiply.[10-15] In this work, we focused on the construction of a miniaturized immunosensing platform that is comprised of domains of defined shape and size (called addresses) to capture a single target cells and other biomolecules. Because of presence of many addresses (> 50000) in a single platform and the exposure of all the addresses to the sample solution at the same time, the selective capturing of a very low number of microorganisms from the solution is possible.

For patterning biomaterials, a number of methods have been reported.[16] One class of techniques involves direct transfer of the biomaterials to a substrate using a master stamp (e.g., microcontact printing (μCP),[17-22] membrane-based patterning,[23] micromolding in capillaries,[19, 24, 25] and laminar flow patterning[19, 24, 26]). However, defects in the transferred antibody coating are occasionally observed during fabrication with μCP.[27] Another class involves the selective chemical or physical modification of the substrate surface to control adhesion (e.g., linking of biomaterial through a covalent bond or protein-protein interaction, manipulation of surface charge,[28] hydrophilicity,[28] and topography.[19, 20, 29] Cell and bacteria were patterned either bio-specifically or non-specifically by different techniques. Cell

patterning has also been accomplished by methods that employ the deposition of metals[30] and self-assembled monolayers (SAMs) of alkylsiloxane on silica/glass by optical,[31, 32] UV,[33, 34] and plasma lithography.[35] Though these methods are useful, they offer limited control over surface chemistry and generate regions differentiated mainly by hydrophilicity.[36] On the other hand, SAMs of alkanethiolates on gold are amenable to more convenient patterning methods (lithographic and nonlithographic). They are structurally well defined at the molecular level; they also offer substantial control over ligand density and environment[37-39] as well as provide great flexibility and precision in specification of the tail (i.e., surface) group.[40] Moreover, μCP of alkanethiolates on gold or silver using a polydimethylsiloxane (PDMS) stamp for the covalent immobilization of proteins[41] or for engineering cell shape and function has been performed.[42, 43]

Nonselective patterning of bacteria within three dimensional heperbranched polymer film templates was performed by Crooks et al.[16] But there are few reports in the literature on the selective capture of bacteria using an immobilized antibody and addressed substrates (e.g., capturing bacteria on bioplastic film (polyurethane)[44]or on array biosensors[27, 45-47]). To our knowledge, no work has appeared for capturing bacteria on 10-μm sized (or smaller) addresses. Our preliminary goal is to create micro-meter size domains of anti-*E. coli* O157:H7 for capturing *E. coli* O157:H7 cell in each address. The general approach to accomplish this is the creation of compositionally patterned alkanethiolate monolayers on gold. Using this approach, monolayers and patterns of proteins and DNA have been previously prepared in our laboratory.[48-54] We chose SAMs of alkanethiolates not only for the advantages described earlier but also because they can be easily and reliably prepared.

Our first experimental focus was to search for a thiolate monolayer that minimizes adhesion of both antibody and antigen (e.g., *E. coli* O157:H7) and for this different functional group terminated thiolate monolayers were studied. The selected monolayer was used to create boundary regions in our patterning approach. *N*-hydroxysuccinimidyl-terminated SAM, i.e., dithio-bis(succinimidyl propionate) (DSP) derived SAM was chosen as the coupling adlayer which can covalently link to proteins via amide bonding. The next steps were to: 1) identify an appropriate blocking solution since cell (e.g., *E. coli* O157:H7) adhesion to a DSP-derived SAM was likely to also occur by the same coupling chemistry; and 2) determine the effect of pH, incubation time, and temperature on the capture step (i.e., binding of *E. coli* O157:H7 to the polyclonal anti-*E. coli* O157:H7). Utilizing the findings of these studies, we achieved selective patterning of *E. coli* O157:H7 onto 7.5-μm addresses. A detailed discussion of these results is presented in the following sections, noting that these miniaturized platforms have tens to thousands of antibody-modified addresses on a single chip which have intriguing attributes with respect to high throughput, reduction of sample volume, and level of detection.

Patterning approach

Figure 1 represents our general approach to the construction of a miniaturized immunosensing platform comprised of domains of specific antibodies covalently coupled to a photolithographically patterned monolayer. SAM I is formed first. The sample is then exposed to UV light through a mask of the desired pattern. The UV irradiation degrades the SAM I within the exposed regions and can be easily removed by washing with a suitable organic solvent. SAM II (based on DSP) is then formed only in the exposed gold regions.

Next, the chip is exposed to the sample containing the target antigen. SAM I therefore functions as a boundary of the address. SAM II, coupled to the antibody, serves as the address that captures the target antigen.

Experimental Section

Materials and reagents. Heat killed *Escherichia coli* O157:H7, *Citrobacter freundii*, *Salmonella choleraesuis*, *Vibro cholerae*, and *Yersinia enterocolitica* were kindly provided by Dr. Nancy Cornick of the Department of Veterinary Microbiology and Preventive Medicine of the Iowa State University. Affinity-purified goat anti-*E. coli* O157:H7 was purchased from USBiological. The DNA stain SYTO 64™ and Alexa fluor 488 goat anti-mouse were obtained from Molecular Probes. Dithio-bis(succinimidyl propionate) (DSP), 16-mercaptohexadecanoic acid (MH, -COOH), 11-mercapto 1-undecanol (MU, -OH), 4-flurobenzenethiol (FBT, -ArF), 1-octadecanethiol (ODT, $-CH_3$), and 2-(2-amino ethoxy) ethanol were acquired from Aldrich. 11-amino-1-undecanethiol, hydrochoride (AUT, $-NH_2$) was purchased from Dojindo, and 1H, 1H, 2H, 2H-perfluorodecyl-1-thiol (PFDT, $-CF_3$) was from SynQuest. 2-(N-morpholino) ethane sulphonic acid (MES), Tris-EDTA buffer, bovine serum albumin (BSA), Tween 20, Tween 80, casein-based blocking buffer, goat serum, and a lipid mixture (mixture of cholesterol, cod liver oil fatty acids, polyoxyethylenesorbitan monooleate, and D-α-tocopherol acetate) were obtained from Sigma. Triton X-100 and sodium azide were purchased from Fisher. Borate buffer was acquired from Pierce. All reagents were used as received.

Instrumentation

Infrared Spectroscopy. Infrared reflection spectra were acquired with a Nicolet 850 FT-IR spectrometer, purged with liquid N_2 boil-off, and equipped with a liquid N_2-cooled HgCdTe detector. Spectra were obtained using *p*-polarized light incident at 82° with respect to the surface normal. The spectra were recorded as $-\log(R/R_0)$, where R is the sample reflectance and R_0 is the reflectance of an octadecanethiolate-d_{37} monolayer-coated Au reference. The spectra are an average of 512 sample and reference scans, taken at 4-cm^{-1} resolution with Happ-Genzel apodization.

Epifluorescence Microscopy. A Nikon Eclipse TE200 inverted microscope, equipped with a Prairie Technologies epifluorescent system that consisted of a uniblitz shutter, a mercury light source with a Prairie Technologies filter wheel, and a Hamamatsu C4742-95 CCD camera (6.7 x 6.7 μm pixels in a 1280 x 1024 pixel format) was used for imaging samples. This system also has a Prairie Technologies NeD microscope attachment for simultaneous imaging at multiple wavelengths. Appropriate filter cubes (96157M (G-2E/C) (TRITC cube) for SYTO 64™ and 96107M (B-2E/C) (FITC cube) for Alexa fluor 488 dye from Nikon Microscopy to match the dye fluorescence wavelength were used. A Metaview system (MetaMorph) from Universal Imaging Corporation was used for image analysis.

Method development

Preparation of glycol terminated thiol.[49] Equal volumes of ethanolic solutions of 0.1 mM DSP and 0.1 M 2-(2-amino ethoxy) ethanol (2-AE) were mixed and allowed to react for 1 h. Gold-coated glass slides (2.5 x 7.5 cm) were then immersed in the solution for 14-18 h. Upon immersion, the slides were rinsed with ethanol (Aaper, USP grade) and dried with a stream of high purity nitrogen (Air products).

Fabrication of gold substrates. Precleaned glass slides (1 x 1 cm) were primed with 15 nm of chromium at a deposition rate of 0.1 nm/s to enhance adherence of gold. This step was followed by the deposition of ~300 nm of 99.99 % gold at 0.1-0.2 nm/s. These samples were then immersed into freshly prepared ethanolic thiol solutions (DSP: 0.1 mM, COOH: 0.2 mM, OH: 2 mM, NH_2: 0.1 mM, -ArF: 2 mM, $-CH_3$: 2 mM, and $-CF_3$: 10 mM) for ~12 h for SAM formation, rinsed with ethanol, and dried under a stream of high purity nitrogen.

Adhesion of *E. coli* O157:H7 to SAMs of different functional groups. The adhered *E. coli* O157:H7 was examined by immersing the various thiol samples into SYTO 64™ stained *E. coli* O157:H7 (5×10^7 cells/mL) in PBS for ~12 h at room temperature. The samples were then extensively rinsed with 10 mM PBS and imaged by epifluorescence microscopy.

Effectiveness of blocking solutions. (i) Identification of optimal blocking solution. A series of common blocking solutions was tested to identify which blocker was the most effective in minimizing *E. coli* O157:H7 adhesion to DSP-derived monolayer because of the expected interaction between any unreacted succinimidyl groups of the monolayer and the protein on the bacteria. For this, DSP-derived SAMs were immersed into different blocking solutions for ~12 h. The solutions were: 1) regular blocking solution (10 mM phosphate buffer saline (PBS) with 5% BSA, 5% goat serum, 0.25% Triton X-100, and 0.02% sodium azide; 2) regular blocking solution with 1% nonfat dry milk (Carnation); 3) 10 mM PBS with 1% nonfat dry milk and 0.1% Tween 20; 4) 50 mM borate buffer with 2% non fat dry milk; 5) casein-based blocking buffer; and 6) regular blocking solution with the noted lipid mixture. The samples were rinsed with PBS and immersed into SYTO™ 64 stained *E. coli* O157:H7 in PBS for ~12 h, then rinsed and imaged by epifluorescence microscopy.

(ii) Effectiveness of optimal blocking solution on antibody-coated surface. The most effective blocker (i.e., the casein-based blocker) determined from the previous experiment, was then tested with respect to minimization of *E. coli* O157:H7 adhesion to a non target antibody that was coupled to the DSP-derived SAM. These tests involved coupling of goat anti-mouse antibodies to the DSP-primed substrate by pipeting 25 μL of a 100 μg/mL goat anti-mouse antibodies in PBS solution onto the sample surface; the coupling reaction was allowed to proceed for ~12 h in a humidity chamber. The antibody-coated samples were then rinsed (3x) with 25 mM borate buffer solution that contained 1% (v/v) Tween 80.

Some of these samples were immersed into the casein-based blocker and some into SYTO™ 64 stained *E. coli* O157:H7 (5×10^7 cells/mL), with the casein-blocked samples then exposed for ~12 h to a solution of the SYTO 64™ stained *E. coli* O157:H7. Finally, all samples were rinsed with PBS and imaged by epifluorescence microscopy.

(iii) Effectiveness of optimal blocking solution for other pathogenic bacteria. The performance of casein-based blocker was also studied with respect to minimization of other bacterial adhesion to the DSP-derived SAM. These experiments paralleled those described earlier, but involved the use of *Citrobacter freundii*, *Salmonella choleraesuis*, *Vibro cholerae*, and *Yersinia enterocolitica*, all of which were stained with SYTO 64™.

Effect of pH on binding of *E. coli* O157:H7 to polyclonal anti-*E. coli* O157:H7. Casein-modified capture substrates were rinsed and immersed for ~12 h into SYTO 64™ stained *E. coli* O157:H7 (9×10^6 cells/mL) with different pH buffers (MES [2-(N-morpholino) ethane sulphonic acid] for pH 5.2 and 6.2, PBS (phosphate buffered saline) for pH 7.2, and Tris-EDTA buffer for pH 8.2 and 9.2) at room temperature. The concentration of all buffer

solutions was 10 mM and contained 150 mM NaCl. After immersion, the samples were rinsed with the same buffer and imaged.

Temperature and time dependent binding of *E. coli* O157:H7 to anti-*E. coli* O157:H7. The effects of temperature (25 and 37°C) on binding were examined by immersing casein-modified capture substrates into SYTO 64™ stained *E. coli* O157:H7 in PBS. At 0.25, 0.5, 1, 2, 4, 8, 12, 24, and 30-h, the samples were removed from the incubation chamber, rinsed, and viewed.

Construction of 3.0 and 7.5 μm-sized addresses. ***Compositionally patterned array from PFDT and DSP.*** Gold-coated glasses were immersed into freshly prepared 10 mM ethanolic solution of PFDT for 12 h. The rinsed and dried substrates were next placed on a chromium photolithography mask (3-μm holes and 10-μm spacings, MicroMask/Microtronics) to form 3-μm sized addresses. On the other hand, to form 7.5 μm size addresses, the substrates were masked with a 2000 mesh nickel transmission electron microscopy grid (TEM) (7.5-μm holes and 5-μm bars, Electron Microscopy Sciences). The samples were exposed for 20 min to UV light from a 200-W, medium-pressure mercury lamp (power: 550 mW/cm^2) (Oriel) that was collimated and reflected off of an air-cooled, dichroic mirror (200-260 nm) and focused by a fused-silica lens. The UV irradiation degrades the PFDT monolayer within the exposed regions through a photo-oxidation mechanism that is only partially understood.[55] The process converts the exposed gold-bound PFDT to various forms of oxygenated sulfur (e.g., RSO_3^-) that can be removed by washing with common organic solvents, e.g., ethanol. The samples were then rinsed, dried, and immediately immersed into 0.1 mM ethanolic solution of DSP for ~12 h.

Covalent immobilization of antibody. Alexa fluor 488 goat anti-mouse was coupled to the substrates with the 3-μm sized patterns and anti-*E. coli* O157:H7 to those with the 7.5-μm addresses. The samples were placed in a humidity chamber for ~12 h. After rinsing with borate buffer, the samples containing Alexa fluor 488 antibody were imaged to assess the effectiveness of the photopatterning process. The samples containing anti-*E. coli* O157:H7 were immersed into casein-based blocker for ~12 h to block any unreacted terminal groups for the DSP-based adlayer.

Capturing E. coli O157:H7 at 7.5 μm addresses. The casein blocked anti-*E. coli* O157:H7 substrates were rinsed with PBS and immersed into SYTO 64™ stained *E. coli* O157:H7 in PBS for ~12 h to capture *E. coli* O157:H7. The samples were then rinsed and viewed.

Results and Discussion

In nearly all experiments, the total number of *E. coli* O157:H7 (5 x 10^7 cells/mL) was in excess of that (3 x 10^7 cells/mL) which could potentially bind to the surface (1 x 1 cm) in a closest packed architecture. However, the pH experiments used solutions in which the number of *E. coli* O157:H7 was approximately one-third of the theoretical maximum so that the effect of pH on the coupling of antibody and bacteria was not overwhelmed by a high bacteria concentration which could possibly compromise the findings because of aggregation. The adhered *E. coli* O157:H7 in the digital images was quantified by measuring the total fluorescent area using Metamorph Image Analysis software. *E. coli* O157:H7 adhesion was expressed as percentage of surface coverage, and calculated as (fluorescent pixel area/total pixel area) x 100. As an alternative approach, the approximate number of

E. coli O157:H7 in each image was also calculated based on the typical area for each *E. coli* O157:H7, ~27 pixels. In each case, 10 or more digital images were analyzed.

Formation of glycol monolayer. Immersion (14-18 h) of gold-coated glass slides resulted in chemisorption of a glycol-terminated monolayer derived from the disulfide formed by the solution reaction between DSP and 2-AE. The three bands around 1800 cm^{-1} in the IRS spectrum of the layer formed from only DSP (Figure 2A) are assigned to the carbonyl stretches of the ester (1812 cm^{-1}) and of the succinimidyl end group (1786 (in-phase) and 1748 cm^{-1} (out-of-phase)).[56] The presence of these bands, along with the succinimidyl C-O stretches at 1219 and 1074 cm^{-1} and the methylene stretches between 3000 and 2800 cm^{-1}, verifies the formation of the DSP-based coating. IRS was also used to confirm presence of a chemisorbed glycol-terminated amide species on the gold surface (Figure 2B). Key features include: 3371 cm^{-1}: NH stretch of 2° amine; 1651 cm^{-1}: C=O stretch of 2° amide (amide I band); and 1554 cm^{-1}: NH deformation of 2° amide (amide II band). The differences in two spectra confirm the presence of a chemisorbed glycol-terminated amide adlayer, with no detectable amounts of an unreacted succinimidyl terminal group.

***E. coli* O157:H7 adhesion to SAMs of different functional groups.** The adhesion of bacteria to surfaces and host cells can occur by a number of mechanisms, both biospecific (carbohydrate-protein, protein-protein) and nonspecific (hydrophobic or electrostatic) interactions.[57] The nonspecific adhesion of bacteria often interferes with and complicates the study of biospecific binding. Surfaces that can resist the nonspecific adhesion of bacteria are, therefore, highly desirable,[58-60] although there are no known materials completely resistant to bacterial adhesion.[61] Figure 3 showed the fluorescence images of *E. coli* O157:H7 adhered

to SAMs with different terminal groups and surface coverage values are summarized in Figure 4.

The largest number of *E. coli* O157:H7 (surface coverage ~26%) was observed on the DSP-derived SAM, which is expected because of the covalent coupling between the succinimidyl terminus of the monolayer and the amines groups of the proteins on the surface of the bacteria. Though bacterial adhesion represents a range of interwoven interaction, the SAMs can be arranged with respect to decreasing surface coverage of *E. coli* O157:H7 as follows: DSP-derived >-COOH >-NH_2 >-Ar-F >Glycol >-OH >-CH_3 >-CF_3. A similar trend was observed by Ista et al. for the adsorption of *Staphylococcus epidermidis* to -COOH, -CH3, and -CF3 terminated monolayers.[58] The hydrophobic CF_3-terminated PFDT monolayer shows the lowest level of *E. coli* O157:H7 adhesion (surface coverage ~0.11%). Based on the propensity to minimize the adhesion of both capture antibody (data not shown) and target bacteria (*E. coli* O157:H7), the PFDT-based monolayer was chosen to serve as the adlayer present as domain boundary between specific antibody addresses.

Effectiveness of blocking solutions. (i) Identification of optimal blocking solution. Different recipes of blocking solutions were tested in order to identify the one that is most effective in minimizing *E. coli* O157:H7 adhesion to the monolayer derived from DSP. Figure 5 presents the fluorescence images of *E. coli* O157:H7 after exposure to a DSP-derived SAM before and after treatment with different blocking solutions; surface coverage values are summarized in Figure 6. A significant number (surface coverage ~26%) of *E. coli* O157:H7 adhered to the SAM prior to blocking. Importantly, all blocking solutions showed a 99% (or better) improvement in resisting the adhesion of *E. coli* O157:H7 (regular blocker ~99.66%, regular blocker with dry milk ~99.76%, PBS with dry milk ~99.75%,

borate buffer with dry milk ~99.37%, casein blocker ~99.94%, and regular blocker with lipid mixture ~99.68%). Casein-based blocking solution performed slightly better in minimizing *E. coli* O157:H7 adhesion than other blockers, and was used in all subsequent studies.

(ii) (a) Effectiveness of optimal blocking solution on antibody-coated surface. The last subsection examined the performance of casein-based blocker to minimize *E. coli* O157:H7 adhesion to the DSP-derived SAM prior to immobilization of the capture antibody. This subsection describes such an experiment that couples an antibody nonspecific to *E. coli* O157:H7 to the DSP-derived adlayer in order to test if the coupled antibody coating has voids large enough for the microorganism to still couple to the terminus of the monolayer. These studies used goat anti-mouse IgG as the nonspecific antibody.

Figure 7 shows the fluorescence images of *E. coli* O157:H7 in case of adhesion to a DSP-based adlayer, the antibody modified surface, and an antibody coupled but casein blocked sample. Surface coverage values in each case are presented in Figure 8. The antibody covered surface showed ~95% improvement in minimizing *E. coli* O157:H7 adhesion. The data also showed that casein-based blocking enhanced the resistance to adhesion to ~99.9%. This result indicates that a blocking solution is needed to minimize the nonspecific adhesion of *E. coli* O157:H7 even when the DSP-derived monolayer is reacted with an antibody.

(ii) (b) Effectiveness of optimal blocking solution for other pathogenic bacteria. The performance of the casein-based blocker was also studied to minimize the adhesion of other bacteria (i.e., *Citrobacter freundii*, *Salmonella choleraesuis*, *Vibro cholerae*, and *Yersinia enterocolitica*) at a DSP-based monolayer. Figure 9 shows fluorescence images from these experiments, and Figure 10 presents the observed surface coverage values. These data

indicate that adhesion is problematic on the unblocked surfaces (surface coverage ~14% for *Citrobacter freundii*, ~9% for *Salmonella choleraesuis*, ~43% for *Vibro cholerae*, and ~7% for *Yersinia enterocolitica*). But when casein-based blocker was applied, a more than 99% improvement in preventing bacterial adhesion is found (improvement ~99.5% for *Citrobacter freundii*, 99.5% for *Salmonella choleraesuis*, 99.8% for *Vibro cholerae*, and 99.7% for *Yersinia enterocolitica*). Therefore, casein-based blocker also effectively minimizes the nonspecific adhesion of other bacteria to the DSP-derived SAM.

Effect of pH on binding of *E. coli* O157:H7 to polyclonal anti- *E. coli* O157:H7. Fluorescence images of *E. coli* O157:H7 bound to anti-*E. coli* O157:H7 at different pHs are shown in Figure 11 and surface coverage values are presented in Figure 12. These results indicate that binding was not greatly affected by the pH of the solution. As shown in Figure 12, surface coverages between 10-12% were found. Slightly higher coverages (~12.6%) were observed between pH 6.2 and 7.2, which is close to physiological conditions.

Temperature and time dependent binding of *E. coli* O157:H7 to anti-*E. coli* O157:H7. The binding of *E. coli* O157:H7 to anti-*E. coli* O157:H7 at room temperature (~25°C) and 37°C as a function of incubation time was also studied. The fluorescence images of bound *E. coli* O157:H7 are shown in Figure 13 and surface coverage values are presented in Figure 14. At room temperature, the surface coverage of *E. coli* O157:H7 increases until 24 h and appears to remain constant (~19%) with longer binding times. However, the surface coverage at 37°C increases until 24 h (~11%) and drops off (~8%) at 30 h. Interestingly, the coverage in both experiments increases comparably up to ~8 h, but then begins to differ.

The drop in surface coverage at 37°C might be due to several factors, e.g., instability of coupled antibody could be a reason. Stability of antibody coupled to DSP-derived SAM

was studied after 24 h both at room temperature and 37°C by IR spectroscopy (data not shown). Coupled antibody was found quite stable at both temperatures and the data also indicated stability of the DSP-derived SAM to which antibody is bound. Larger growth of other microorganisms as contaminants as well as sample degradation at 37°C compared to that of at room temperature could be another issue. Detail investigation is needed to fully understand the phenomenon. However, from the results we conclude that the maximum *E. coli* O157:H7 binding to antibody can be achieved by incubating the samples at room temperature rather than 37°C for ~24 h.

Performance of photopatterning approach. After completing the above studies, the performance of photopatterning approach to forming capture substrates was tested by patterning fluorescent antibody into 3-μm addresses that are separated by 10 μm. Figure 15 indicates that fluorescent antibody was clearly coupled to DSP-derived surface in the addresses. No detectable adhesion of the antibody to PFDT reference monolayer was observed. Therefore, it can be concluded that PFDT is performing effectively as a "nonstick" filter in the gridded regions between addresses.

Capturing *E. coli* O157:H7 into specific addresses. Drawing on these data, investigations were initiated on the selective patterning of *E. coli* O157:H7 at the substrates with 7.5 x 7.5 μm addresses. Each address was modified with anti-*E. coli* O157:H7. When the chip was exposed to sample, the *E. coli* O157:H7 was selectively bound to the addresses not in the boundary region. Figure 16 clearly shows that the bacteria confined to antibody regions produced well defined optical patterns that can be easily detected. Aggregated bacteria were observed in some of the addresses probably due to presence of high concentration of *E. coli* O157:H7 in the sample solution. Since the addresses are bigger than

E. coli O157:H7, more that one bacterium was observed in most addresses. However, when the size of the address will be of similar size as bacteria, selective capturing of single bacteria is expected. Our laboratory is currently working on making smaller addresses, testing cross reactivity, and finding limit of detection of such immunosensing platform.

Conclusion and Future Directions

We have described a simple technique for fabrication of antibody addresses (microarrays) capable of capturing selective bacteria in predetermined locations, separated by a defined spacing. The miniaturized immunosensing platform was comprised of micrometer-sized domains (i.e., addresses) of anti-*E. coli* O157:H7 formed by covalent coupling to DSP-derived SAM. Each address was separated by micrometer-sized spacing composed of a monolayer from a fluorine-terminated thiolate, which owes to its propensity to minimize the nonspecific adsorption of both the capture antibody and target bacteria (i.e., *E. coli* O157:H7). The future goal is to use this platform to capture bacteria at low levels of concentration. Since one platform has ~62000 addresses localized in a 3 x 3 mm area, all addresses can be exposed to sample solution concurrently. We believe this miniaturized platform comprised of arrays of thousands of addresses for the target analyte on a small a chip will provide some useful and desirable features such as high throughput, reduction of sample volume as well as low level of detection. The ultimate objective of this project is to capture one bacterium on one address by making the addresses same size as the target bacteria. Then, various detection techniques (e.g., fluorescence, Raman spectroscopy, and giant magnetoresistance etc.) can be employed to "digitally" enumerate the captured bacteria.

Acknowledgments

The authors express appreciation to Dr. Nancy Cornick of VMPM department of Iowa State University for providing *E. coli* O157:H7. Funding for this work was provided by the United State Department of Agriculture Cooperative State Research, Education, and Extention Service (UDSA CSREES award number 20002-35201-12659) and by the Institute of Combinatorial Discovery of Iowa State University through the Roy J. Carver Laboratory for Ultra High Resolution Biological Microscopy. The Ames Laboratory is operated for the U.S. Department of Energy by Iowa State University under Contract W-7405-Eng-82.

References

(1) Hobson, N. S.; Tothill, I.; Turner, A. P. F. *Biosens. Bioelectron.* **1996**, *11*, 455-477.

(2) Ho, J. A. A.; Hsu, H. W.; Huang, M. R. *Anal. Biochem.* **2004**, *330*, 342-349.

(3) Abdel-Hamid, I.; Ivnitski, D.; Atanasov, P.; Wilkins, E. *Biosens. Bioelectron.* **1999**, *14*, 309-316.

(4) Belgrader, P.; Benett, W.; Hadley, D.; Richards, J.; Stratton, P.; Mariella, R.; Milanovich, F. *Science* **1999**, *284*, 449-450.

(5) Gehring, A. G.; Patterson, D. L.; Tu, S. I. *Anal. Biochem.* **1998**, *258*, 293-298.

(6) Su, X. L.; Li, Y. B. *Anal. Chem.* **2004**, *76*, 4806-4810.

(7) Tortorello, M. L.; Stewart, D. S. *Appl. Environ. Microbiol.* **1994**, *60*, 3553-3559.

(8) Weimer, B. C.; Walsh, M. K.; Beer, C.; Koka, R.; Wang, X. *Appl. Environ. Microbiol.* **2001**, *67*, 1300-1307.

(9) Yu, H.; Bruno, J. G. *Appl. Environ. Microbiol.* **1996**, *62*, 587-592.

(10) Bukhari, Z.; Weihe, J.; LeChevallier, M. *Water Sci. Technol.* **2004**, *50*, 233-237.

(11) Gooding, C. M.; Choudary, P. V. *J. Dairy Res.* **1997**, *64*, 87-93.

(12) Goodridge, L.; Chen, J. R.; Griffiths, M. *Appl. Environ. Microbiol.* **1999**, *65*, 1397-1404.

(13) Tims, T. B.; Lim, D. V. *J. Microbiol. Methods* **2003**, *55*, 141-147.

(14) Tu, S. I.; Patterson, D.; Briggs, C.; Irwin, P.; Yu, L. *J. Ind. Microbiol. Biotechnol.* **2001**, *26*, 345-349.

(15) Yu, L. S. L.; Reed, S. A.; Golden, M. H. *J. Microbiol. Methods* **2002**, *49*, 63-68.

(16) Rowan, B.; Wheeler, M. A.; Crooks, R. M. *Langmuir* **2002**, *18*, 9914-9917.

(17) Tan, J. L.; Tien, J.; Chen, C. S. *Langmuir* **2002**, *18*, 519-523.

(18) Mrksich, M.; Whitesides, G. M. *Trends Biotechnol.* **1995**, *13*, 228-235.

(19) Kane, R. S.; Takayama, S.; Ostuni, E.; Ingber, D. E.; Whitesides, G. M. *Biomaterials* **1999**, *20*, 2363-2376.

(20) Craighead, H. G.; James, C. D.; Turner, A. M. P. *Curr. Opin. Solid State Mater. Sci.* **2001**, *5*, 177-184.

(21) Mrksich, M. *Chem. Soc. Rev.* **2000**, *29*, 267-273.

(22) St John, P. M.; Davis, R.; Cady, N.; Czajka, J.; Batt, C. A.; Craighead, H. G. *Anal. Chem.* **1998**, *70*, 1108-1111.

(23) Ostuni, E.; Kane, R.; Chen, C. S.; Ingber, D. E.; Whitesides, G. M. *Langmuir* **2000**, *16*, 7811-7819.

(24) Chiu, D. T.; Jeon, N. L.; Huang, S.; Kane, R. S.; Wargo, C. J.; Choi, I. S.; Ingber, D. E.; Whitesides, G. M. *PNAS* **2000**, *97*, 2408-2413.

(25) Papra, A.; Bernard, A.; Juncker, D.; Larsen, N. B.; Michel, B.; Delamarche, E. *Langmuir* **2001**, *17*, 4090-4095.

(26) Takayama, S.; McDonald, J. C.; Ostuni, E.; Liang, M. N.; Kenis, P. J. A.; Ismagilov, R. F.; Whitesides, G. M. *PNAS* **1999**, *96*, 5545-5548.

(27) Howell, S. W.; Inerowicz, H. D.; Regnier, F. E.; Reifenberger, R. *Langmuir* **2003**, *19*, 436-439.

(28) Ito, Y. *Biomaterials* **1999**, *20*, 2333-2342.

(29) Chen, C. S.; Mrksich, M.; Huang, S.; Whitesides, G. M.; Ingber, D. E. *Science* **1997**, *276*, 1425-1428.

(30) Shay, J. W.; Porter, K. R.; Krueger, T. C. *Exp. Cell Res.* **1977**, *105*, 1-8.

(31) Kleinfeld, D.; Kahler, K. H.; Hockberger, P. E. *J. Neurosci.* **1988**, *8*, 4098-4120.

(32) Britland, S.; Clark, P.; Connolly, P.; Moores, G. *Exp. Cell Res.* **1992**, *198*, 124-129.

(33) Stenger, D. A.; Georger, J. H.; Dulcey, C. S.; Hickman, J. J.; Rudolph, A. S.; Nielsen, T. B.; Mccort, S. M.; Calvert, J. M. *J. Am. Chem. Soc.* **1992**, *114*, 8435-8442.

(34) Mooney, J. F.; Hunt, A. J.; McIntosh, J. R.; Liberko, C. A.; Walba, D. M.; Rogers, C. T. *PNAS* **1996**, *93*, 12287-12291.

(35) Vargo, T. G.; Thompson, P. M.; Gerenser, L. J.; Valentini, R. F.; Aebischer, P.; Hook, D. J.; Gardella, J. A. *Langmuir* **1992**, *8*, 130-134.

(36) Lopez, G. P.; Albers, M. W.; Schreiber, S. L.; Carroll, R.; Peralta, E.; Whitesides, G. M. *J. Am. Chem. Soc.* **1993**, *115*, 5877-5878.

(37) Bain, C. D.; Whitesides, G. M. *Angewandte Chemie-International Edition in English* **1989**, *28*, 506-512.

(38) Ulman, A. *Chem. Rev.* **1996**, *96*, 1533-1554.

(39) Ostuni, E.; Yan, L.; Whitesides, G. M. *Colloids Surf., B* **1999**, *15*, 3-30.

(40) Prime, K. L.; Whitesides, G. M. *Science* **1991**, *252*, 1164-1167.

(41) Zaugg, F. G.; Spencer, N. D.; Wagner, P.; Kernen, P.; Vinckier, A.; Groscurth, P.; Semenza, G. *J. Mater. Sci.-Mater. Med.* **1999**, *10*, 255-263.

(42) Singhvi, R.; Kumar, A.; Lopez, G. P.; Stephanopoulos, G. N.; Wang, D. I. C.; Whitesides, G. M.; Ingber, D. E. *Science* **1994**, *264*, 696-698.

(43) Mrksich, M.; Dike, L. E.; Tien, J.; Ingber, D. E.; Whitesides, G. M. *Exp. Cell Res.* **1997**, *235*, 305-313.

(44) Koepsel, R. R.; Russell, A. J. *Biomacromolecules* **2003**, *4*, 850-855.

(45) Rowe, C. A.; Tender, L. M.; Feldstein, M. J.; Golden, J. P.; Scruggs, S. B.; MacCraith, B. D.; Cras, J. J.; Ligler, F. S. *Anal. Chem.* **1999**, *71*, 3846-3852.

(46) Morhard, F.; Pipper, J.; Dahint, R.; Grunze, M. *Sens. Actuators, B* **2000**, *70*, 232-242.

(47) Sapsford, K. E.; Rasooly, A.; Taitt, C. R.; Ligler, F. S. *Anal. Chem.* **2004**, *76*, 433-440.

(48) Jones, V. W.; Kenseth, J. R.; Porter, M. D.; Mosher, C. L.; Henderson, E. *Anal. Chem.* **1998**, *70*, 1233-1241.

(49) Duhachek, S. D.; Kenseth, J. R.; Casale, G. P.; Small, G. J.; Porter, M. D.; Jankowiak, R. *Anal. Chem.* **2000**, *72*, 3709-3716.

(50) O'Brien, J. C.; Stickney, J. T.; Porter, M. D. *Langmuir* **2000**, *16*, 9559-9567.

(51) O'Brien, J. C.; Jones, V. W.; Porter, M. D.; Mosher, C. L.; Henderson, E. *Anal. Chem.* **2000**, *72*, 703-710.

(52) O'Brien, J. C.; Stickney, J. T.; Porter, M. D. *J. Am. Chem. Soc.* **2000**, *122*, 5004-5005.

(53) Kenseth, J. R.; Harnisch, J. A.; Jones, V. W.; Porter, M. D. *Langmuir* **2001**, *17*, 4105-4112.

(54) Takano, H.; Sul, J. Y.; Mazzanti, M. L.; Doyle, R. T.; Haydon, P. G.; Porter, M. D. *Anal. Chem.* **2002**, *74*, 4640-4646.

(55) Love, J. C.; Estroff, L. A.; Kriebel, J. K.; Nuzzo, R. G.; Whitesides, G. M. *Chem. Rev.* **2005**, *105*, 1103-1169.

(56) Frey, B. L.; Corn, R. M. *Anal. Chem.* **1996**, *68*, 3187-3193.

(57) Habash, M.; Reid, G. *J. Clin. Pharmacol.* **1999**, *39*, 887-898.

(58) Ista, L. K.; Fan, H. Y.; Baca, O.; Lopez, G. P. *FEMS Microbiol. Lett.* **1996**, *142*, 59-63.

(59) Chapman, R. G.; Ostuni, E.; Liang, M. N.; Meluleni, G.; Kim, E.; Yan, L.; Pier, G.; Warren, H. S.; Whitesides, G. M. *Langmuir* **2001**, *17*, 1225-1233.

(60) Qian, X. P.; Metallo, S. J.; Choi, I. S.; Wu, H. K.; Liang, M. N.; Whitesides, G. M. *Anal. Chem.* **2002**, *74*, 1805-1810.

(61) Ostuni, E.; Chapman, R. G.; Liang, M. N.; Meluleni, G.; Pier, G.; Ingber, D. E.; Whitesides, G. M. *Langmuir* **2001**, *17*, 6336-6343.

Figure Captions

Figure 1. General approach to construct miniaturized immunosensing platform.

Figure 2. Infrared spectra of DSP-derived self-assembled monolayer (SAM) (A) and glycol terminated disulfide formed (B) from the solution reaction between DSP and 2-AE.

Figure 3. Fluorescence images of SYTO 64™ stained *E. coli* O157:H7 adhered to SAMs of different functional groups.

Figure 4. Percentage of surface coverage (fluorescent pixel area/total pixel area x 100) of *E. coli* O157:H7 on thiolate monolayers of different functional groups. Approximate number of *E. coli* O157:H7 is shown in red color.

Figure 5. Fluorescence images of SYTO 64™ stained *E. coli* O157:H7 adhered to DSP-derived SAM before and after blocked with different composition of blocking solutions.

Figure 6. Percentage of surface coverage of *E. coli* O157:H7 adhered to DSP-derived SAM before and after blocked with different composition of blocking solutions: 1) no blocking solution; 2) regular blocking solution; 3) regular blocking solution with 1% nonfat dry milk; 4) 10 mM PBS with 1% nonfat dry milk and 0.1% Tween 20; 5) 50 mM borate buffer with 2% non fat dry milk; 6) casein-based blocking buffer, and 7) regular blocking solution with lipid mixture. Approximate number of *E. coli* O157:H7 is shown in red color.

Figure 7. Fluorescence images of SYTO 64™ stained *E. coli* O157:H7 adhered to unreacted DSP-derived SAM (1), DSP-derived SAM reacted with non target (goat anti-mouse) antibody (2), and DSP-derived SAM reacted with non target antibody and also blocked with casein-based blocking solution (3).

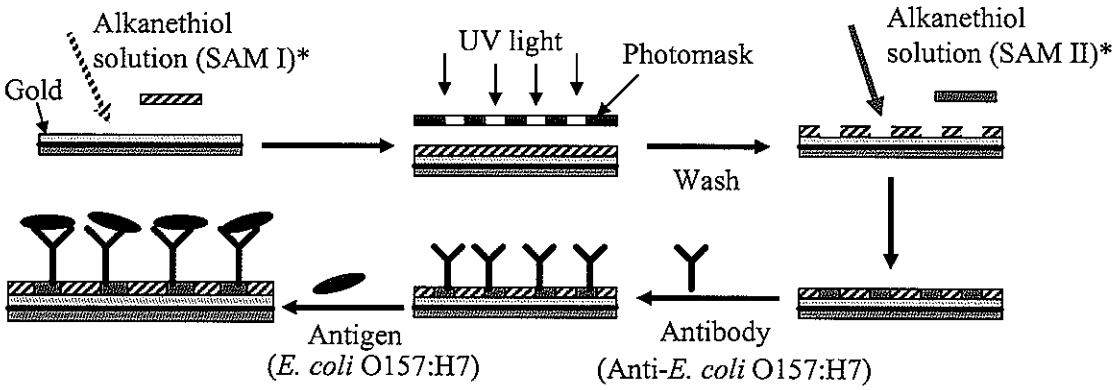

* Self-assembled monolayer (SAM)

Figure 1

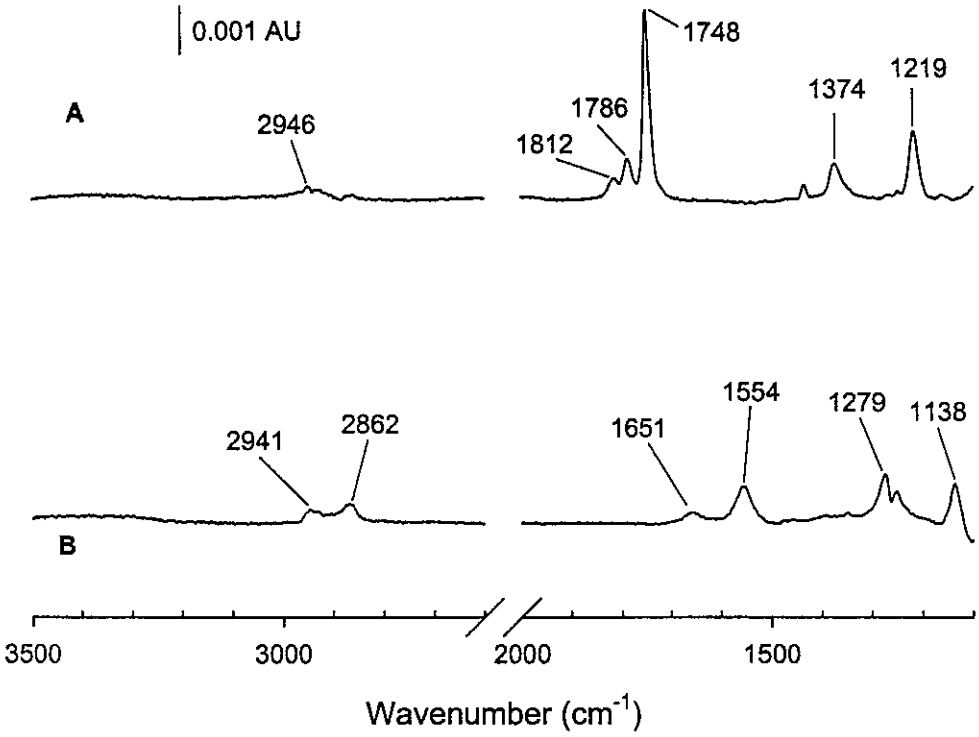
0.001 AU
A
2946
1812
1786
1748
1374
1219
2941
2862
1651
1554
1279
1138
B
3500
3000
2000
1500
Wavenumber (cm-1)

Figure 2

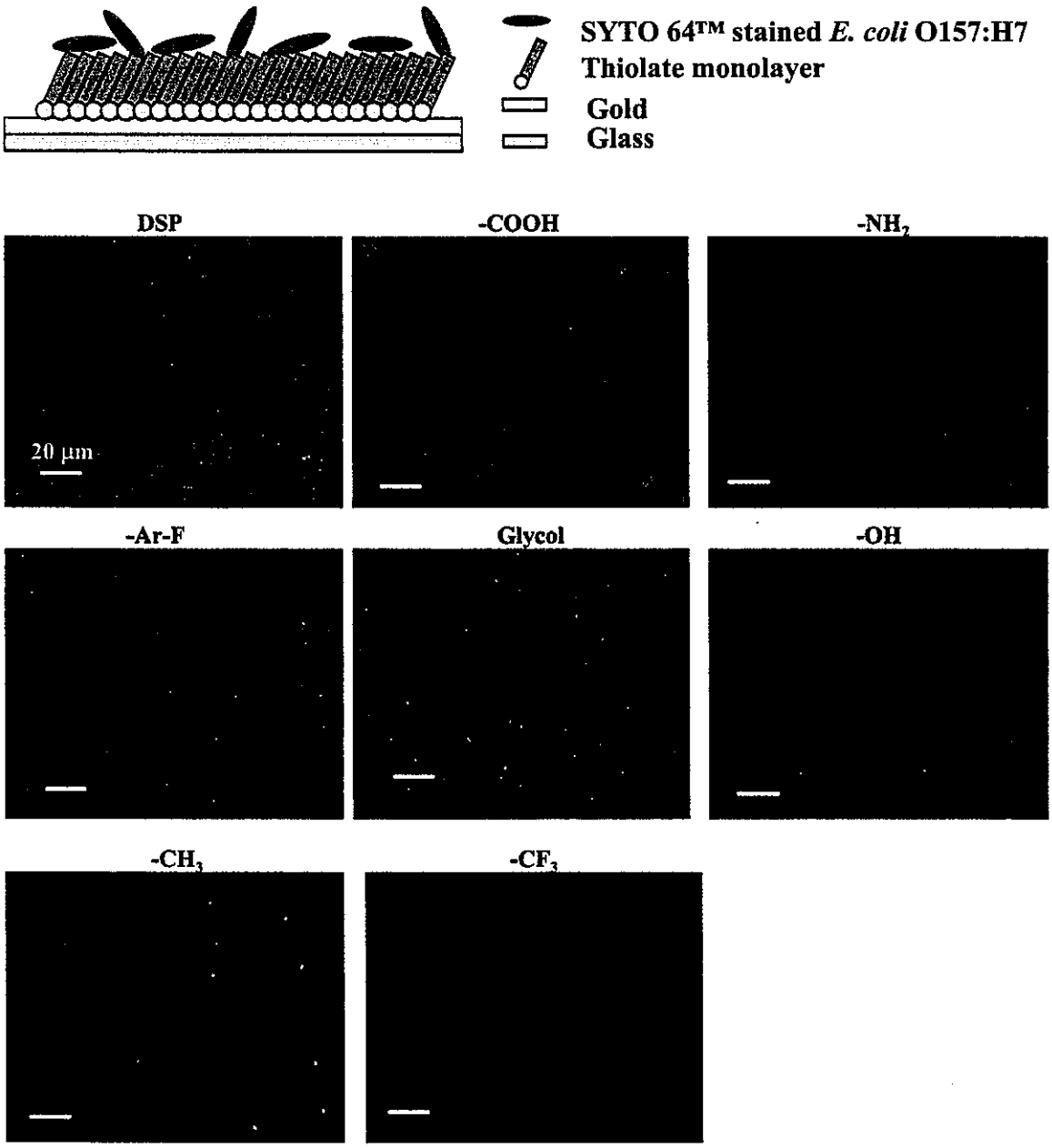
SYTO 64™ stained E. coli O157:H7
Thiolate monolayer
Gold
Glass
DSP
-COOH
-NH2
20 μm
-Ar-F
Glycol
-OH
-CH3
-CF3

Figure 3

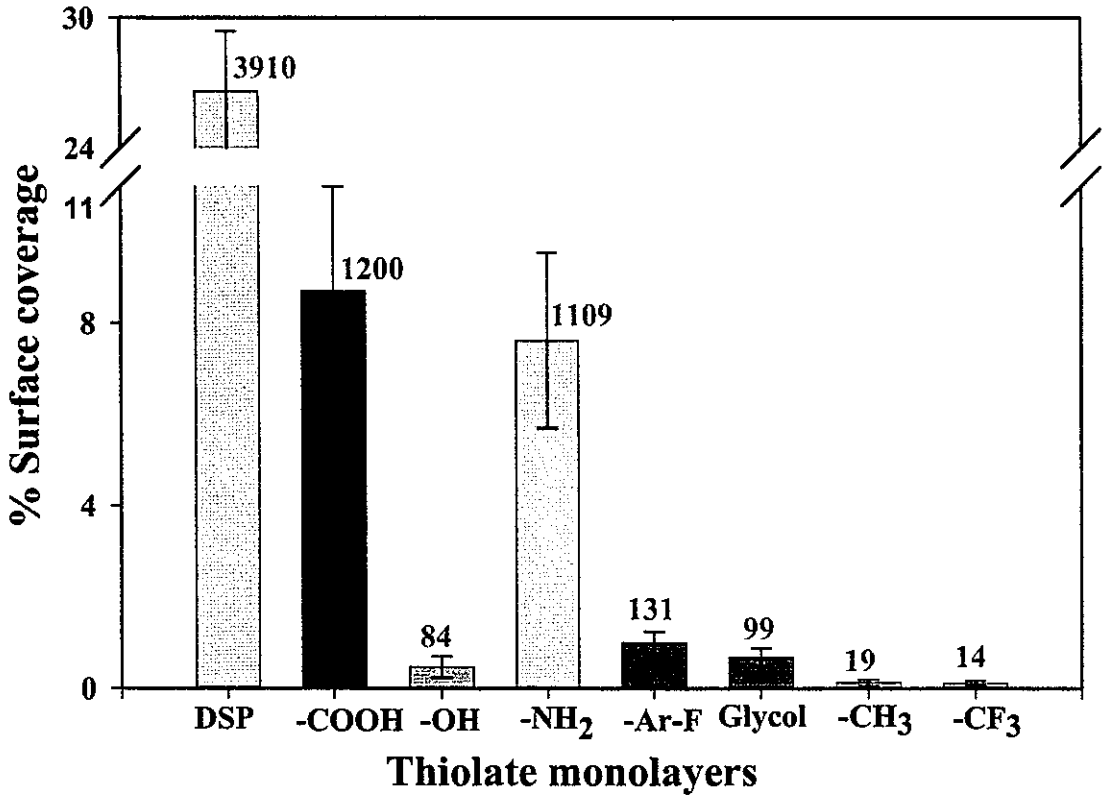
30
24
11
8
4
0
% Surface coverage
3910
1200
84
1109
131
99
19
14
DSP
-COOH
-OH
-NH2
-Ar-F
Glycol
-CH3
-CF3
Thiolate monolayers

Figure 4

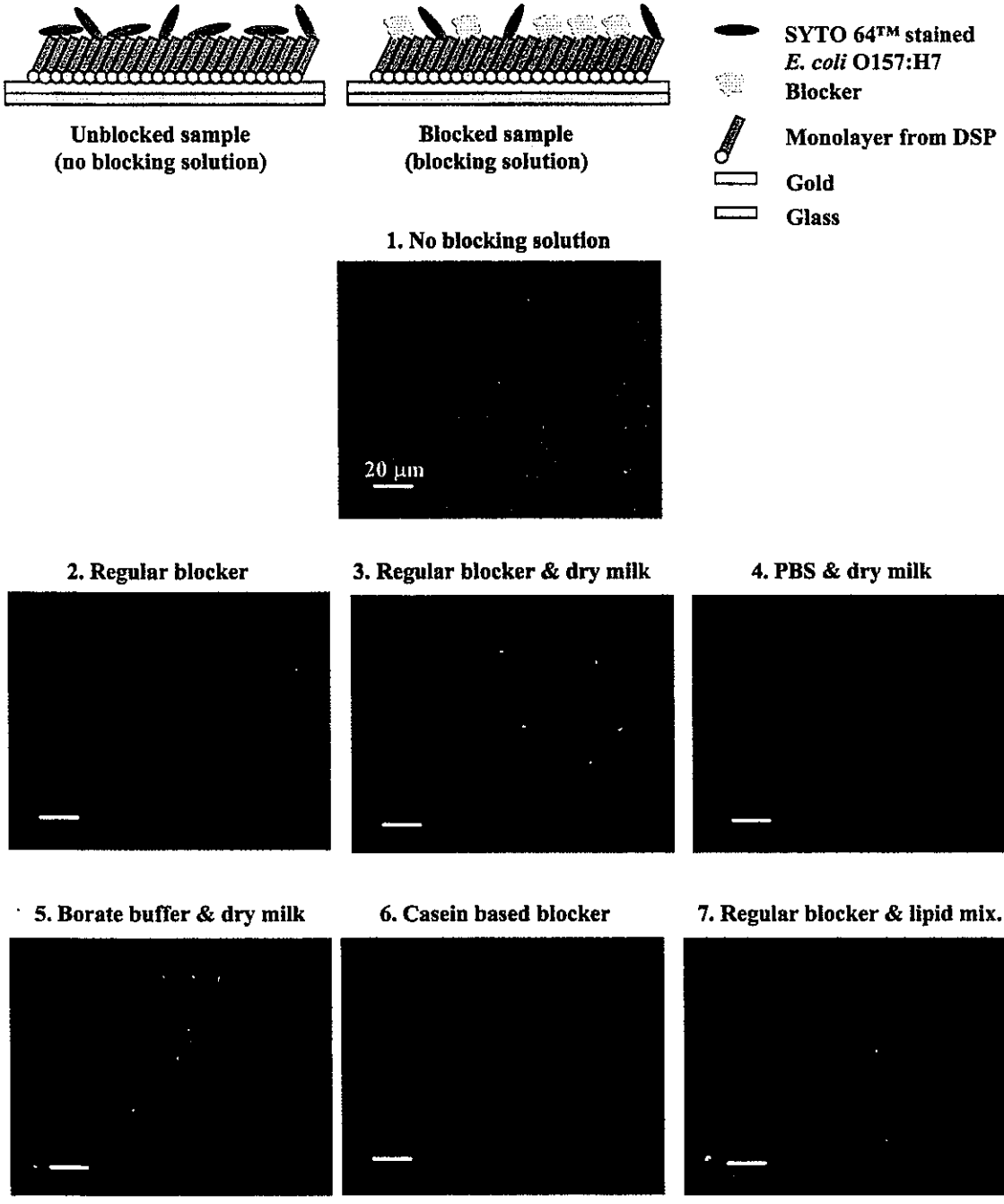
Unblocked sample
(no blocking solution)
Blocked sample
(blocking solution)
SYTO 64™ stained
E. coli O157:H7
Blocker
Monolayer from DSP
Gold
Glass
1. No blocking solution
20 μm
2. Regular blocker
3. Regular blocker & dry milk
4. PBS & dry milk
5. Borate buffer & dry milk
6. Casein based blocker
7. Regular blocker & lipid mix.

Figure 5

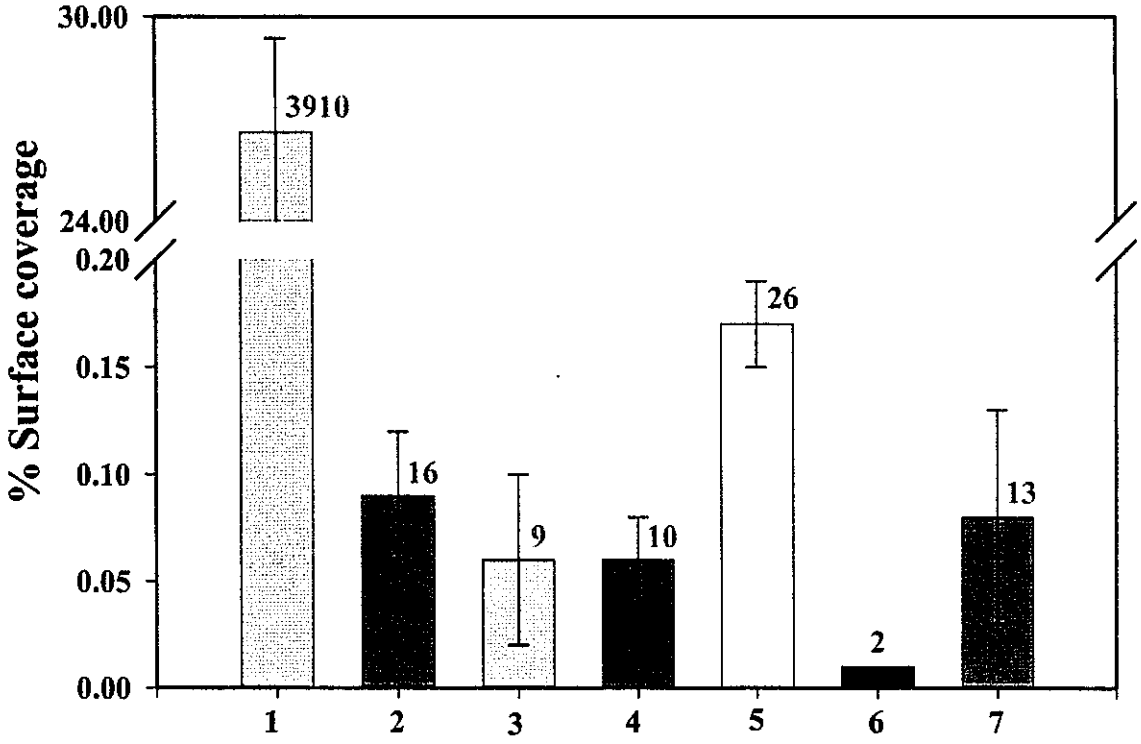
30.00
24.00
0.20
0.15
0.10
0.05
0.00
% Surface coverage
3910
16
9
10
26
2
13
1
2
3
4
5
6
7

Figure 6

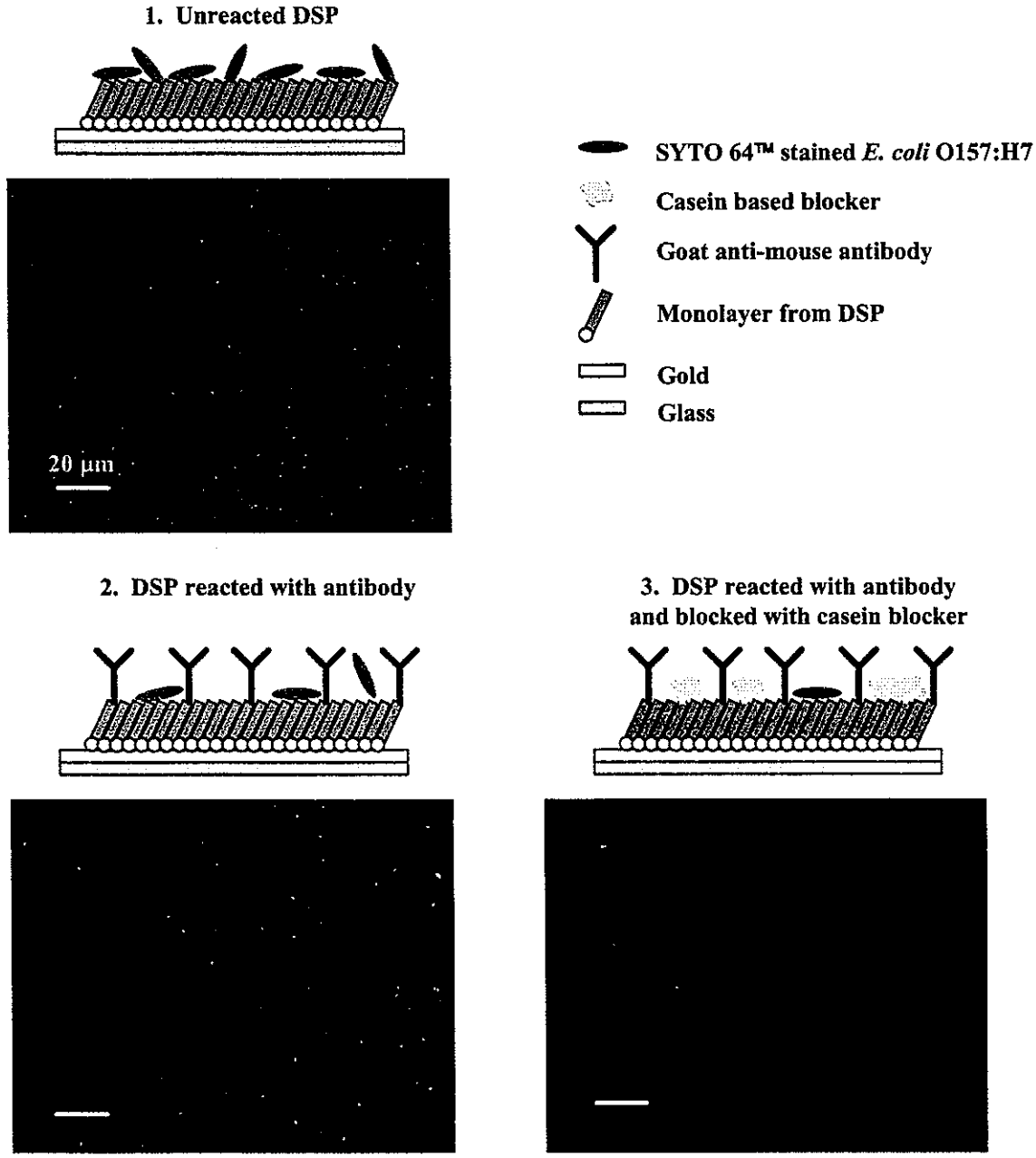
1. Unreacted DSP
20 µm
SYTO 64™ stained E. coli O157:H7
Casein based blocker
Goat anti-mouse antibody
Monolayer from DSP
Gold
Glass
2. DSP reacted with antibody
3. DSP reacted with antibody
and blocked with casein blocker

Figure 7

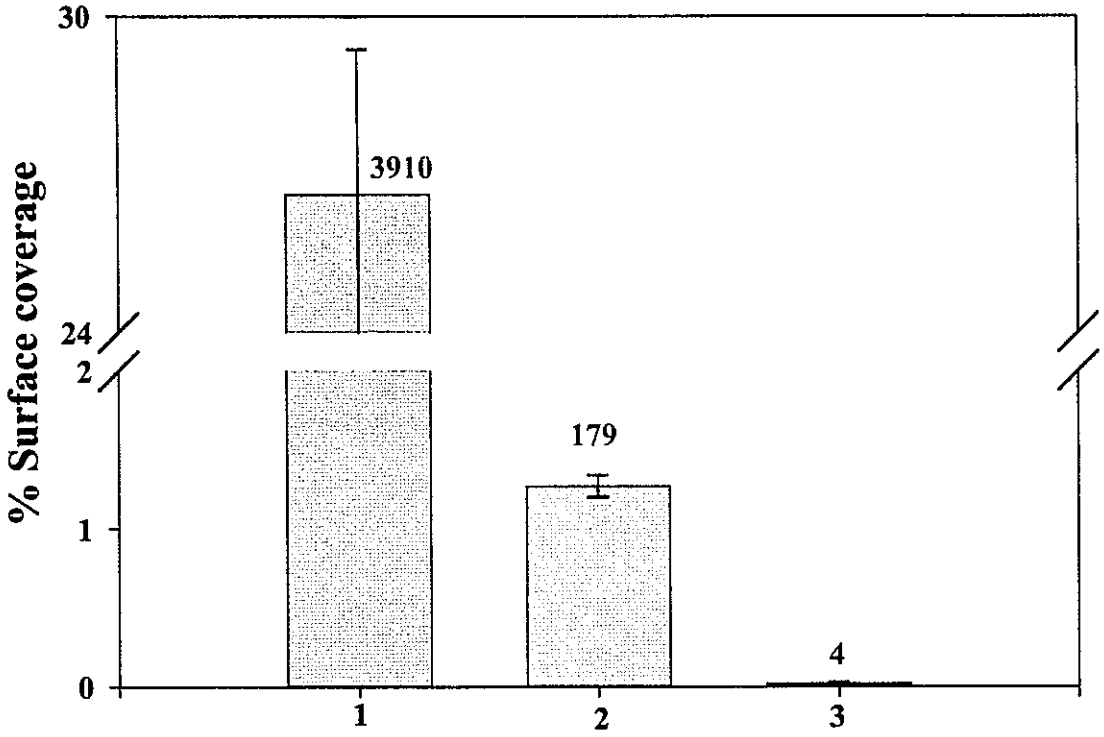

Figure 8

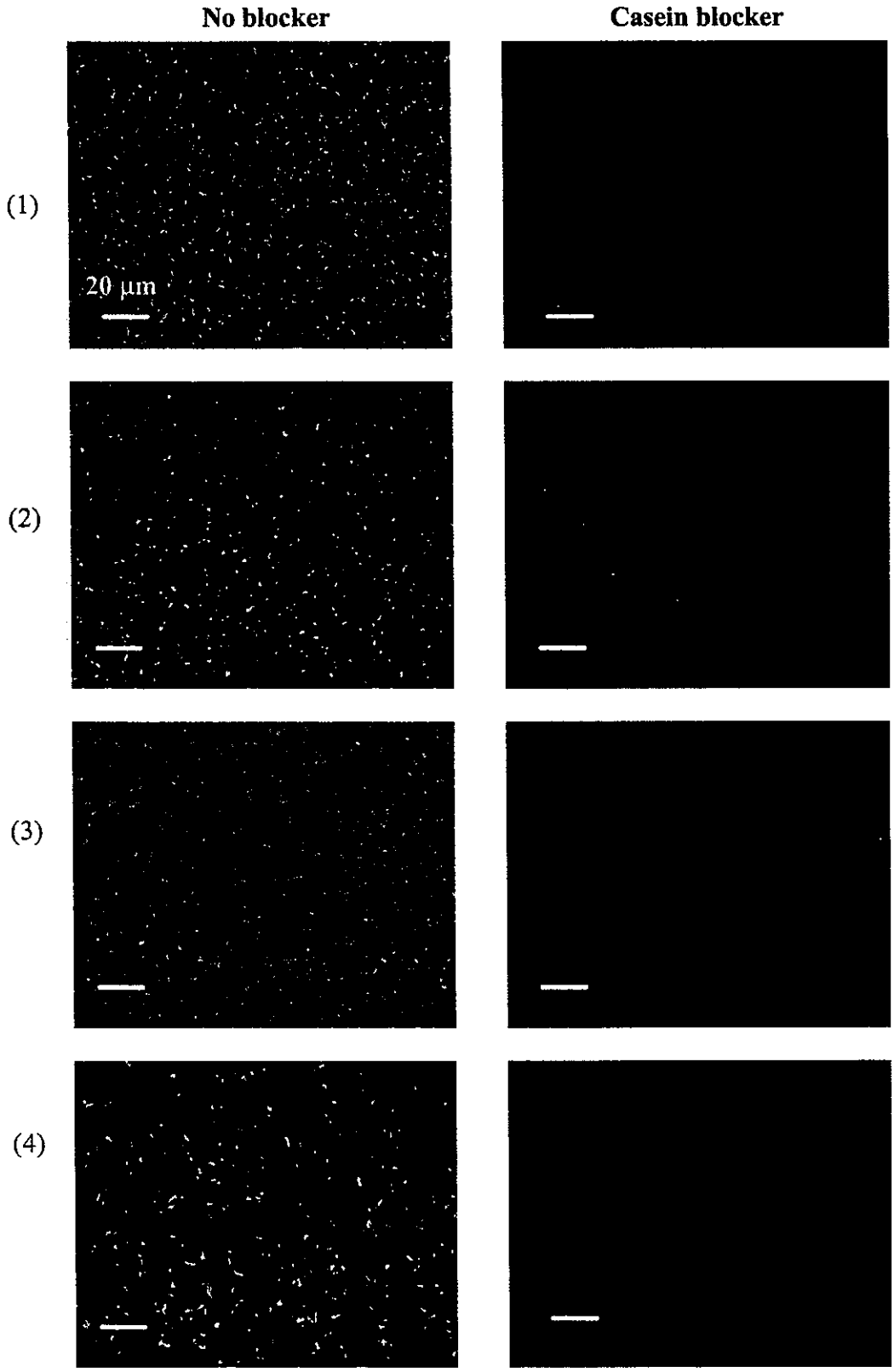

Figure 9

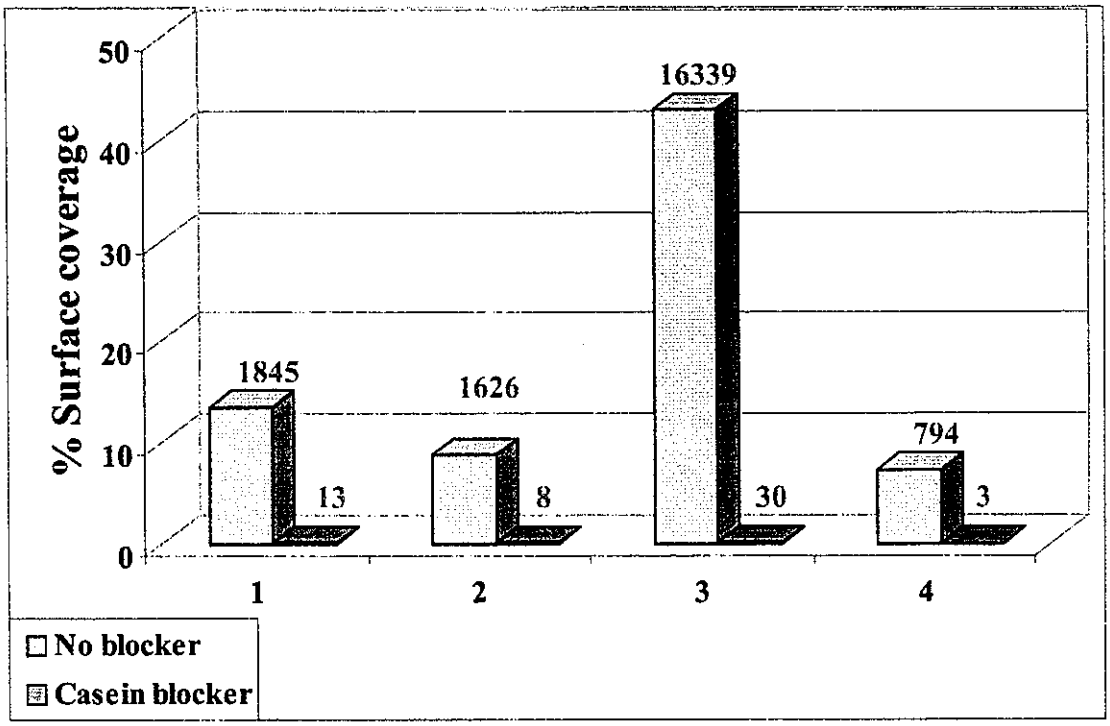
% Surface coverage
50
40
30
20
10
0
1845
13
1626
8
16339
30
794
3
1
2
3
4
No blocker
Casein blocker

Figure 10

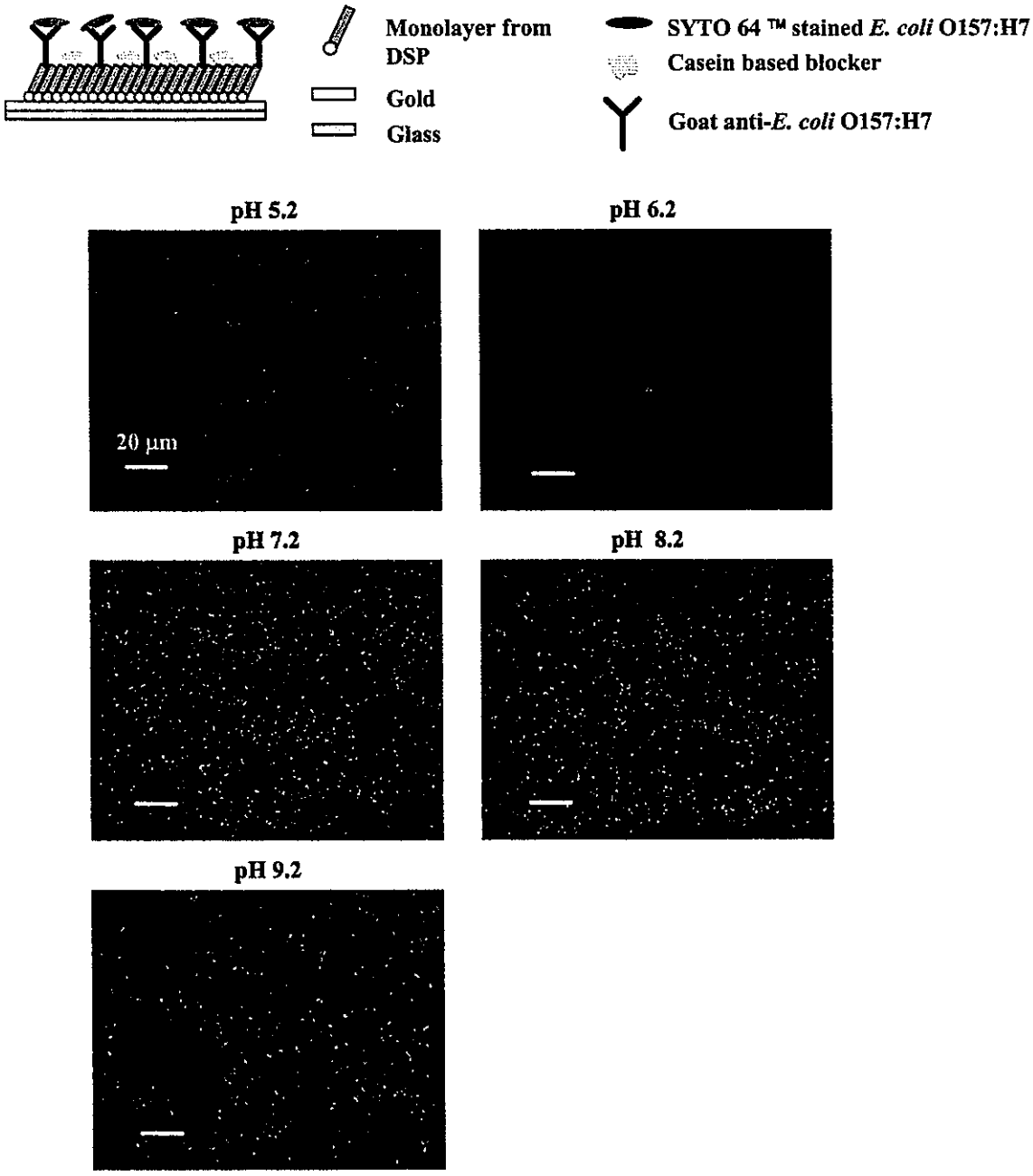
Monolayer from DSP
Gold
Glass
SYTO 64 ™ stained E. coli O157:H7
Casein based blocker
Goat anti-E. coli O157:H7
pH 5.2
pH 6.2
20 μm
pH 7.2
pH 8.2
pH 9.2

Figure 11

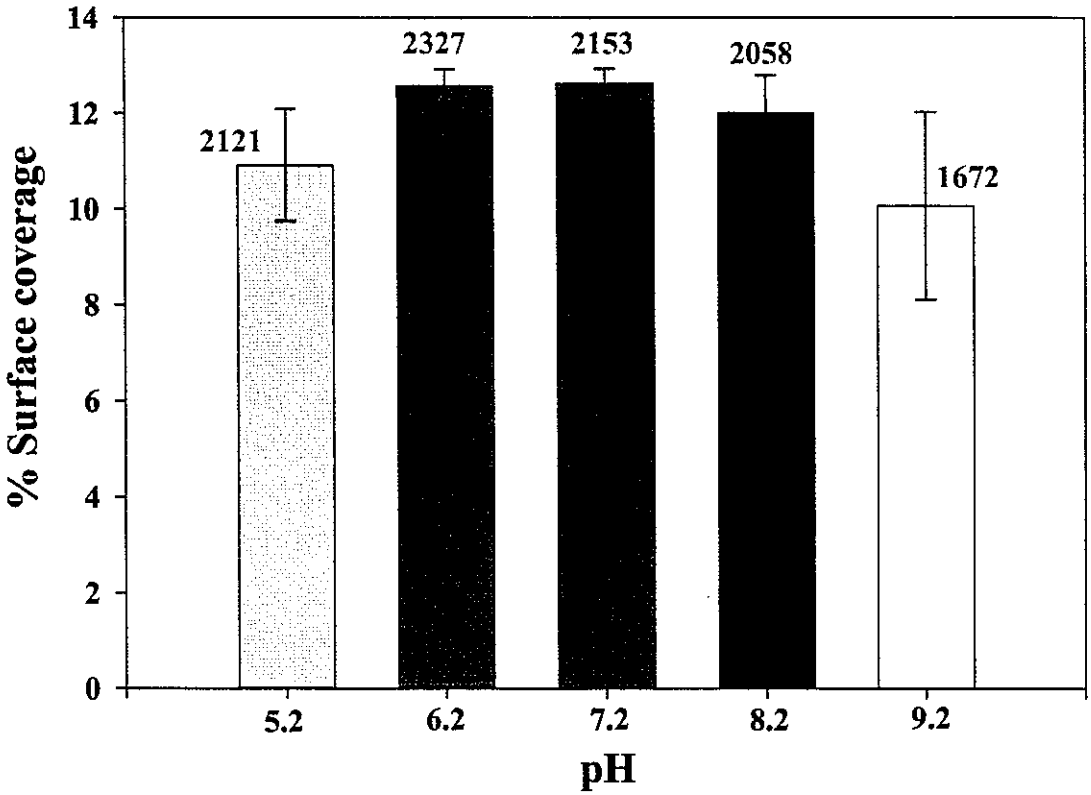
14
12
10
8
6
4
2
0
% Surface coverage
2121
2327
2153
2058
1672
5.2
6.2
7.2
8.2
9.2
pH

Figure 12

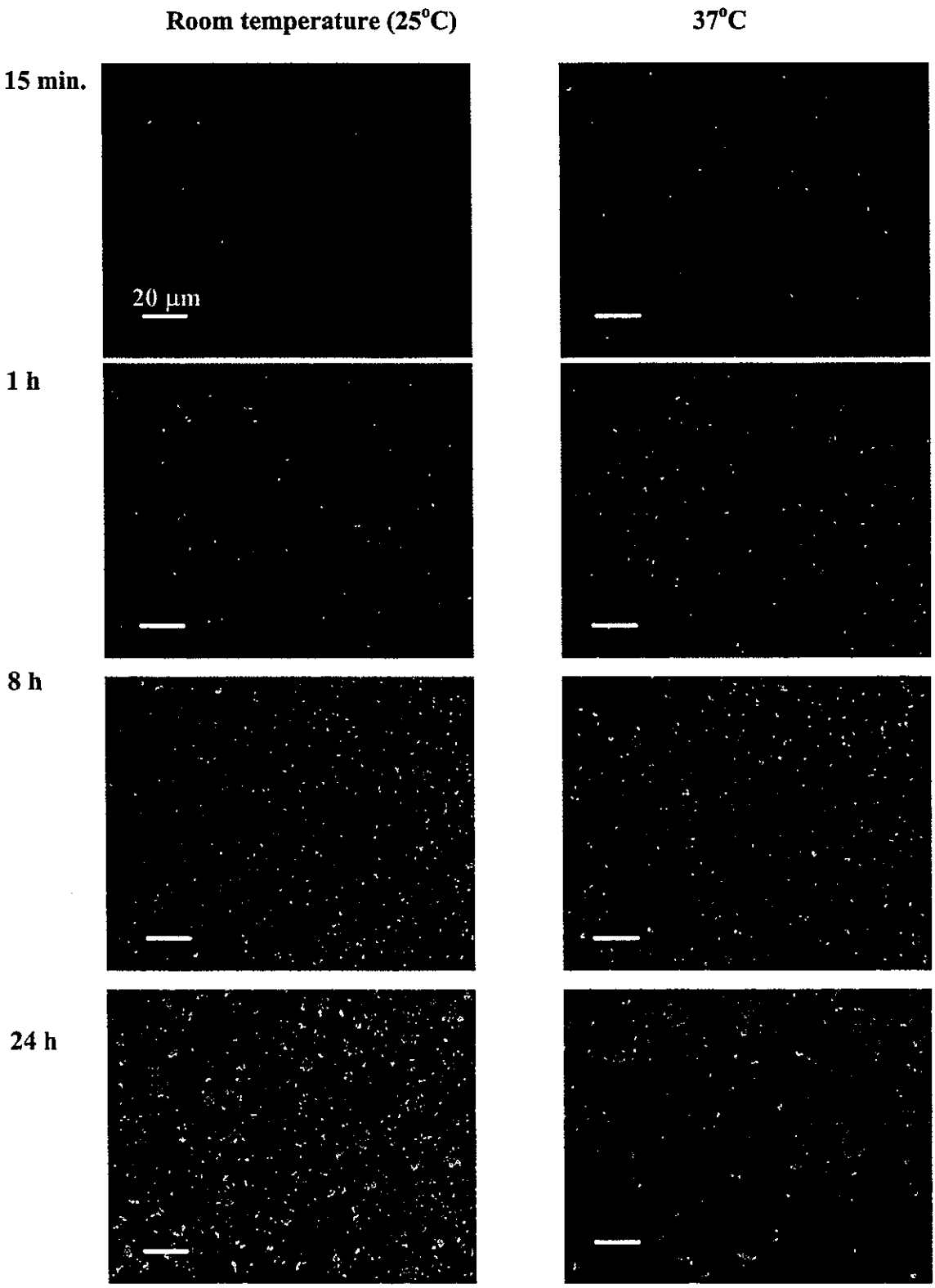

Figure 13

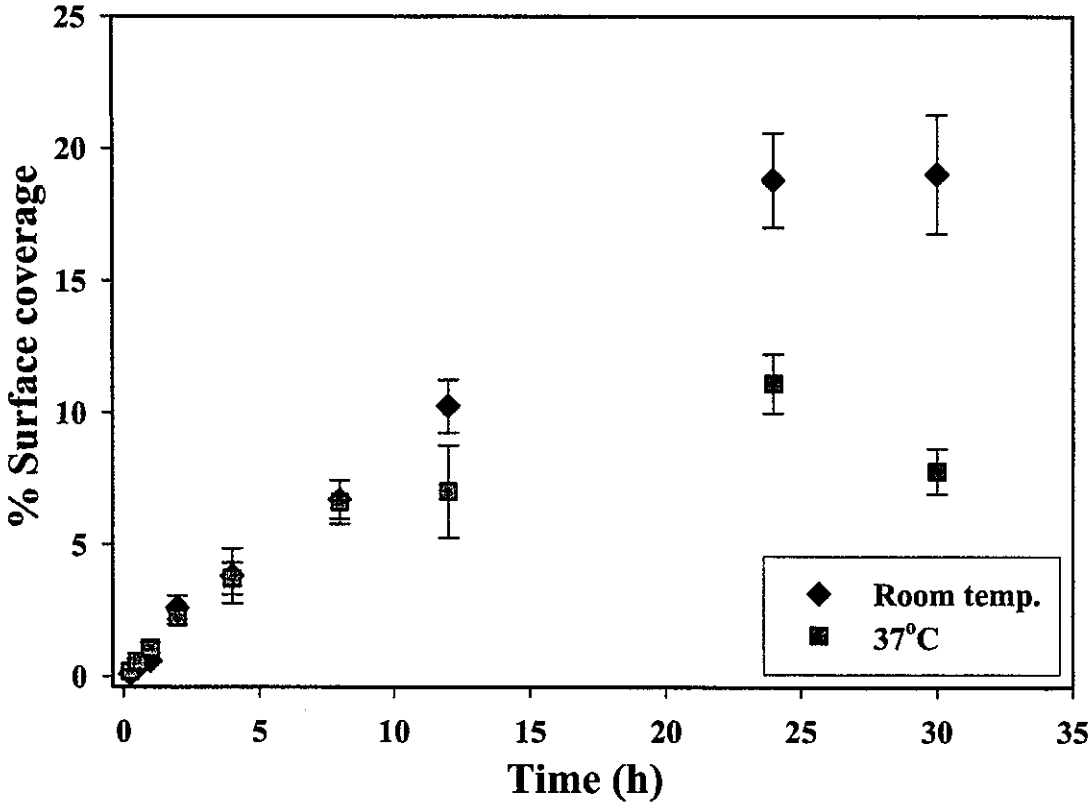

Figure 14

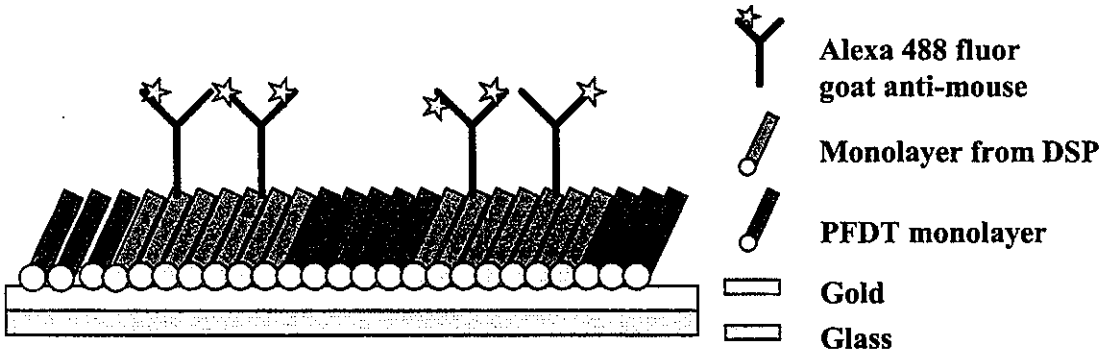
Alexa 488 fluor
goat anti-mouse
Monolayer from DSP
PFDT monolayer
Gold
Glass

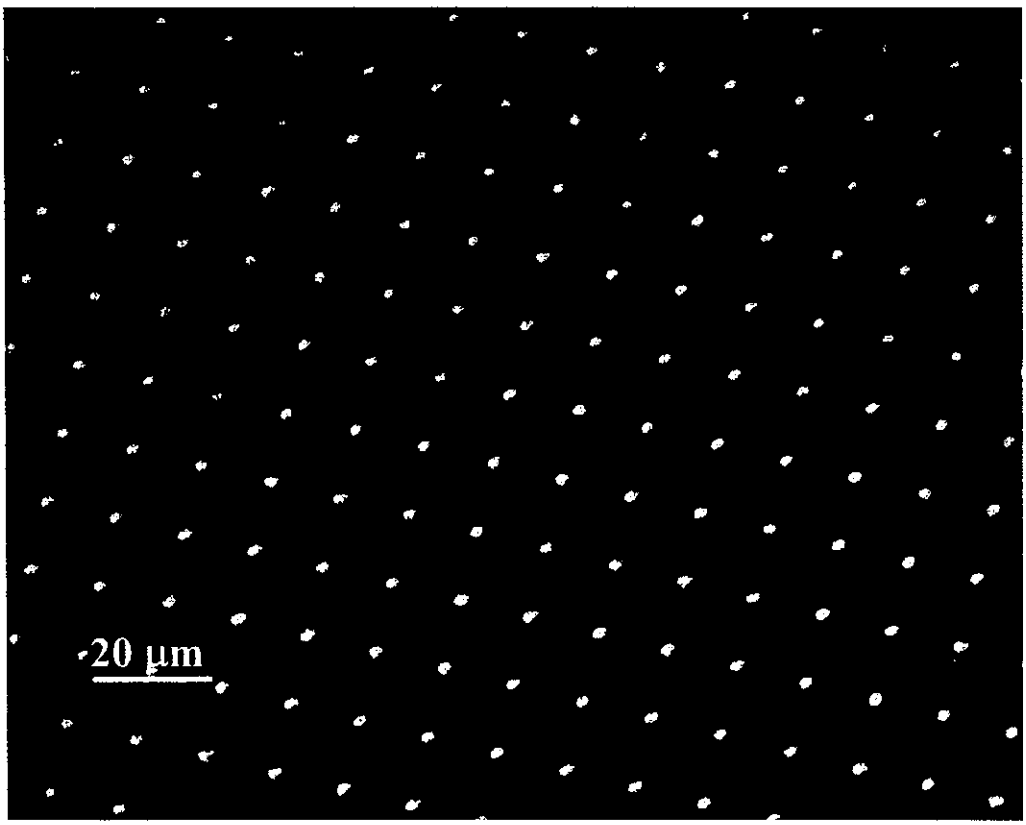
20 µm

Figure 15

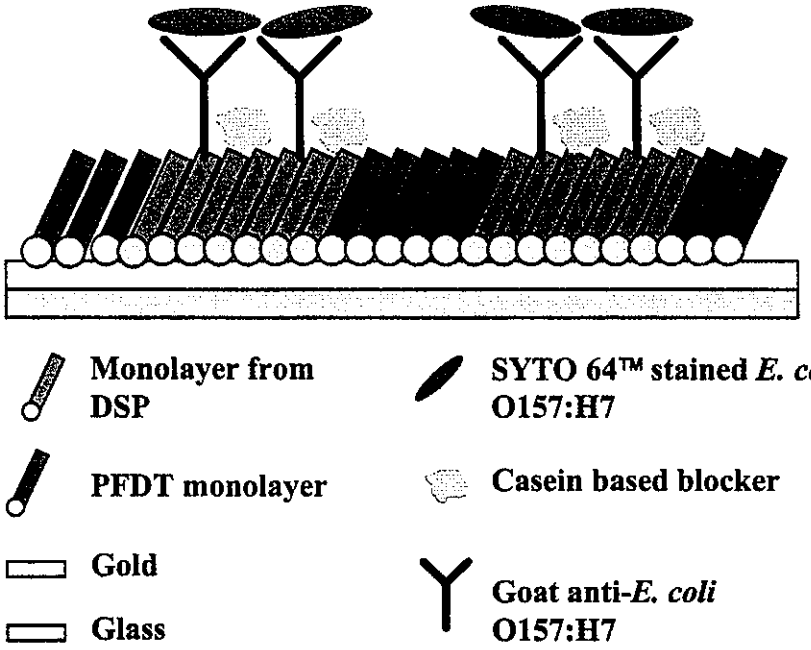
Monolayer from DSP
PFDT monolayer
Gold
Glass
SYTO 64™ stained E. coli O157:H7
Casein based blocker
Goat anti-E. coli O157:H7

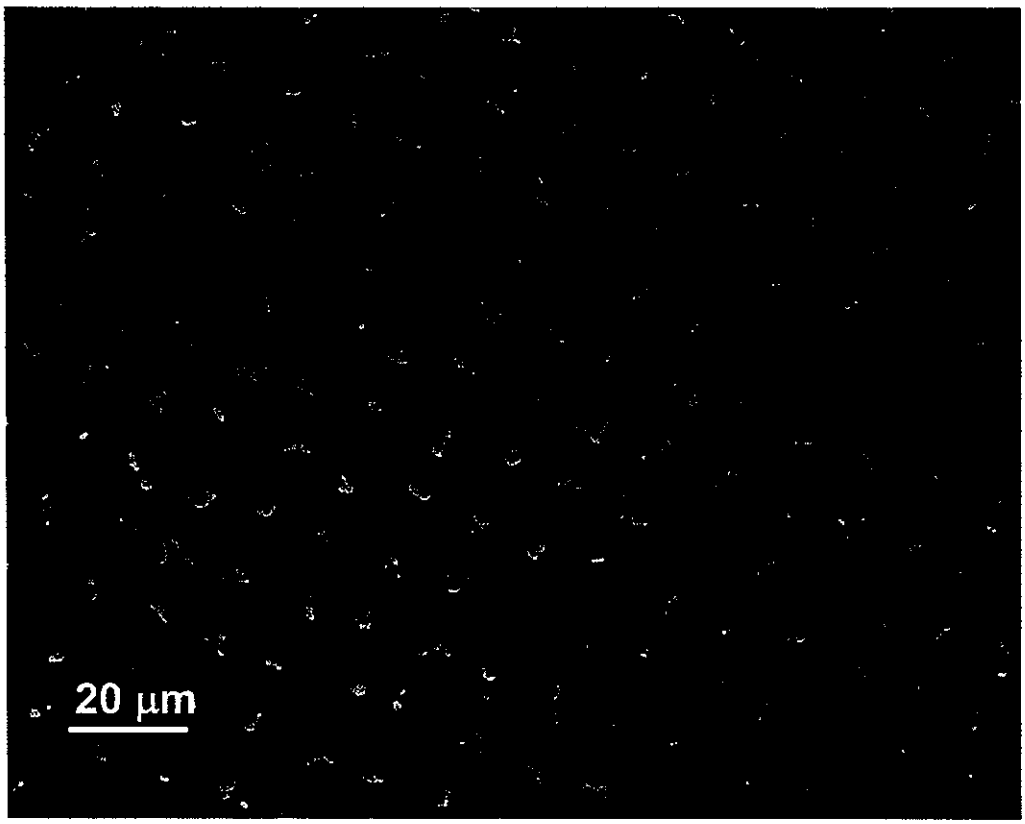
20 µm

Figure 16

CHAPTER 2: CHARACTERIZATION OF 1H, 1H, 2H, 2H-PERFLUORODECYL-1-THIOL (PFDT) AND DITHIO-BIS(SUCCINIMIDYL PROPIONATE) (DSP)-DERIVED MONOLAYERS THAT HAVE BEEN USED TO CONSTRUCT MICROMINIATURIZED IMMUNOSENSING PLATFORM FOR BACTERIA DETECTION BY IRS, XPS, AND EQCM TECHNIQUES

A paper in preparation for submission to *Langmuir*

Salma Rahman, Tosikazu Kawaguchi, Robert J. Lipert, and Marc D. Porter *

Institute of Combinatorial Discovery, Ames laboratory-USDOE, and Department of Chemistry and of Chemical and Biological Engineering, Iowa State University, Ames, IA 50011 USA

Abstract

1H, 1H, 2H, 2H-perfluorodecyl-1-thiol (PFDT)- and dithio-bis(succinimidyl propionate (DSP)-derived monolayers have been employed previously in our laboratory to create microminiaturized immunosensing platforms prepared by patterning specific capture addresses for the target bacteria (e.g., *E. coli* O157:H7).[1] DSP-based monolayers were used as coupling agents to immobilize antibodies (e.g., anti-*E. coli* O157:H7) in micrometer-sized addresses via amide linkages. The capture addresses were surrounded by PFDT-based monolayers because of the propensity these monolayers to minimize the nonspecific adsorption of both the capture antibody and target bacteria. The paper herein describes the results from a structural characterization of PFDT-based monolayer and DSP-derived monolayer. As principal characterization techniques, infrared reflection spectroscopy (IRS), electrochemical quartz crystal microbalance (EQCM), and X-ray photoelectron spectroscopy (XPS) have been employed. Both IRS and XPS validated the formation and reactivity of the

coupling agent DSP utilized in the covalent attachment of the antibody to the substrate. EQCM data provided further insights into the adlayer structure, e.g., the surface coverage of the thiolate monolayers (i.e., $4.2\pm0.5\times10^{-10}$ mol cm^{-2} in case of PFDT- and $6.6\pm0.9\times10^{-10}$ mol cm^{-2} in case of DSP-derived monolayers using more exacting treatments), mass change, or mass change per mole of electrons (*mpe*). This technique also indicated that the PFDT- and DSP-derived monolayers were associated with ~2.2 and ~0.6 solvated cations at the interface in the electrolyte solution, respectively. The data obtained from the structural characterization of the two adlayers will serve as a basis for our efforts in the construction of a wide range of immunosensing platforms.

* Corresponding Author

Introduction

Numerous readout techniques for bioassays have been developed in the past decade. The most recent readout instruments can measure hundreds of analytes at once, and typically function in a chip-scale format. Analytes can be labeled with a fluorescent dye,[2] Raman active nanosphere,[3] radioactive material,[4] or magnetic or electroactive tag.[5] Other strategies read these platforms with methods like surface plasmon resonance[6] and atomic force microscopy,[7] which have the advantages of not requiring a labeling step.

In each of these cases, performance is often compromised by nonspecific adsorption.[8] In our previous work,[1] we investigated the resistance of various functional groups, based on end-group modified alkanethiolates on gold, to the nonspecific adsorption of a variety of antibodies and microorganisms, the latter being the principal focus of the investigation. That

study showed that a fluorinated thiolate, formed from 1H, 1H, 2H, 2H-perfluorodecyl-1-thiol (PFDT), was strongly resistant to nonspecific adsorption by bacteria and several antibodies.

Based on this work, we also employed *N*-hydroxysuccinimidyl-terminated self-assembled monolayers (NHS-SAM) as coupling agents to immobilize proteins (i.e., antibodies) on the substrate, which eliminates the activation steps typically used in the covalent attachment of amines. The self-assembly method for the anchoring biomolecules shows a number of advantages, e.g., high reproducibility, molecular level control (e.g., distribution across the surface), and control over the distance from the surface.[9] With an NHS-SAM, the succinimidyl group reacts with the amines of the lysine residues of the antibody to form an amide linkage.[7] Dithio-bis(succinimide undecanote) (DSU), synthesized in-house,[3, 7, 10, 11] was used as NHS-SAM in our group previously. In contrast, dithio-bis(succinimidyl propionate) (DSP), a shorter chain version of DSU, can be employed as purchased. Previous studies concerning the reactivity of DSP-derived SAMs have shown they undergo hydrolysis in basic solutions, losing the terminal NHS moieties and forming a carboxylate ion.[12, 13] However, recent work in our and other laboratories have shown that integrity of the DSP-derived monolayer is maintained at neutral pH for 24 h or more,[1, 10] the usual condition for biomolecular applications.[14]

Previously in our group, photolithographic techniques have been used for the construction of a bifunctional surface for the creation of an immnunosensing platform to capture bacteria.[1, 7] The platforms were prepared by the use of DSP as a coupling agent to immobilize anti-*E. coli* O157:H7 in micrometer-sized addresses that were surrounded by PFDT-based domains between the capture addresses. Results demonstrated selective binding for *E. coli* O157:H7 at the capture address and a low level of nonspecific adsorption at the

PFDT domains. The work herein reports on the structural characterization of the two adlayers, and on the adlayer after coupling to the antibody as well as to the target bacteria (i.e., *E. coli* O157:H7). We have used infrared reflection spectroscopy (IRS), X-ray photoelectron spectroscopy (XPS), and electrochemical quartz crystal microbalance (EQCM) as principal characterization techniques. IRS and XPS are invaluable tools to probe the functional group composition of the surface species.[15-20] Both IRS and XPS were employed to validate the formation and reactivity of the adlayer formed from DSP.[3, 13, 15] XPS can, in addition, delineate details regarding the interaction between the sulfhydryl group of the adsorbate precursor and gold surface. On the other hand, EQCM serves as a highly sensitive means to monitor the mass of surface materials at low nanogram levels.[21, 22] With EQCM, alkanethiolate SAMs have been characterized by cross correlations with the voltammetrically driven reductive desorption of SAMs, yielding a quantitative measure of adsorbate surface concentration.[20] Collectively, these data are applied to the development of general structural descriptions of the two adlayers, serving as a basis for our ongoing efforts in the application of patterned adlayers in the protein-based bioassays.

Experimental Section

Materials and reagents. DSP and semiconductor grade potassium hydroxide (99.99 %) were purchased from Aldrich. PFDT was obtained from SynQuest. Ethanol (absolute 200 proof) was obtained from AAPER. The quartz crystals (AT-cut, 5MHz) for EQCM measurement were acquired from MAXTEK. Heat killed *Escherichia coli* O157:H7 was kindly provided by Dr. Cornick of the Iowa State University Department of Veterinary

Microbiology and Preventive Medicine. Affinity-purified goat anti-*E. coli* O157:H7 was purchased from USBiological.

Instrumentation. (i) Infrared Spectroscopy. IRS spectra were acquired with a Nicolet 850 FT-IR spectrometer, purged with liquid N_2 boil off, and equipped with a liquid N_2-cooled HgCdTe detector. Spectra were obtained using *p*-polarized light incident at 80° with respect to the surface normal. The spectra were recorded as $-\log(R/R_0)$, where R is the sample reflectance and R_0 is the reflectance of an octadecanethiolate-d_{37} monolayer-coated gold reference. The spectra are an average of 512 sample and reference scans, taken at 4-cm^{-1} resolution with Happ-Genzel apodization.

(ii) X-ray photoelectron spectroscopy (XPS). XPS characterizations were performed at room temperature with a Physical Electronics Industries 5500 multitechnique surface analysis system. This system is equipped with a hemispherical analyzer, a toroidal monochromator, a multichannel detector, and monochromatic Al-Kα excitation radiation (1486.6 eV, 250 W). The base pressure of the chamber during analysis was less than 9×10^{-10} Torr and the sampling area was ~2 mm^2. Photoelectrons were collected with integration time of 20 min. The resolution was ~0.3 eV. The Au($4f_{7/2}$) emission band served as an internal reference for binding energy.

(iii) EQCM measurements. Gold-coated quartz crystals (AT-cut, 5 MHz, MAXTEK) were used as the working electrode. Ag/AgCl (saturated KCl) and platinated platinum were used as reference and counter electrodes, respectively. The quartz crystal was fixed on the QCM sensor head (MAXTEK), and was connected to a frequency counter (Hewlett Packard, 53131A) and potentiostat (EG & G Princeton Applied Research, model 273). The frequency and current with respect to applied potential were collected on a personal computer (Dell,

Optiplex GX260) through a DAQ board (National Instrument, PCI-6025E) and GP-IB interface board (National Instruments).

Method development. (i) Sample preparation for IR spectroscopy. Precleaned glass slides (2.5 x 7.5 cm) were primed with 15-nm of chromium (0.1nm/s), following by ~300-nm of gold (0.1-0.2 nm/s). These substrates were then immersed into freshly prepared ethanolic solutions of thiols (10 mM PFDT or 0.1-1 mM DSP) for ~12 h, rinsed with ethanol, and dried with a stream of nitrogen gas (Air products). IRS measurements of the samples were then performed.

Anti-*E. coli* O157:H7 (100x the amount theoretically needed to fully cover the test area) was pipetted onto some of the samples (DSP) and placed in a humidity chamber for ~12 h. The samples were rinsed (3x) with 25 mM borate buffer and de-ionized water, and dried with nitrogen.

(ii) Sample preparation for XPS. These samples were prepared by the same procedure used for the IRS studies except the size of glass slide was 1 x 1 cm.

(iii) Working electrode preparation for EQCM. All quartz crystals were etched with aqua regia and manually polished with 0.3-μm alumina to remove the coated metal layers present on the as-received materials. They were then rinsed and sonicated in Milli-Q water for 10 min, dried with nitrogen gas, and cleaned by RF-plasma treatment (20 W) in an air plasma at 250 mtorr for 5 min. These substrates were then coated with a titanium adhesion layer (1 nm) and 200-nm gold film at 200 °C. Finally, the substrates were immersed in ethanolic solutions of 0.1-1 mM DSP or 10 mM PFDT for ~12 h immediately after flame-annealing and quenching with argon. As prepared, these surfaces have a strong Au(111) surface texture, as revealed by sharp oxidation peak at +1.43 V in a cyclic voltammogram in 0.1 M

sulfuric acid had.[23-25] A roughness factor of 1.37 was estimated from the surface oxide reduction peak at +0.9 V in the same set of scans.[26]

Results and Discussion

Characterizations by IRS.

Formation of PFDT monolayer. The immersion of gold-coated glass slides in PFDT solution resulted in the chemisorption of a fluorine-terminated PFDT monolayer. Figure 1 shows the resulting IRS spectrum, which compares well with that of an earlier report in both the location and numbers of features as well as their intensities.[27] The features between 1400 and 1050 cm^{-1} are therefore consistent with presence of the highly fluorinated adlayer. That is, the peaks at 1337, 1295, and 1277 cm^{-1} are associated with asymmetric CF_2 stretches, that at 1370 cm^{-1} with a symmetric CF_2 stretch, and that at 1239 cm^{-1} with both CF_3 and asymmetric CF_2 stretches. The peak intensities of several (but not all) of these bands can also be used to estimate an average chain tilt for the adlayer, which detailed in our earlier work yielded a chain tilt of ~20° with respect to the surface normal.[27] We did not observe any features associated with methylene stretching modes, as expected for a monolayer containing only two methylene groups in its alkyl chain.[27] This result indicates that the adlayer is devoid of detectable hydrocarbon contamination.

Coupling of antibody to surface via monolayer from DSP. The capture antibody substrate consisted of anti-*E. coli* O157:H7 bound to a gold-coated glass substrate via the DSP-derived monolayer. DSP chemisorbs to gold through cleavage of the sulfur-sulfur bond,[3] and the formation of the resulting gold-bound thiolate and its subsequent coupling to anti-

E. coli O157:H7 can be readily confirmed by IRS. These results are presented in Figure 2. The three bands around 1800 cm^{-1} in the spectrum of the layer formed from DSP (Figure 2a) are assigned to the carbonyl stretches of the ester (1812 cm^{-1}) and of the succinimidyl end group (1786 (in-phase) and 1749 cm^{-1} (out-of-phase)).[28] The presence of these bands, along with the C-O stretch at 1219 cm^{-1} and the methylene stretches between 3000 and 2800 cm^{-1}, verifies the formation of the DSP-based coating.

IRS was also used to qualitatively confirm the covalent binding of anti-*E. coli* O157:H7 to the terminal group of the gold-bound coupling layer (Figure 2b). Since the acyl carbon of the succinimidyl ester group is strongly susceptible to nucleophilic attack, its reaction with the sterically accessible amines of the protein will immobilize the antibody via amide linkages. As is evident, treatment of the DSP-modified substrate with anti-*E. coli* O157:H7 causes a marked decrease in the magnitude of the bands for the succinimidyl group (e.g., 1749 and 1219 cm^{-1}). Moreover, three readily identifiable bands, which are located at 3300 (N-H stretch), 1652 (amide I), and 1539 cm^{-1} (amide II), have appeared. The new bands reflect the presence of amides inherent in the native antibody as well as those formed by the reaction of the succinimidyl groups of DSP with amines in the protein. We add that the presence of residual succinimide groups is expected because of the lack of registry between the amines of the protein and the end groups of the adlayer and the voids between neighboring, immobilized proteins. Coupled with earlier reports,[7, 10, 29] which studied the hydrolysis rate of the succinimidyl terminal group of DSU-derived monolayer under similar conditions,[7] the differences in the two spectra in Figure 2 support the covalent attachment of anti-*E. coli* O157:H7 to the underlying substrate.

Characterizations by XPS. Figures 3a, 4a show the S(2p) binding region for the PFDT and DSP-derived monolayers, respectively. The observed binding energy (162.4 eV) of the marginally resolved S(2p) couplet (i.e., S2($p_{1/2}$) and S($2p_{3/2}$)) is consistent the presence of gold-bound thiolate.[30] Moreover, the attenuation in the intensities in this region after immobilization of anti-*E. coli* O15:H7 and then the capture of *E. coli* O15:H7 are indicative of the attenuation of photoelectrons by the subsequent overlayers on the DSP-based adlayer.[31, 32]

The XPS data in the F(1s) and C(1s) binding regions for the PFDT monolayer are shown in Figures 3b,c, respectively. The binding energy of F(1s) peak at 688.5 eV is consistent with the positions of fluorocarbon chains, i.e., -$(CF_2)_n$- in the XPS database,[33] which were between 688.1 eV and 691.0 eV. In contrast, the C(1s) region of the PFDT monolayer has three peaks: 284.8 eV, 291.0 eV, and 293.3 eV; these positions corresponded to those for methylene groups (-CH_2-), and fluorocarbon groups, i.e., -$(CF_2)_n$-, and -CF_3, respectively.[33] The relative intensities are also qualitatively consistent with the numbers of each functional group in the expected adlayer.

The binding energies of the O(1s), N(1s), and C(1s) features in Figures 4b-d are further support of the presence of each structural component. These features were identified by using the NIST database.[33] Thus, the O(1s) peak at 532.3 eV, which corresponds to carbonyl oxygens, were observed in both the DSP-derived monolayer and the surface after capture of *E. coli* O157:H7;[33] the latter reflects in part the large number of carboxyl groups[34] on the bacterial cell wall. Only one O(1s) peak (533.3 eV) was observed on the anti-*E. coli* O157:H7 modified surface. This feature, which is asymmetric on the low energy side, is assigned to carbonyl oxygen and to oxygen as part of amide linkage.

The N(1s) and C(1S) regions qualitatively complete the structural assessment. The N(1s) region has only one observable feature (400.5 eV), which is attributed to the nitrogen of an amide bond. We add that the binding energy of nitrogen that is part of the *N*-hydroxysuccinimide group of DSP appears at almost the same position as an amide nitrogen. Lastly, the C(1s) signal from *E. coli* O157:H7 and anti-*E. coli* O157:H7 is not readily assignable, and probably represents the superposition of the many types of carbons in both materials. However, the C(1s) peaks of the DSP-derived adlayer at 285.3 eV and 289.0 eV are in close agreement with those for the carbon of the *N*-hydroxysuccinimide group and the ester carbonyl group, respectively.[35]

The sequential increase in the thickness of material on gold surfaces after each modification step is supported by Au(4f) spectra for the DSP-derived monolayer, anti-*E. coli* O157:H7 coupled to DSP-derived film, and the *E. coli* O157:H7 captured on anti-*E. coli* O157:H7 coupled to DSP-derived film in Figure 4e. The Au(4f) peaks at 87.8 eV and 84.0 eV are assigned to Au($4f_{5/2}$) and Au($4f_{7/2}$), respectively. As the thickness of the layer increased by binding of either anti-*E. coli* O157:H7 or *E. coli* O157:H7, the intensity of the Au(4f) systematically decreased. These changes reflect the increase in photoelectron attenuation as the overall thickness of the coating increases.

Characterization by EQCM. EQCM responses for the reductive desorption process of DSP- and PFDT- derived monolayers on pseudo-Au (111) are shown in Figure 5. Alkanethiolate monolayers can be desorbed in alkaline solution from gold by the one-electron reduction reaction in eq. 1.[36-41] Eq. 1 also shows that the reverse process can oxidatively deposit the adlayer.[42]

$$RS\text{-}Au + 1e^- \leftrightarrows RS^- + Au(0) \quad (1)$$

As evident, the linear cathodic sweep at the DSP-derived monolayer yields a single desorption wave with a peak at -1.03 V, whereas the sweep at the PFDT-based monolayer has waves at -0.92 V and -1.20 V. The responses correspond to the desorption of the adlayer from the heavily Au(111)-terraced surface in the case of both adlayers. That is, the wave for the DSP-based adlayer arises from the desorption of the adlayer, with the corresponding product rapidly lost to solution. The response for the PFDT adlayer, in contrast, reflects a mixed process, representing first the partial desorption of the adlayer and then the desorption of the remainder of the adlayer along with insoluble aggregates formed at the electrode surface from the first desorption wave.[43]

The voltammetric responses are accompanied by increases in the resonance frequency (Δf), which from the Sauerbrey equation,[44] reflects a decrease in the mass of material adsorbed on the electrode. Moreover, the evolution of the QCM response tracks with the voltammetric profiles. In other words, there was no detectable change in Δf until current began to flow from the reductive desorption process. We also note that the changes near the end of the cathodic scan arise from the evolution of hydrogen and the competition of this reaction with the interaction of the cations attached into the electrical double layer.[20]

These data can also be analyzed to gain further insights into the adlayer structure. The observed desorption charge (Q_{rd}), which is determined by integrating the area under the wave, can be directly translated to the surface coverage (Γ) of the thiolate monolayer by the following equation:

$$\Gamma = Q_{rd}/(nFA) \tag{2}$$

where n is the number of electrons in the reaction, F is Faraday constant, and A is surface area of the electrode after accounting for surface roughness. There are two approaches to the analysis of such data with respect to accounting for the nonfaradaic current that flows to charge the double layer as a consequence of adlayer desorption (Q_{dl}), and the background faradaic process that results from the low level of hydrogen generation (Q_f). These treatments both recognize that the total charge flow during desorption has three contributions, as expressed in eq. 3.

$$Q_{total} = Q_{rd} + Q_{dl} + Q_f \tag{3}$$

The first approach simply estimates the contributions of Q_{dl} and Q_f by a linear extrapolation from the current prior to the onset of desorption to that after desorption is completed.[27] The second approach determines the values of Q_{dl} and Q_f in a more exacting manner.[20] In this case, Q_{dl} is given by

$$Q_{dl} = (-E_{rd,e} - E_{PZC,Au})\, C_{dl,Au} - (-E_{rd,i} - E_{PZC,SAM})\, C_{dl,SAM} \tag{4}$$

where $E_{rd,e}$ represents a value of applied potential after the current that flows to desorb the adlayer has decayed to background levels; $E_{PZC,Au}$ is the potential of zero charge for an uncoated gold electrode in only supporting electrolyte; $C_{dl,Au}$ is the double layer capacitance

of an uncoated gold electrode in only supporting electrolyte, $E_{rd,i}$ is a value of applied potential chosen to represent the system prior to any flow of desorption current; $E_{PZC,SAM}$ is the potential of zero charge for gold electrode coated with the adlayer; and $C_{dl,SAM}$ is the double layer capacitance of a gold electrode coated with the adlayer. Table 1 summarizes the results of these analysis and all the experimental values for this analysis, noting that $E_{rd,e}$ was set at -1.35 V and $E_{rd,i}$ was fixed at -0.50 V.

The results of the two analyses, given as $\Gamma_{rd,1}$ and $\Gamma_{rd,2}$ to represent the values from the extrapolation and more exacting treatments, respectively, yield comparable surface concentrations (Γ_{rd}) for both types of adlayers. Interestingly, the experimental values of Γ_{rd} for the DSP-based adlayers are close to that for a model based on closest packing considerations,[45] whereas those for PFDT-based monolayers are indicated of a lower surface concentration. We do not, at present, have any tenable explanation for this difference, noting that our earlier work gave an indistinguishable difference between experiment and theory.[27] We suspect the difference may be due to surface roughness, but do not have evidence to realistically support this possibility.

Further insight into the structure can be gained can be gained from a detailed examination of Δf, which can be converted to a mass change (Δm) by the simplified Sauerbrey equation:

$$\Delta m = S\,\Delta f \tag{5}$$

where S is a proportionality constant, which expresses the sensitivity of 5 MHz AT-cut quartz crystal (17.7 ng cm^{-2} Hz^{-1}).[44] This result can be further examined by calculation of the mass change per mole of electrons (*mpe*), which is defined as:

$$mpe = \Delta m/(Q_{rd}/(FA)) \quad (6)$$

Thus, the observed *mpe*-value for the DSP-based monolayer is 28% of that found for the PFDT-monolayer. This difference, however, is much smaller than expected based on the molecular weights of the thiolates for the two adsorbates. The 41% of the discrepancy is attributed to the observed values of mpe reflecting only the net mass change.

In earlier work, the observed *mpe* was shown to arise not only from the desorption loss of a monolayer of gold-bound alkanethiolate, but also the electrosorption of solvated potassium cations, each roughly as a 3:1 ethanol: potassium ion unit (MW ~177 g/mol). In other words, the mass discrepancy between the *mpe* for a monolayer of alkanethiolates (ideal surface packing concentrations on a Au(111) surface (i.e., 7.6 x 10^{-10} mol/cm^2)) indicated that each desorb thiolate was replaced by this ethanol-potassium ion unit. Following this analysis, the lower surface concentration for the DSP-adlayer yielded a slightly larger relative mass for the electrosorbed solvated cation (149 g/mol). Thus, the net mass changes given as the *mpe* value of 165 g/mol, translate to a total desorption of an adsorbate with an associated molecular weight of 313 g/mol. This value, however, is 112 g/mol greater than that for the adsorbate alone, and if we assign this differences to the solvated cations, roughly 0.6 of these units are then associated with each adsorbate prior to desorption. A parallel analysis, summarized in Table 1, yields an association number of 2.2.

The solvated cations can be associated into two different sites of the monolayer, e.g., terminus of the monolayer or void volumes between adsorbates. In case of PFDT-based monolayer, the solvated cation units are likely associated via hydrophobic terminus of the monolayer (hydrophobic-hydophobic interaction) or trapped in voids. Whereas, in case of DSP-derived monolayer, the solvated cation units are probably associated via hydrogen bonding between the –OH regions of the cation and the –C=O regions of the succinimidyl terminus of the monolayer. Moreover, as presented in Table 1, surface coverage of PFDT-based monolayer was much smaller than the theoretical closest packing expectation, which may be the source of void volume. We presently believe, it is the contribution of all these factors that are responsible for the difference between the numbers of associated solvated cations into the two types adlayers.

Conclusions

This paper has presented the results of a multitechnique study of the structure of fluorine-terminated PFDT monolayers and *N*-hydroxysuccinimidyl (NHS) group terminated DSP-derived monolayers before and after coupling to proteins. These monolayers were employed to create a microminiaturized immunosensing platform prepared by patterning specific capture addresses for the target bacteria.[1] IRS spectra confirmed the presence of a highly fluorinated adlayer, and also the formation of DSP-derived monolayer. The coupling of antibody to DSP-derived monolayer was qualitatively confirmed by IRS via decrease in the magnitude of succinimidyl group bands and presence of amides inherent in the native antibody as well as those formed by the reaction of the succinimidyl groups of DSP with amines in the protein. In addition, the binding energy regions of various structural

components in XPS spectra also support the presence of gold-bound thiolates as well as immobilization of antibody and capturing of bacteria. The attenuation in the intensities after immobilization of biomolecules was indicative of the attenuation of photoelectrons by the subsequent overlayers. In EQCM measurement, the voltammetric responses are accompanied by increases in the resonance frequency which reflects a decrease in the mass of material adsorbed on the electrode. These data can be analyzed to gain further insights into the adlayer structure, e.g., the surface coverage of the thiolate monolayers (i.e., $4.2\pm0.5\times10^{-10}$ mol cm^{-2} in case of PFDT- and $6.6\pm0.9\times10^{-10}$ mol cm^{-2} in case of DSP-derived monolayers using more exacting treatments), mass change, or mass change per mole of electrons (*mpe*). The observed *mpe* arised both from the desorption loss of gold-bound alkanethiolate monolayer and the electrosorption of solvated potassium cations. It was observed that PFDT- and DSP-derived monolayers were associated with 2.2 and 0.64 solvated cations, respectively. Differences in the terminus of the monolayers as well as that of surface coverage values are probably responsible for the discrepancy between the numbers of associated solvated cations units into the two adlayers. The results will serve as a basis for our ongoing efforts in the construction of a wide range of immunosensing platforms.

Acknowledgments

The authors express appreciation to Dr. Nancy Cornick of VMPM department of Iowa State University for providing *E. coli* O157:H7. Funding for this work was provided by the United State Department of Agriculture Cooperative State Research, Education, and Extention Service (UDSA CSREES award number 20002-35201-12659) and by the Institute of Combinatorial Discovery of Iowa State University through the Roy J. Carver Laboratory

for Ultra High Resolution Biological Microscopy. The Ames Laboratory is operated for the U.S. Department of Energy by Iowa State University under Contract W-7405-Eng-82.

References

(1) Rahman, S.; Lipert, R. J.; Porter, M. D. *Manuscript in preparation* **2005**.

(2) Brown, P. O.; Botstein, D. *Nat. Genet.* **1999**, *21*, 33-37.

(3) Grubisha, D. S.; Lipert, R. J.; Park, H. Y.; Driskell, J.; Porter, M. D. *Anal. Chem.* **2003**, *75*, 5936-5943.

(4) Diamandis, E. P., Christopoulos, T. K. *Immunoassay*; Academic Press: New York, 1996.

(5) Millen, R. L.; Kawaguchi, T.; Granger, M. C.; Tondra, M.; Porter, M. D. *Anal. Chem.* **2005**, *77*, 6581-6587.

(6) Cullen, D. C.; Lowe, C. R. *Sens. Actuators, B* **1990**, *1*, 576-579.

(7) Jones, V. W.; Kenseth, J. R.; Porter, M. D.; Mosher, C. L.; Henderson, E. *Anal. Chem.* **1998**, *70*, 1233-1241.

(8) Rowan, B.; Wheeler, M. A.; Crooks, R. M. *Langmuir* **2002**, *18*, 9914-9917.

(9) Gooding, J. J.; Erokhin, P.; Losic, D.; Yang, W. R.; Policarpio, V.; Liu, J. Q.; Ho, F. M.; Situmorang, M.; Hibbert, D. B.; Shapter, J. G. *Anal. Sci.* **2001**, *17*, 3-9.

(10) Wagner, P.; Hegner, M.; Kernen, P.; Zaugg, F.; Semenza, G. *Biophys. J.* **1996**, *70*, 2052-2066.

(11) Niemz, A.; Jeoung, E.; Boal, A. K.; Deans, R.; Rotello, V. M. *Langmuir* **2000**, *16*, 1460-1462.

(12) Dordi, B.; Schonherr, H.; Vancso, G. J. *Langmuir* **2003**, *19*, 5780-5786.

(13) Grubor, N. M.; Shinar, R.; Jankowiak, R.; Porter, M. D.; Small, G. J. *Biosens. Bioelectron.* **2004**, *19*, 547-556.

(14) Cabrita, J. F.; Abrantes, L. M.; Viana, A. S. *Electrochim. Acta* **2005**, *50*, 2117-2124.

(15) Kenseth, J., Wong, S. -S., Takano, H., Jones, V., Porter, M. D., Tokyo, Japan 1999; 179-182.

(16) Naselli, C.; Swalen, J. D.; Rabolt, J. F. *J. Chem. Phys.* **1989**, *90*, 3855-3860.

(17) Mate, C. M.; Lorenz, M. R.; Novotny, V. J. *J. Chem. Phys.* **1989**, *90*, 7550-7555.

(18) Chidsey, C. E. D.; Loiacono, D. N. *Langmuir* **1990**, *6*, 682-691.

(19) Chau, L. K.; Porter, M. D. *Chem. Phys. Lett.* **1990**, *167*, 198-204.

(20) Kawaguchi, T.; Yasuda, H.; Shimazu, K.; Porter, M. D. *Langmuir* **2000**, *16*, 9830-9840.

(21) Bruckenstein, S.; Swathirajan, S. *Electrochim. Acta* **1985**, *30*, 851-855.

(22) Shimazu, K.; Kita, H. *J. Electroanal. Chem.* **1992**, *341*, 361-367.

(23) Sotto, M. *J. Electroanal. Chem.* **1976**, *69*, 229-237.

(24) Sotto, M. *J. Electroanal. Chem.* **1976**, *72*, 287-306.

(25) Angersteinkozlowska, H.; Conway, B. E.; Barnett, B.; Mozota, J. *J. Electroanal. Chem.* **1979**, *100*, 417-446.

(26) Angersteinkozlowska, H.; Conway, B. E.; Hamelin, A.; Stoicoviciu, L. *J. Electroanal. Chem.* **1987**, *228*, 429-453.

(27) Alves, C. A.; Porter, M. D. *Langmuir* **1993**, *9*, 3507-3512.

(28) Frey, B. L.; Corn, R. M. *Anal. Chem.* **1996**, *68*, 3187-3193.

(29) Duhachek, S. D.; Kenseth, J. R.; Casale, G. P.; Small, G. J.; Porter, M. D.; Jankowiak, R. *Anal. Chem.* **2000**, *72*, 3709-3716.

(30) Lindberg, B. J., Harmin, K., Johanson, G., Gelius, U., Fahlman, A., Nordling, C., Siegbahn, K. *Phys. Scr.* **1970**, *1*, 286-298.

(31) Briggs, D., Seah, M. P. *Practical Surface Analysis by Auger and X-ray Photoelectron Spectroscopy*; Wiley: Chichester, 1983.

(32) Smith, E. L.; Alves, C. A.; Anderegg, J. W.; Porter, M. D.; Siperko, L. M. *Langmuir* **1992**, *8*, 2707-2714.

(33) www.nist.gov.

(34) http://pps98.man.poznan.pl/assignment/projects/castro/bacwall.html.

(35) Vaidya, B.; Chen, J. H.; Porter, M. D.; Angelici, R. J. *Langmuir* **2001**, *17*, 6569-6576.

(36) Walczak, M. M.; Popenoe, D. D.; Deinhammer, R. S.; Lamp, B. D.; Chung, C. K.; Porter, M. D. *Langmuir* **1991**, *7*, 2687-2693.

(37) Weisshaar, D. E.; Lamp, B. D.; Porter, M. D. *J. Am. Chem. Soc.* **1992**, *114*, 5860-5862.

(38) Widrig, C. A.; Chung, C.; Porter, M. D. *J. Electroanal. Chem.* **1991**, *310*, 335-359.

(39) Zhong, C. J.; Porter, M. D. *J. Am. Chem. Soc.* **1994**, *116*, 11616-11617.

(40) Zhong, C. J.; Porter, M. D. *J. Electroanal. Chem.* **1997**, *425*, 147-153.

(41) Zhong, C. J.; Zak, J.; Porter, M. D. *J. Electroanal. Chem.* **1997**, *421*, 9-13.

(42) Sumi, T.; Wano, H.; Uosaki, K. *J. Electroanal. Chem.* **2003**, *550*, 321-325.

(43) Hobara, D.; Miyake, O.; Imabayashi, S.; Niki, K.; Kakiuchi, T. *Langmuir* **1998**, *14*, 3590-3596.

(44) Sauerbrey, G. *Z. Phys.* **1959**, *155*, 206-222.

(45) Wagner, P.; Zaugg, F.; Kernen, P.; Hegner, M.; Semenza, G. *J. Vac. Sci. Technol., B* **1996**, *14*, 1466-1471.

Figure Captions

Figure 1. Infrared reflection spectra of PFDT-based monolayer on gold.

Figure 2. Infrared reflection spectra DSP-derived monolayer on gold before (a) and after (b) coupling with anti-*E. coli* O157:H7.

Figure 3. XPS in the (a) S(2p), (b) F(1s), and (c) C(1s) regions for monolayers from PFDT at gold.

Figure 4. XPS in the (a) S(2p), (b) O(1s), (c) N(1s), (d) C(1s), and (e) Au(4f) regions for DSP-derived monolayer/Au (solid line), anti-*E. coli* O157:H7/DSP-derived monolayer/Au (long dash line), and *E. coli* O157:H7/anti-*E. coli* O157:H7/ DSP-derived monolayer/Au (dotted line).

Figure 5. EQCM responses for the reductive desorption of DSP-derived monolayer (a), and PFDT-based monolayer (b) on pseudo-Au(111). The supporting electrolyte was 0.1 M KOH/ethanol, and sweep rate equalled 0.1 V s^{-1}.

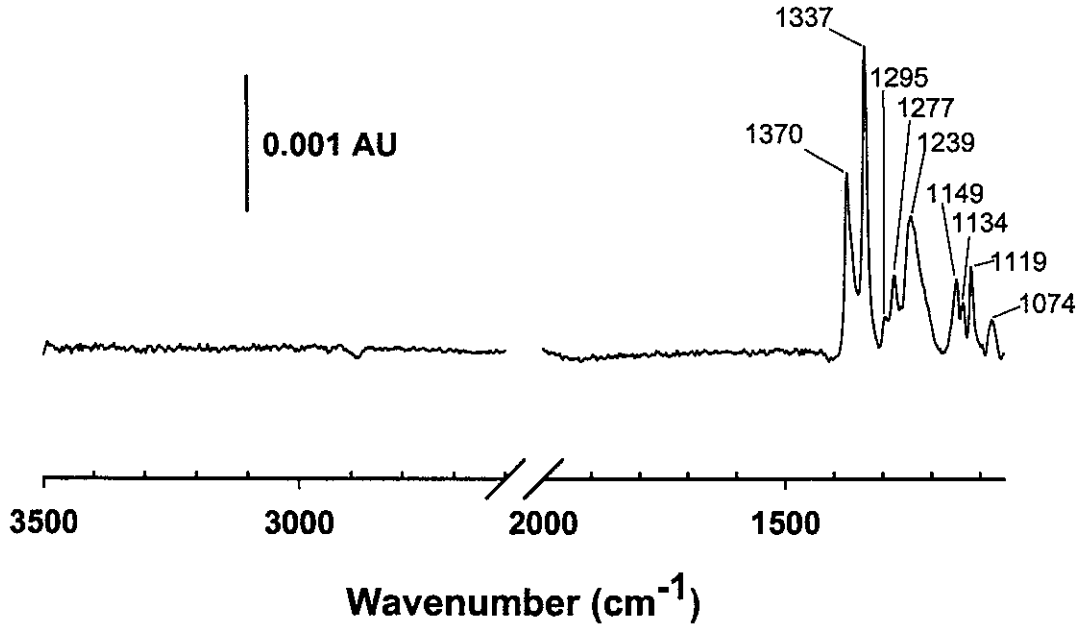
1337
1295
1277
1370
1239
1149
1134
1119
1074
0.001 AU
3500
3000
2000
1500
Wavenumber (cm-1)

Figure 1

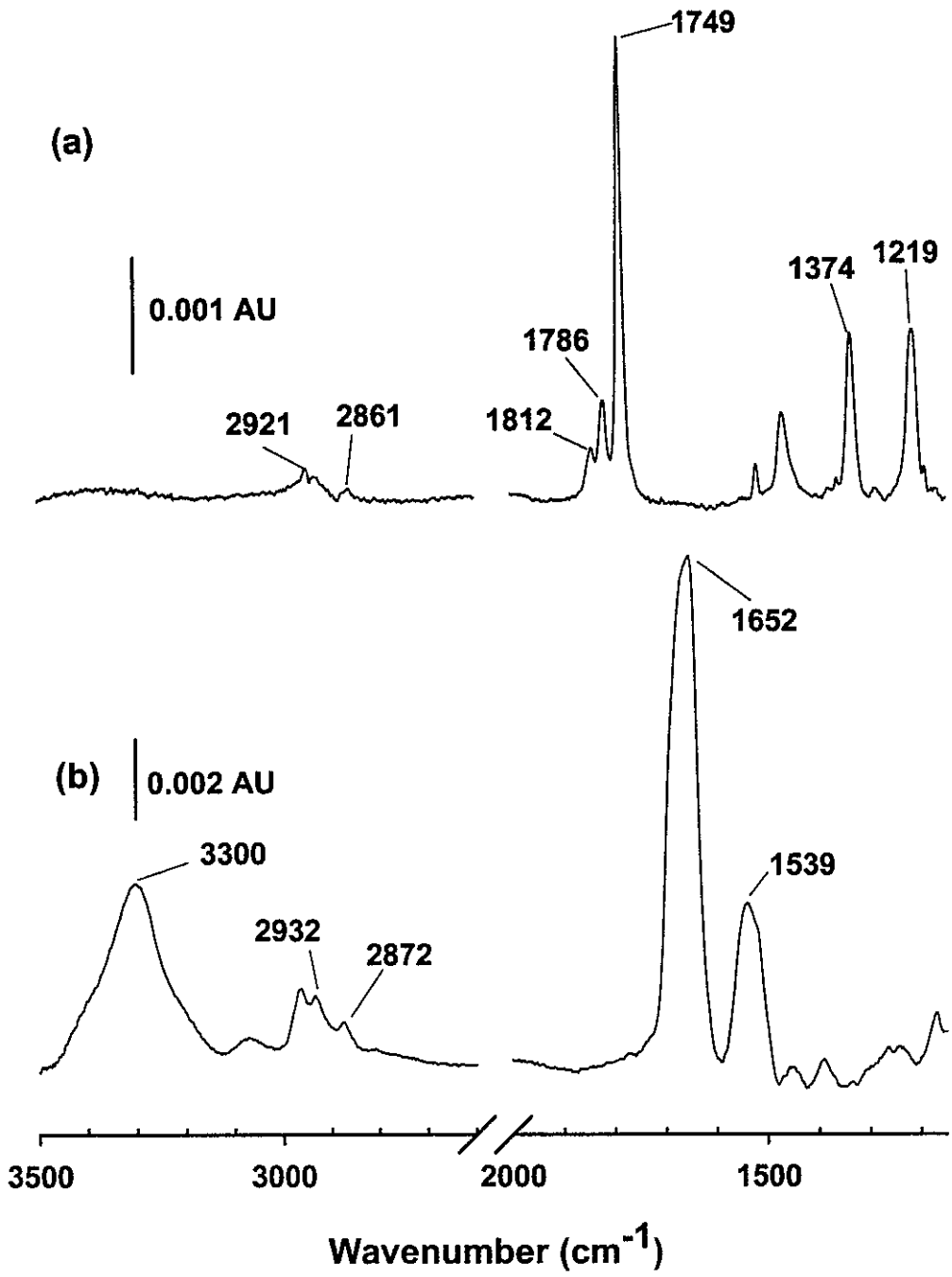
(a)
0.001 AU
1749
1786
1812
1374
1219
2921
2861
(b)
0.002 AU
1652
3300
1539
2932
2872
3500
3000
2000
1500
Wavenumber (cm-1)

Figure 2

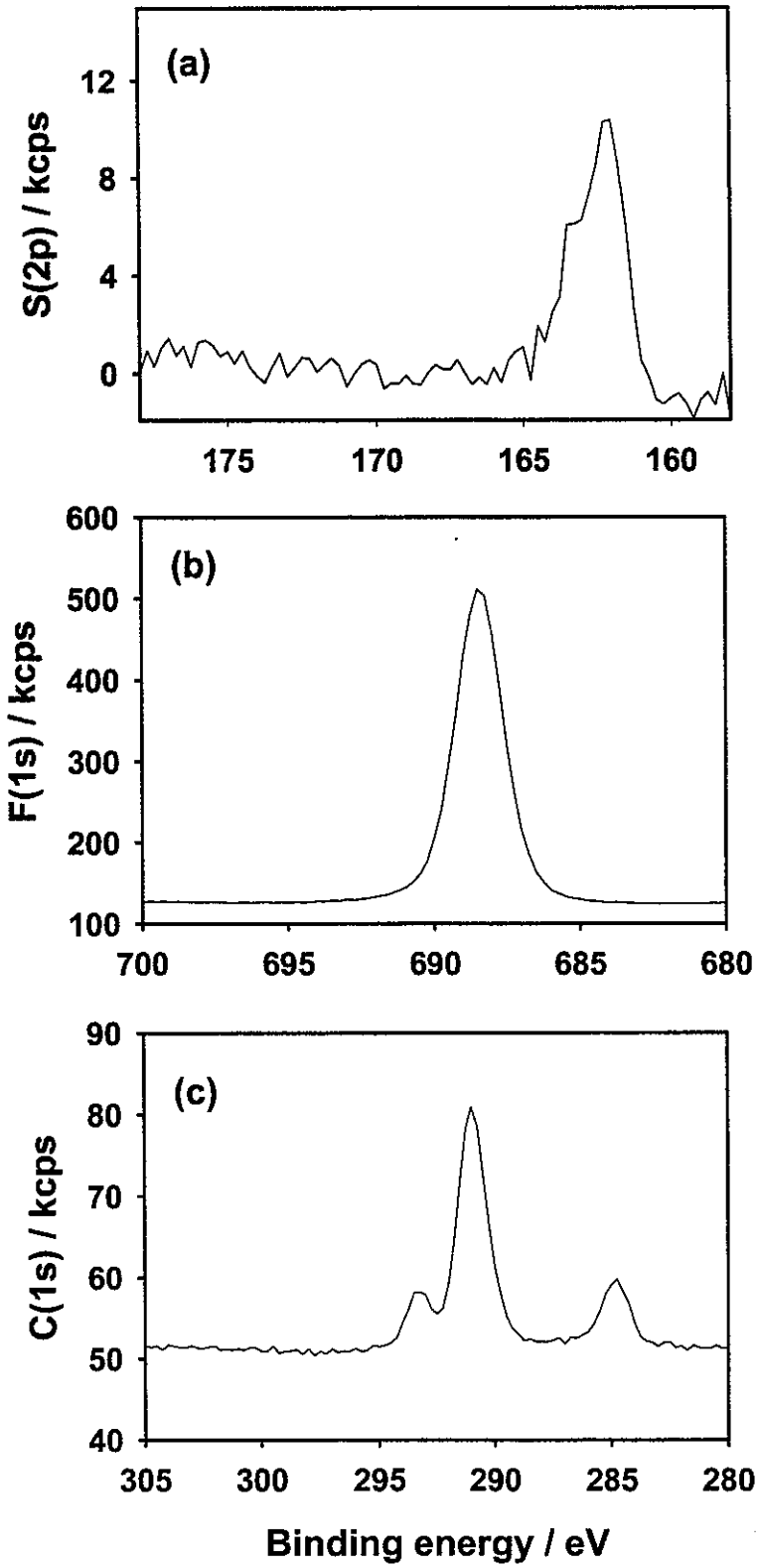
(a)
S(2p) / kcps
12
8
4
0
175
170
165
160
(b)
F(1s) / kcps
600
500
400
300
200
100
700
695
690
685
680
(c)
C(1s) / kcps
90
80
70
60
50
40
305
300
295
290
285
280
Binding energy / eV

Figure 3

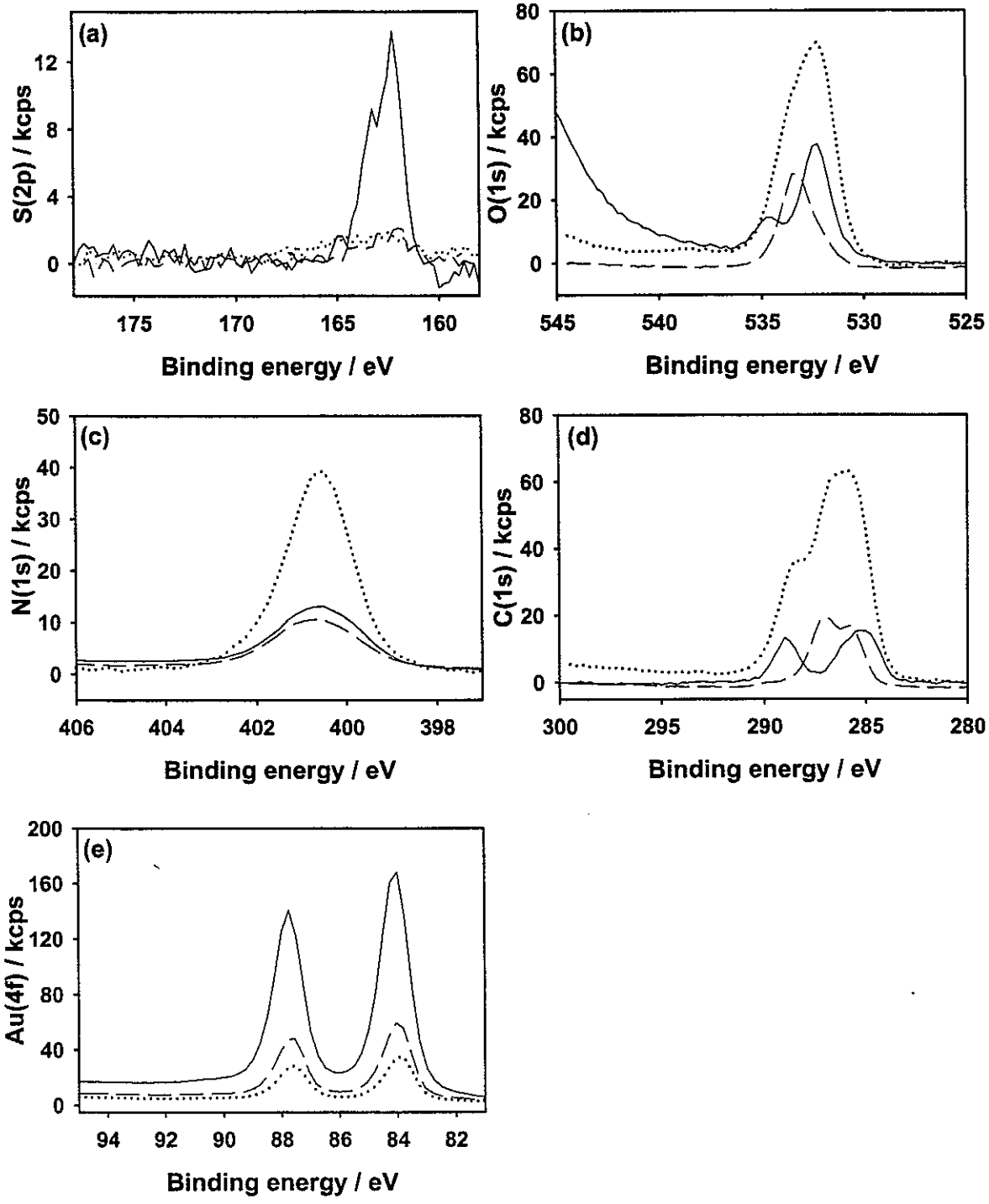
(a)
S(2p) / kcps
12
8
4
0
175
170
165
160
Binding energy / eV
(b)
O(1s) / kcps
80
60
40
20
0
545
540
535
530
525
Binding energy / eV
(c)
N(1s) / kcps
50
40
30
20
10
0
406
404
402
400
398
Binding energy / eV
(d)
C(1s) / kcps
80
60
40
20
0
300
295
290
285
280
Binding energy / eV
(e)
Au(4f) / kcps
200
160
120
80
40
0
94
92
90
88
86
84
82
Binding energy / eV

Figure 4

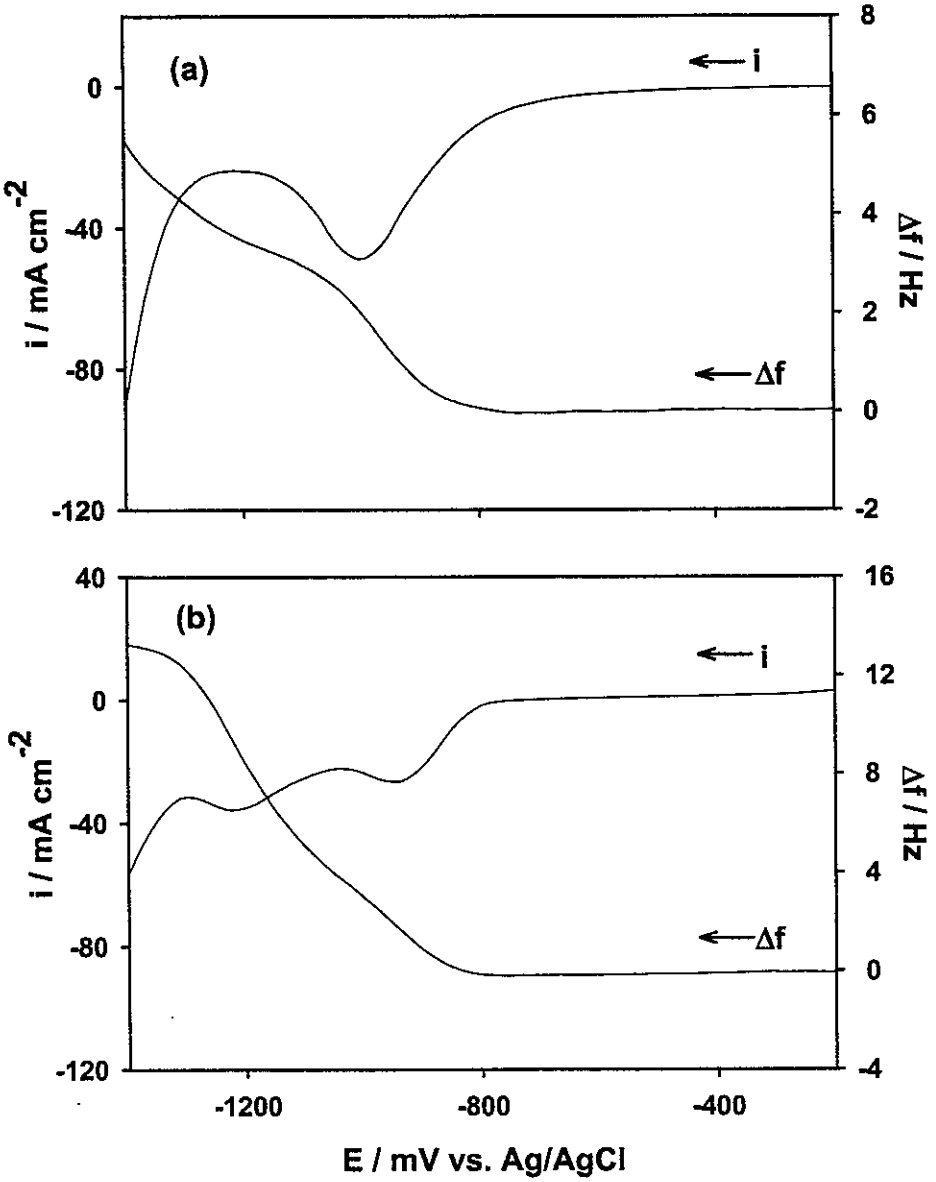
(a)
i
Δf
i / mA cm-2
Δf / Hz
0
-40
-80
-120
8
6
4
2
0
-2
(b)
i
Δf
i / mA cm-2
Δf / Hz
40
0
-40
-80
-120
16
12
8
4
0
-4
-1200
-800
-400
E / mV vs. Ag/AgCl

Figure 5

Table 1. Electrochemical values of self-assembled monolayers (SAMs) and bare gold in 0.1 M potassium hydroxide ethanolic solution (Charge (Q) was integrated current from -0.5 V to -1.35 V).

	DSP-derived SAM	**PFDT-derived SAM**	**Uncoated gold**
E_{PZC}[a] /V	+0.043±0.007	-0.250±0.010	+0.018
C_{dl}[b] /μF cm^{-2}	7.5±2.3	0.090±0.03	57.5
Q_{total}[c] /μC cm^{-2}	179.2	169.9	
Q_f[d] /μC cm^{-2}	40.8	50.7	
Q_{dl}[e] /μC cm^{-2}	75.2	78.6	
Q_{rd}[f] /μC cm^{-2}	63.2	40.5	
$\Gamma_{rd,2}$[g] /mol cm^{-2}	6.6±0.9 x10^{-10}	4.2±0.5x10^{-10}	
Q_{linear}[h] /μC cm^{-2}	51.6±7.3	44.3±4.8	
$\Gamma_{rd,1}$[i] /mol cm^{-2}	5.4±0.8x10^{-10}	4.6±0.5x10^{-10}	
$\Gamma_{expected}$[j] /mol cm^{-2}	5.9x10^{-10}	5.4x10^{-10}	
Δf[k] /Hz	6.06±0.64	13.81±0.64	
Δm[l] /ng cm^{-2}	107.26±11.3	244.35±11.3	
mpe[m] /g mol^{-1}	165	581.8	
Final mass /g mol^{-1}	148.5	229.8	
Initial mass /g mol^{-1}	313.5	811.6	
Molecular weight of corresponding thiolate /g mol^{-1}	201.2	480.9	
Mass of associated solvated cation /g mol^{-1}	112.3	400.7	
Association number of solvated cation per thiol	0.64	2.2	

a. Potential of zero charge determined by measurement of differential capacitance curve in 10 mM KOH in ethanol at 0.01V s^{-1}. b. Double layer capacitance measured by cyclic voltammogram in 0.1 M KOH in ethanol at 0.1 V s^{-1}. c. $Q_{total} = Q_{rd} + Q_{dl} + Q_f$ d. Background faradaic process that results from the low level of hydrogen generation. Q_f was simulated by Tafel plot in hydrogen generation region (under -1.35 V) in the cyclic voltammogram of reductive desorption of thiolate in 0.1 M KOH in ethanol solution at 0.1 V s^{-1}. e. Nonfaradaic current that flows to charge the double layer as a consequence of adlayer desorption. f. Observed desorption charge. g. Surface coverage calculated from more exacting treatments. h. Reduction charge estimated from linear extrapolation. i. Surface coverage calculated from Q_{linear} j. Calculated based on closest packed models. k. Change in resonance frequency. l. Mass change. m. Mass change per mole of electrons

CHAPTER 3: RAPID DETECTION OF PATHOGENIC BACTERIA USING A FIELD DEPLOYABLE HAND HELD DIFFUSE REFLECTANCE SPECTROMETER

A paper in preparation for submission to *Analytica Chimica Acta*

Salma Rahman, Robert J. Lipert, and Marc D. Porter *

Institute of Combinatorial Discovery, Ames laboratory-USDOE, and Department of Chemistry and of Chemical and Biological Engineering, Iowa State University, Ames, IA 50011 USA

Abstract

A new methodology for the rapid identification and quantification of pathogenic bacteria (e.g., *E. coli* O157:H7) is described. It combines the selectivity of dye-labeled antibodies, the sample concentration capability of solid phase extraction, and the facile readout of the extracted, dye-labeled microorganisms by diffuse reflectance spectroscopy. The amount of captured bacteria is directly determined in only 2 s by using a hand-held diffuse reflectance spectrometer via comparisons of the result with a calibration curve based on the Kubelka-Munk function. Details about the selection of proper membrane filter, optimization of the amount of labeled antibody relative to the target, detection of target bacteria in different sample media, and evaluation of specificity of the assay are also discussed. The calibration curve for *E. coli* O157:H7 by this technique has a working range of 5×10^5–5×10^8 cells/mL with a correlation coefficient of 0.982. The overall work up time is ~45 min, and the measurement can be performed almost anywhere. Overall, this assay system offers high speed, simplicity, and low cost, making it a potential alternative for the field screening of bacterial contaminated samples.

*Corresponding Author

Introduction

Bacterial contamination of food and water is a long standing problem around the globe.[1] The Center for Disease Control and Prevention (CDC) has estimated that in the United States microbial pathogens in food cause 76 million cases of human illness, 325000 hospitalizations, and up to 5000 deaths annually.[2] The breadth of the problem is further underscored by the concomitant loss of billions of dollars every year due to medical costs and low productivity. Clinical, environmental, and industrial analysts therefore continue to seek breakthroughs in the development of rapid, inexpensive, and easy-to-use methodologies to investigate microbial contamination.[3] Ideal requirements of a microbial detection system are as follows: accuracy, rapid response time, sensitivity, reproducible, facile (if any) sample pretreatment, negligible interference from the culture, sample matrix, or other enrichment conditions, and a large dynamic range. The instrument should also be easy to calibrate, portable, user friendly, and operable at low cost.[4] Despite significant improvements, there is no single method that is completely satisfactory for determining bacterial contaminations.[4]

Although traditional culture-based bacteria detection techniques are sensitive, they are labor intensive, cumbersome, and time consuming (2-5 days for completion).[2, 5, 6] In the event of an outbreak, rapid methods can improve the probability of identifying the source, and ultimately, controlling the spread of contaminations.[7] Many of the current analytical methods require long sample-preparation and analysis times, as well as complex instrumentation. Common methods employed for the identification and enumeration of bacteria include counting and analyzing cells by optical microscopy or by flow cytometry, measuring physical parameters by piezocrystals, impedimetry, redox reactions, optical methods, and calorimetry; and detecting cellular compounds such as ATP (by

bioluminescence), DNA, proteins and lipid derivatives by biochemical methods, and radioactive labeling.[1] Low level of detection (e.g., ~10^3 cells/mL) in a short time period (~1h) has only been possible using PCR, fluorescence, ELISA, electrochemistry, and electrochemiluminesence techniques without a lengthy pre-enrichment step.[8-16] However, pre-enrichment steps are required by most of the methods in order to allow the target organism to multiply[17-23] and even without pre-enrichment, some methods are lengthy (>6 h).[2, 7, 24]

Immunoanalytical methods are attractive because antibodies can be developed not only for recognizing proteins, but also for the surface antigens of microorganisms and for low-molecular-weight compounds. The specificity and high affinity of the antibody–analyte interaction significantly simplifies sample pretreatment.[25] Most of the immunoanalytical procedures, including immunosensor systems, are based on multistep assays and deliver a signal some time after the introduction of the analyte.[25] Several immunosensor systems using labels (e.g., radioisotopes, fluorophores, enzymes) or no labels (e.g., acoustic or optical) have been developed. Label-free mass-sensitive detection methods for whole cells, with specific antibodies immobilized on the transducer surface, are potentially ideal because they offer a real time output, simplicity of use, and low cost.[1, 26] However, acoustic sensors are of only limited reusability[27] and also immobilized antibodies may have a sterically limited access to cell-surface antigens. Alternatively, surface plasmon resonance (SPR) has been used to detect bacteria, but sensitivity (5-7 x 10^7 CFU/mL) remains a challenge[28] and the high degree of non-specific binding can prove problematic.[29]

Many microbial assays are currently based on solid phase enzyme linked immunoassays (ELISA), with detection limits of ~10^5 cells/mL.[20, 30] Although ELISA is

quite sensitive and has high throughput, it requires long incubation time, extensive sample manipulation, and tends to yield positive results that cannot be confirmed by culturing.[6, 31, 32]

Flow cytometry based instruments have outstanding resolution and capacity for real time measurements,[33-37] but hardware cost and the need for skilled personnel for sample preparation and operation limit its portability.[38, 39]

Electrochemical techniques were also used for bacteria detection. Impedimetric and conductimetric methods dictate lengthy incubation times in order to achieve a detectable signal. The same challenge limits the use of potentiometry[4] and amperometry.[40 41, 42] Amperometry may also been affected by interfering redox reactions.[43]

DNA based analytical methods, e.g., detection of a specific DNA sequence by amplification using PCR and hybridization of the products to immobilized oligonucleotides (DNA chip), are the most sensitive approaches for detecting microorganisms.[9, 44-50] However, they require the extraction of DNA from the sample, specialized personnel and equipment,[2, 25] and are comparatively expensive.[19] Sometimes, the total process can be long (>8 h)[51] and may involve a pre-enrichment step for low level detection.[21, 52] Also, PCR techniques can be inhibited by components of the sample matrix[21] which limits the examination of environmental samples due to widespread presence of common genes (e.g., shiga toxins 1 and 2) in bacteria.[6]

In this paper, we report a new rapid methodology for the identification and quantification of target bacteria that combines the selectivity of a dye-labeled antibody, the sample concentration capability of solid phase extraction, and the facile and rapid readout of diffuse reflectance spectroscopy. As a starting point, we used *E. coli* O157:H7, a food borne pathogenic bacteria. Infections caused by *E. coli* O157:H7 may progress to life-threatening

complications such as hemolytic uremic syndrome and hemorrhagic colitis in humans.[53] Our technique is based on staining the target bacteria with dye labeled antibodies followed by concentration of the bacteria using membrane filtration, and direct measurement (within 2 s) on membrane using diffuse reflectance spectroscopy. The complete process takes less than 1 h to complete. For staining target bacteria, we used Cy5™-anti-*E. coli* O157:H7 because Cy5™ is not only a fluorophore compound but a dye with a high molar extinction coefficient. The DRS instrument employed is compact, hand-held, portable, and sensitive, which is ideal for field applications. Our laboratory has previously demonstrated, and continues to advance, the development of colorimetric solid-phase extraction (C-SPE) and DRS as an on-membrane readout technique to meet the operational requirements imposed by NASA for on-orbit biocide determinations in spacecraft water.[54-59] This work builds on that background.

Experimental Section

Materials and reagents. Heat-killed *E. coli* O157:H7, *Salmonella typhimurium*, *Staphylococcus aureus*, and *Listeria monocytogenes* were kindly provided by Dr. Cornick of the Department of Veterinary Microbiology and Preventive Medicine, Iowa State University. Affinity-purified goat anti-*E. coli* O157:H7 was acquired from USBiological. Anti-*E. coli* O157:H7 was conjugated with Cy5™ bisfunctional dye (*N*-hydroxysuccinimide ester linker) using FluoroLink-Ab-Cy5™ kit (GE Health Care, formally Amersham Pharmacia Biotechnology). Membra-Fil® and Anopore® membrane filters (13 mm) were obtained from Whatman. Durapore®, Millipore Express®, and Isopore™ (13 mm) were purchased

from Millipore. Swinnex filter holders (13 mm, part # 09-753-10ASX00 0013 00) were acquired from Fisher.

Instrumentation. (i) Diffuse reflectance spectrometer. A BYK-Gardner color-guide sphere *d*/8° spin diffuse reflectance spectrophotometer (model PCB-6830) was used to acquire the spectral data from the membrane filters. This hand-held spectrophotometer is small (8.1 × 17.8 × 9.4 cm), light in weight (0.5 kg), battery operated (4 AA batteries), and acquires reflectance data from 400 to 700 nm at 20-nm intervals in ~2 s. The aperture of the integrating sphere is 11 mm, which matches the area of the membrane surface exposed to the sample.

(ii) Epifluorescence microscopy. A Nikon Eclipse TE200 inverted microscope, equipped with a Prairie Technologies epifluorescent system that consisted of a uniblitz shutter, a mercury light source with a Prairie Technologies filter wheel, and a Hamamatsu C4742-95 CCD camera (6.7 x 6.7 μm pixels in a 1280 x 1024 pixel format), was employed for fluorescence imaging. This system also has a Prairie Technologies NeD microscope attachment for simultaneous imaging at multiple wavelengths. A filter cube, i.e., XF110/E/XC102 for Cy5™ (Omega Optical), was used to match the fluorescence emission of the Cy5™ dye. Images were analyzed with a Metaview system (MetaMorph) from Universal Imaging Corporation.

Method development. (i) Labeling antibody with Cy5™ dye. Anti-*E. coli* O157:H7 (1 mL, 1 mg/mL) was conjugated with Cy5™ by following the vendor specified protocol which is designed for labeling the amine groups of 1 mg of protein. The average dye/protein molar ratio was estimated from the absorbance values obtained by transmission spectrophotometry of the Cy5™ dye and antibody at 650 nm and 280 nm, respectively, using

the following expression: [Cy5™ dye]/[Antibody] = ([A_{650}/250000 M^{-1} cm^{-1}]/[A_{280} - (0.05 x A_{650})]/170000 $M^{-1}cm^{-1}$).[60] This procedure yielded a dye/protein molar ratio of ~4, with the molar ratio estimated for each new batch of labels.

(ii) General protocol for *E. coli* O157:H7 staining and diffuse reflectance measurements. Stock *E. coli* O157:H7 (~10^8 cells/mL, exact values determined before each experiment by flow cytometry measurement at the Cell and Hybridoma Facility of the Iowa State University) was diluted with phosphate buffered saline (PBS) to yield a final volume of 1.0 mL. Cy5™-labeled anti-*E. coli* O157:H7 (see below for details about optimization of this step) was added and the solution was incubated at 37°C for 45 min with mild rotation (85 rpm) in a rotary incubator shaker. Blank samples, devoid of *E. coli* O157:H7, were prepared by the same procedure.

Figure 1 represents the general detection scheme.[59] A 1-mL plastic syringe is filled with 0.85 ± 0.01 mL of an *E. coli* O157:H7 sample, then connected to the membrane holder via a Luer Lock fitting, which captures the bacteria from the sample upon its passage through a membrane mounted in the holder. The membrane filter is then dried by passing ~60 mL of air from another syringe. Next, the filter holder is disassembled and the membrane removed. The membrane is then placed in the sample locator for the spectrometer and a diffuse reflectance spectrum is acquired. This entire process, beginning with syringe filling, requires ~60 s.

(iii) Data manipulation. After collecting a spectral data set, the spectrophotometer was interfaced to a computer using a serial cable. The reflectance spectra were downloaded into a MS-Excel spreadsheet and the Kubelka–Munk function was calculated using an in-house-modified version of BYK-Gardner QC-Link software. The Kubelka-Munk (K-M) equation

provides an effective approach for relating the observed signal to the sample concentration for diffuse reflectance measurements.[61] The K-M function, *F(R)*, is defined as:

$$F(R) = (1-R)^2 / 2R$$

where R is the reflectance measured with respect to a standard white tile. The value of *F(R)* can be related to analyte concentration (C) by[62]

$$F(R) = 2.303\ \varepsilon C / s$$

where ε is the absorptivity of the analyte and s is the scattering coefficient of the membrane surface. By assuming the scattering coefficient and absorptivity of all membrane surfaces are constant at a given wavelength, *F(R)* can then be directly related to analyte concentration.

(iv) Selection of membrane filter. Five different membrane filters, all having a low affinity for nonspecific protein adsorption, were tested: Membra-Fil® (mixed cellulose esters, 80:20 ratio of cellulose nitrate to cellulose acetate), Anopore® (high purity alumina matrix), Durapore® (polyvinylidene fluoride), Millipore Express® (polyethersulfone), and Isopore™ (polycarbonate). All membranes had a diameter of 13 mm; all pore sizes were 0.45 μm except Millipore Express®, which was 0.22 μm. *E. coli* O157:H7 (50 μL, 1.2 x 10^8 cells/mL) was labeled with Cy5™-anti-*E. coli* O157:H7 (40 μL) and extracted on the membrane filters as detailed earlier.

(v) Optimization of amount of antibody. Different volumes of Cy5™-anti-*E. coli* O157:H7 (e.g., 10, 20, 30, 40, and 50 μL) were added to *E. coli* O157:H7 (100 μL, 3.6 x 10^8 cells/mL). The sample\blank was then diluted with PBS to a final volume of 1.0 mL. The solution was incubated and extracted on a Membra-Fil® membrane as described earlier.

Evaluation of assay specificity by determining *E. coli* O157:H7 in presence of other bacteria. Cy5™ anti-*E. coli* O157:H7 (45 μL) was added to *E. coli* O157:H7 solution (50 μL, 1.5 x 10^8 cells/mL) or to 100 μL of 1:1 (volume) mixture of *E. coli* O157:H7 (1.5 x 10^8 cells/mL) and second pathogenic bacterium [*Salmonella typhimurium* (3.3 x 10^8 cells/mL), *Staphylococcus aureus* (2.6 x 10^8 cells/mL), or *Listeria monocytogenes* (1.4 x 10^7 cells/mL)]. The solution was made up to 1.0 mL with PBS, incubated, and extracted on the Membra-Fil® membrane filter as described earlier.

Results and Discussion

In all experiments, the number of captured *E. coli* O157:H7 on the membrane filter was calculated based on the concentration of *E. coli* O157:H7 in solution and the volume of sample passed through the membrane (0.85 mL). The wavelength of maximum absorbance and the molar extinction coefficient of Cy5™ dye in aqueous solution are 649 nm and 250000 $M^{-1}cm^{-1}$, respectively. Because of the 20-nm resolution of the spectrometer, *F(R)* values at 660 nm were used to quantitate Cy5™ anti-*E. coli* O157:H7 labeled *E. coli* O157:H7.

Selection of membrane filter. Passage of solutions containing antibody-stained bacteria through each membrane filter (pore size <0.5 μm) results in the concentration of the sample on the membrane. Figures 2 (a) and (b) present the diffuse reflectance spectra for extracted samples (*E. coli* O157:H7 (5.1 x 10^6 cells) + Cy5™ anti-*E. coli* O157:H7) and blanks (only Cy5™ anti-*E. coli* O157:H7) that were obtained using each of the membrane filters. Interestingly, the response for the each membrane differed throughout the collected spectral

region for both the sample and blank experiments. At 660 nm, the *F(R)* values were: Membra-Fil®: sample 0.067, blank 0.024; Anopore®: sample 0.054, blank 0.033; Durapore®: sample 0.025, blank 0.010; Millipore Express®: sample 0.014, blank 0.005, and Isopore™: sample 0.031, blank 0.017.

From a purely filtration perspective, the response for the samples is expected to be independent of membrane material. There are, however, a variety of factors that likely contribute to the observed difference. These factors span differences in the optical properties of the membrane material and the impact of the chemical composition of the membrane material on nonspecific antibody adsorption. The former relates to the diffuse reflection process. When light impinges upon a textured sample, such as analyte captured membrane, a substantial portion of the incident radiation penetrates into the sample interior. This penetrating radiation undergoes a combination of scattering and wavelength-dependent absorption events and then re-emerges from the sample. The re-emitted light constitutes diffuse reflection. As a consequence, *F(R)* depends on scattering coefficient of the membrane surface, texture, and sampling depth as well as distribution of sample within the membrane and on the surface.

These optical effects are superimposed on the strong likelihood that the amount of nonspecific binding of the dye-labeled antibody to each type of membrane is compositionally dependent. We have not, however, attempted to assess the relative contribution of the different factors. Based on Figure 2, the membranes can be ranked in terms of performance by the subtraction of the signal of the blank from that of the sample. The ranking in descending order is: Membra-Fil® >Anopore® >Durapore® >Isopore™ > Express®. Thus, from a detection viewpoint, the Membra-Fil® membrane is the most effective of those tested.

Moreover, the physical handing of the Membra-Fil® membrane, due to its rigidity, is reasonably facile. On the other hand, the Anopore® membranes are mechanically brittle whereas the Isopore™ membranes are compliant. Both properties complicated the physical manipulations needed to mount the membranes in the filter holder and the sample position locator of the spectrometer. Taken together, these factors led to the selection of the Membra-Fil® membrane filters for all subsequent experiments.

Another criterium central to the overall assay is the ability to exhaustively collect all of the bacteria in a sample on the filter. We therefore checked whether all of the *E. coli* O157:H7 in a sample were captured by the membrane by probing for the presence of labeled *E. coli* O157:H7 in a sample by using epifluorescence microscopy before and after filtration. Roughly 10 images were analyzed for each case. Examples of these findings are shown in Figure 3. The images of the solution before filtration showed the presence of a large number of labeled *E. coli* O157:H7 (Figure 3a). Numerous individual and a few small aggregates of the labeled organisms are evident, and are superimposed on the fluorescence response of the excess labeled antibody. On the other hand, all the images of the solution after filtration are devoid of the presence of *E. coli* O157:H7 (Figure 3b). Thus, we concluded that the Membra-Fil® membrane is highly effective in the capture of these labeled microorganisms.

These data also can be used to estimate the concentration factor obtained in the filtration step. If we assume that the filtration step is fully exhaustive, the ratio of the sample to membrane volume yields one measure of the concentration factor. Based on the volume of sample (0.85 mL) and the thickness (0.013 cm) and radius (0.55 cm) of the membrane exposed to the sample, which translate to a membrane volume of 0.012 mL, a concentration factor of ~70 is obtained. We believe that this result is an underestimation of the

concentration factor due to the fact that the membrane pore size is much smaller than that of the organism and therefore the bacteria is not distributed throughout the entire volume of the membrane. Moreover, an earlier work with C-SPE has suggested concentration factors at least an order of magnitude larger.

Optimization of amount of Cy5™-anti-*E. coli* O157:H7. Figure 4 presents results for samples (a) and blanks (b) for the same number of *E. coli* O157:H7 (3.1×10^7 cells) stained with different amounts of Cy5™ anti-*E. coli* O157:H7. When the concentration of dye (i.e., amount of labeled antibody) is high, the large background from unbound labeled antibody may limit the ability to discriminate the signal between two samples with different *E. coli* O157:H7 concentrations. On the other hand, when concentration of dye is low, the signal from the labeled *E. coli* O157:H7 may also prove problematic. An effective determination therefore requires a compromise in the amount of dye-labeled antibody used to tag the organism.

As shown in Figure 4, *F(R)* values increased with both the sample and blank as the volume of Cy5™ anti-*E. coli* O157:H7 increases. In case of the blank, the signal originates from antibody nonspecifically adsorbed on the membrane, whereas the sample situation is more complicated. The sample signal is combination of two components: signal from antibody labeled *E. coli* O157:H7 and from excess antibody that is nonspecifically adsorbed on the membrane (i.e., background). Insights into the contributions of both can be roughly estimated as follows. If most of the labeled antibodies are bound to the microorganisms, there will be little left to nonspecifically bind to the membrane. At 40 μL, the ratio of Cy5™ anti-*E. coli* O157:H7 (40 μL, 0.48 mg/mL) to *E. coli* O157:H7 (3.1×10^7 cells) is calculated to be 2.5×10^6, which is approximately equal to the number of lipopolysaccharides (i.e.,

antigens) that are present on the outer cell membrane of Gram-negative bacteria (i.e., 2 x 10^6 molecules per cell).[63] This number at 30 μL is 1.8 x 10^6, a little less than the number of surface antigens. While only an idealized analysis, the 30 μL volume would leave little (if any) unbound labeled antibody to yield a background response.

Next, if we assume most of the captured bacteria reside on the surface of the membrane because of its small pore size (0.45 μm); the sample signal will grow at the expense of the response of the background if the bacterial surfaces are saturated with antibody. We suspect that the discontinuity observed between the 30 and 40 μL antibody volume arises from this occurence. Thus, the total signal will always represent a complex contribution from both factors that is only further complicated by the diversity in the size of the organisms in different stages of their life cycle. Keeping all the factors in mind, the optimum volume of Cy5™-anti-*E. coli* O157:H7 is between 40-50 μL in case of detection of ~1 mL *E. coli* O157:H7 solution but this optimum volume can vary from one batch of Cy5™ labeled antibody to another depending on the dye : antibody molar ratio.

Calibration plot. Solutions with different concentrations of *E. coli* O157:H7 (2.4 x 10^5, 4.8 x 10^5, 2.4 x 10^6, 4.8 x 10^6, 4.8 x 10^7, and 4.8 x 10^8 cells/mL) were prepared from the stock (4.8 x 10^8 cells/mL). Cy5™-anti-*E. coli* O157:H7 (45 μL) was added to each *E. coli* O157:H7 solution (955 μL), and the mixture was then incubated at 37 °C for ~45 min. The sample was extracted on the Membra-Fil® membrane filter, and a spectrum was acquired as described earlier; this process required ~60 s.

Figure 5 presents signals for different numbers of captured *E. coli* O157:H7 stained with the optimal amount of antibody. As mentioned in earlier section, both labeled *E. coli* O157:H7 and adsorbed excess antibody (i.e., background) constitute the signal. A

linear relationship between the Kubelka-Munk function *F(R)* and logarithmic value of *E. coli* O157:H7 concentration was observed in a range of concentration from 5 x 10^5–5 x 10^8 cells/mL, with a correlation coefficient (R^2) of 0.982, as presented in Figure 6. The inset in Figure 6 presents the results simply as a plot of the number of *E. coli* O157:H7. For each concentration, three sample solutions were passed through three separate membranes. The different points in the graph correspond to the average of the three replicates. The limit of detection (LOD), calculated by adding three times the standard deviation of the blank to the average of the blank, is ~2 x 10^5 cells/mL. This value is comparable with LOD achieved by other techniques (e.g., optical biosensor,[7, 64] piezoelectric biosensor,[1, 65-67] electrical impedance biosensors,[53, 68] surface plasmon resonance biosensor,[28, 69]) and commercial instruments[1, 4] for detection of bacteria. Moreover, the sensitivity of this system is similar to that of widely used ELISA based microbial assays (~10^5 cells/mL).[20, 30]

***E. coli* O157:H7 detection in different sample media.** Different sample media (e.g., 905 μL of PBS, tap water, and apple juice) were spiked with the same number of *E. coli* O157:H7 (50 μL, 2.9 x 10^8 cells/mL). The pH of apple juice was adjusted to 7.4 using sodium hydroxide before spiking with *E. coli* O157:H7, while tap water was used as collected. Real samples usually contain interfering matter and particulates. Therefore, pretreatment prior to analysis is needed. For pretreatment, we simply used a filtration step with a 5-μm pore size Membra-Fil® membrane filter. Cy5™-anti-*E. coli* O157:H7 (45 μL) was added to the filtered solution. The solution was incubated, extracted on the Membra-Fil® membrane filter (0.45 μm), and a diffuse reflectance spectrum was acquired.

Figure 7 presents signals for the same number of *E. coli* O157:H7 (1.2 x 10^7 cells) stained with same volume of Cy5™ anti-*E. coli* O157:H7 but in the three different sample

media. The *F(R)* values observed at 660 nm are: PBS ~0.089, tap water ~0.070, and pH-adjusted apple juice ~0.082. The adjustment of pH primarily arises from the acid-base chemistry of cyanine dyes.[70] The pK_a value, for example, of pentamethine cyanine dye (i.e., Cy5™) is ~7.5, with the pH of apple juice sample (originally pH ~3.8) then adjusted to ~7.4. Nevertheless, we attribute to lower *F(R)* values found for the tap water and apple juice samples to the absorptive loss of bacteria to debris and other macroscopic objects in the sample matrix.

Evaluation of specificity of the assay. To evaluate the specificity of the assay, *E. coli* O157:H7 was detected in the presence of other pathogenic bacteria. Figure 8 presents *F(R)* values observed for the same number of *E. coli* O157:H7 (6.4×10^6 cells) stained with the same volume of Cy5™ anti-*E. coli* O157:H7 in presence of other pathogenic bacteria. *F(R)* did not change significantly when other nontarget bacteria were present at the same or higher level of target bacteria (e.g., *F(R)* values at 660 nm: only *E. coli* O157:H7 ~0.077, mixture of *E. coli* O157:H7 and *Salmonella typhimurium* ~0.087, *E. coli* O157:H7 and *Staphylococcus aureus* ~0.085, and *E. coli* O157:H7 and *Listeria monocytogenes* ~0.077). The signal varied by ~13% in the of mixture of *E. coli* O157:H7 and *Salmonella typhimurium*, ~10% in the mixture of *E. coli* O157:H7 and *Staphylococcus aureus*, and only ~1% for the mixture of *E. coli* O157:H7 and *Listeria monocytogenes*. Thus, this procedure allows the detection of *E. coli* O157 in the presence of other notable pathogenic bacteria.

Conclusions and Future Work

The successful development and application of an analytical technique mainly depends on the ease of use, accuracy, sensitivity, analysis time, and cost effectiveness. In

this paper, we present a new rapid, sensitive, and portable solid phase extraction and diffuse reflection-based technique for the detection of *E. coli.* O157:H7 microorganisms. This technique can be easily adapted for the assay of other microorganisms and may be a basis for a new class of sensitive bioanalytical devices for rapid quantitative detection of bacteria. The calibration curve for *E. coli* O157:H7 by this technique has a working range of 5×10^5–5×10^8 cells/mL. The limit of detection (LOD ~10^5 cells/mL), achieved without any pre-enrichment step, is comparable with other techniques (e.g., by fluorescent labeled antibody based optical biosensor,[7, 64] by quartz crystal microbalance based piezoelectric biosensor,[1, 65-67] by electrical impedance biosensors,[53, 68] and by using surface plasmon resonance biosensor,[28, 69]). This LOD is also comparable with that of some commercial instruments (e.g., bioluminescence detection based Lumac Biocounter, electronic particle analysis based Ramus 265, surface plasmon resonance based BIA-core, impedimetry based Bactometer 32, conductance based Malthus 2000, amperometry based Midas Pro, and piezoelectric method based PZ 106 immuno-biosensor system[1, 4]). Our approach also uses a low level of costly reagents (i.e., the dye labeled antibody). Our developed technique is also fairly selective with respect to cross-reactivity to several other important pathogenic bacteria. Furthermore, our technique features a small, inexpensive, easy-to-use, and portable instrument for detection, and perhaps the greatest advantage is the total sample workup takes less than 1 h and the actual sample readout requires ~2 s.

Although the LOD for *E. coli* O157:H7 is higher than the infectious dose of *E. coli* O157:H7 (~10-100 cells),[31] it can be further improved by applying different concentration techniques, e.g., by using immunomagnetic separation or increasing the sample volume for filtration. We are currently exploring strategies to this end. Even without further

preconcentration, this technique can be applied to the detection of several other bacteria that have higher infectious doses, e.g., *Salmonella* ($>10^6$ cells),[12] simply by using the appropriate antibody. Therefore, although this technique has been demonstrated for a particular food borne pathogen, the method may be generalized to identify other microbes or groups of microbes, provided that appropriate dye-antibody probes are available. With combinations of different antibodies, each with a unique dye label, the concurrent analysis of two or more bacteria may be possible. Finally, the attributes of this assay system are very attractive with respect to high speed, simplicity, and low cost field deployment.

Acknowledgments

The authors express appreciation to Dr. Nancy Cornick of VMPM department of Iowa State University for providing all the bacteria. Funding for this work was provided by the United State Department of Agriculture Cooperative State Research, Education, and Extention Service (UDSA CSREES award number 20002-35201-12659) and by the Institute of Combinatorial Discovery of Iowa State University through the Roy J. Carver Laboratory for Ultra High Resolution Biological Microscopy. The Ames Laboratory is operated for the U.S. Department of Energy by Iowa State University under Contract W-7405-Eng-82.

References

(1) Ivnitski, D.; Abdel-Hamid, I.; Atanasov, P.; Wilkins, E. *Biosens. Bioelectron.* **1999**, *14*, 599-624.

(2) Kourkine, I. V.; Ristic-Petrovic, M.; Davis, E.; Ruffolo, C. G.; Kapsalis, A.; Barron, A. E. *Electrophoresis* **2003**, *24*, 655-661.

(3) Perez, F. G.; Mascini, M.; Tothill, I. E.; Turner, A. P. F. *Anal. Chem.* **1998**, *70*, 2380-2386.

(4) Hobson, N. S.; Tothill, I.; Turner, A. P. F. *Biosens. Bioelectron.* **1996**, *11*, 455-477.

(5) Dey, B. P., Lattuuada, C. P. *Microbiology laboratory guidebook, U. S. Department of Agriculture*, 3rd ed.: Washington, D. C., 1998.

(6) Oda, M.; Morita, M.; Unno, H.; Tanji, Y. *Appl. Environ. Microbiol.* **2004**, *70*, 527-534.

(7) Pyle, B. H.; Broadaway, S. C.; McFeters, G. A. *Appl. Environ. Microbiol.* **1999**, *65*, 1966-1972.

(8) Abdel-Hamid, I.; Ivnitski, D.; Atanasov, P.; Wilkins, E. *Biosens. Bioelectron.* **1999**, *14*, 309-316.

(9) Belgrader, P.; Benett, W.; Hadley, D.; Richards, J.; Stratton, P.; Mariella, R.; Milanovich, F. *Science* **1999**, *284*, 449-450.

(10) Brewster, J. D.; Mazenko, R. S. *J. Immunol. Methods* **1998**, *211*, 1-8.

(11) Gehring, A. G.; Patterson, D. L.; Tu, S. I. *Anal. Biochem.* **1998**, *258*, 293-298.

(12) Ho, J. A. A.; Hsu, H. W.; Huang, M. R. *Anal. Biochem.* **2004**, *330*, 342-349.

(13) Su, X. L.; Li, Y. B. *Anal. Chem.* **2004**, *76*, 4806-4810.

(14) Tortorello, M. L.; Stewart, D. S. *Appl. Environ. Microbiol.* **1994**, *60*, 3553-3559.

(15) Weimer, B. C.; Walsh, M. K.; Beer, C.; Koka, R.; Wang, X. *Appl. Environ. Microbiol.* **2001**, *67*, 1300-1307.

(16) Yu, H.; Bruno, J. G. *Appl. Environ. Microbiol.* **1996**, *62*, 587-592.

(17) Bukhari, Z.; Weihe, J.; LeChevallier, M. *Water Sci. Technol.* **2004**, *50*, 233-237.

(18) Gooding, C. M.; Choudary, P. V. *J. Dairy Res.* **1997**, *64*, 87-93.

(19) Goodridge, L.; Chen, J. R.; Griffiths, M. *Appl. Environ. Microbiol.* **1999**, *65*, 1397-1404.

(20) Seo, K. H.; Brackett, R. E.; Frank, J. F. *Intl. J. Food Microbiol.* **1998**, *44*, 115-123.

(21) Tims, T. B.; Lim, D. V. *J. Microbiol. Methods* **2003**, *55*, 141-147.

(22) Tu, S. I.; Patterson, D.; Briggs, C.; Irwin, P.; Yu, L. *J. Ind. Microbiol. Biotechnol.* **2001**, *26*, 345-349.

(23) Yu, L. S. L.; Reed, S. A.; Golden, M. H. *J. Microbiol. Methods* **2002**, *49*, 63-68.

(24) DeCory, T. R.; Durst, R. A.; Zimmerman, S. J.; Garringer, L. A.; Paluca, G.; DeCory, H. H.; Montagna, R. A. *Appl. Environ. Microbiol.* **2005**, *71*, 1856-1864.

(25) Bilitewski, U. *Anal. Chem.* **2000**, *72*, 692A-701A.

(26) Fung, Y. S.; Wong, Y. Y. *Anal. Chem.* **2001**, *73*, 5302-5309.

(27) Guilbault, G. G.; Luong, J. H. T. In *Food Sci. Technol. (N. Y.)*, 1994; Vol. 60, pp 151-172.

(28) Fratamico, P. M.; Strobaugh, T. P.; Medina, M. B.; Gehring, A. G. *Biotechnol. Tech.* **1998**, *12*, 571-576.

(29) Cullen, D. C.; Lowe, C. R. *Sens. Actuators, B* **1990**, *1*, 576-579.

(30) Acheson, D. W. K.; Lincicome, L. L.; DeBreucker, S.; Keusch, G. T. *J. Food Prot.* **1996**, *59*, 344-349.

(31) Blackburn, C. D.; McCarthy, J. D. *Intl. J. Food Microbiol.* **2000**, *55*, 285-290.

(32) Chapman, P. A.; Malo, A. T. C.; Siddons, C. A.; Harkin, M. *Appl. Environ. Microbiol.* **1997**, *63*, 2549-2553.

(33) Gunasekera, T. S.; Veal, D. A.; Attfield, P. V. *Intl. J. Food Microbiol.* **2003**, *85*, 269-279.

(34) McClain, M. A.; Culbertson, C. T.; Jacobson, S. C.; Ramsey, J. M. *Anal. Chem.* **2001**, *73*, 5334-5338.

(35) Mcclelland, R. G.; Pinder, A. C. *J. Appl. Bacteriol.* **1994**, *77*, 440-447.

(36) Pinder, A. C.; Purdy, P. W.; Poulter, S. A. G.; Clark, D. C. *J. Appl. Bacteriol.* **1990**, *69*, 92-100.

(37) Shapiro, H. M. *Cytometry* **2001**, *43*, 223-226.

(38) Rieseberg, M.; Kasper, C.; Reardon, K. F.; Scheper, T. *Appl. Microbiol. Biotechnol.* **2001**, *56*, 350-360.

(39) Vives-Rego, J.; Lebaron, P.; Nebe-von Caron, G. *FEMS Microbiol. Rev.* **2000**, *24*, 429-448.

(40) Ghindilis, A. L.; Atanasov, P.; Wilkins, M.; Wilkins, E. *Biosens. Bioelectron.* **1998**, *13*, 113-131.

(41) Brewster, J. D.; Gehring, A. G.; Mazenko, R. S.; VanHouten, L. J.; Crawford, C. J. *Anal. Chem.* **1996**, *68*, 4153-4159.

(42) Rishpon, J.; Ivnitski, D. *Biosens. Bioelectron.* **1997**, *12*, 195-204.

(43) Mello, L. D.; Kubota, L. T. *Food Chem.* **2002**, *77*, 237-256.

(44) Bopp, D. J.; Sauders, B. D.; Waring, A. L.; Ackelsberg, J.; Dumas, N.; Braun-Howland, E.; Dziewulski, D.; Wallace, B. J.; Kelly, M.; Halse, T.; Musser, K. A.; Smith, P. F.; Morse, D. L.; Limberger, R. J. *J. Clin. Microbiol.* **2003**, *41*, 174-180.

(45) Grant, M. A. *J. Food Prot.* **2003**, *66*, 18-24.

(46) Heller, L. C.; Davis, C. R.; Peak, K. K.; Wingfield, D.; Cannons, A. C.; Amuso, P. T.; Cattani, J. *Appl. Environ. Microbiol.* **2003**, *69*, 1844-1846.

(47) Ibekwe, A. M.; Grieve, C. M. *J. Appl. Microbiol.* **2003**, *94*, 421-431.

(48) Imamura, O.; Arakawa, H.; Maeda, M. *Luminescence* **2003**, *18*, 107-112.

(49) McKillip, J. L.; Jaykus, L. A.; Drake, M. *J. Food Prot.* **2002**, *65*, 1775-1779.

(50) Wang, G. H.; Clark, C. G.; Rodgers, F. G. *J. Clin. Microbiol.* **2002**, *40*, 3613-3619.

(51) Sharma, V. K.; Dean-Nystrom, E. A.; Casey, T. A. *Mol. Cell. Probe.* **1999**, *13*, 291-302.

(52) Campbell, G. R.; Prosser, J.; Glover, A.; Killham, K. *J. Appl. Microbiol.* **2001**, *91*, 1004-1010.

(53) Yang, L. J.; Li, Y. B.; Erf, G. F. *Anal. Chem.* **2004**, *76*, 1107-1113.

(54) Arena, M. P.; Porter, M. D.; Fritz, J. S. *Anal. Chem.* **2002**, *74*, 185-190.

(55) Arena, M. P.; Porter, M. D.; Fritz, J. S. *Anal. Chim. Acta* **2003**, *482*, 197-207.

(56) Fritz, J. S.; Arena, M. P.; Steiner, S. A.; Porter, M. D. *J. Chromatogr., A* **2003**, *997*, 41-50.

(57) Gazda, D. B.; Fritz, J. S.; Porter, M. D. *Anal. Chem.* **2004**, *76*, 4881-4887.

(58) Gazda, D. B.; Fritz, J. S.; Porter, M. D. *Anal. Chim. Acta* **2004**, *508*, 53-59.

(59) Gazda, D. B.; Lipert, R. J.; Fritz, J. S.; Porter, M. D. *Anal. Chim. Acta* **2004**, *510*, 241-247.

(60) Mujumdar, R. B.; Ernst, L. A.; Mujumdar, S. R.; Lewis, C. J.; Waggoner, A. S. *Bioconjugate Chem.* **1993**, *4*, 105-111.

(61) Kortum, G. *Reflectance spectroscopy: Principles, Methods, Applications*; Springer-Verlag: New York, 1969.

(62) Blitz, J. P. *Modern Techniques in Applied Molecular Spectroscopy*; John Wiley & Sons: New York, 1998.

(63) Philips, R. J., "Real Time Monitoring of Foodborne Pathogens: *State-of-the-Art Report*," Food Manufacturing Coalition, **1997**.

(64) Plomer, M.; Guilbault, G. G.; Hock, B. *Enzyme Microb. Tecnol.* **1992**, *14*, 230-235.

(65) Deisingh, A. K.; Thompson, M. *Analyst* **2002**, *127*, 567-581.

(66) Ivnitski, D.; Abdel-Hamid, I.; Atanasov, P.; Wilkins, E.; Stricker, S. *Electroanalysis* **2000**, *12*, 317-325.

(67) Ye, J. M.; Letcher, S. V.; Rand, A. G. *J. Food Sci.* **1997**, *62*, 1067-&.

(68) Silley, P.; Forsythe, S. *J. Appl. Bacteriol.* **1996**, *80*, 233-243.

(69) Koubova, V.; Brynda, E.; Karasova, L.; Skvor, J.; Homola, J.; Dostalek, J.; Tobiska, P.; Rosicky, J. *Sens. Actuators, B* **2001**, *74*, 100-105.

(70) Briggs, M. S.; Burns, D. D.; Cooper, M. E.; Gregory, S. J. *Chem. Commun.* **2000**, 2323-2324.

Figure Captions

Figure 1. General scheme for bacteria detection employing diffuse reflectance measurement of stained bacteria (e.g., *E. coli* O157:H7) captured on a membrane filter. Arrows indicate direction of fluid flow.

Figure 2. (a) Kubelka–Munk responses for *E. coli* O157:H7 (5×10^6 cells) labeled with Cy5™ anti-*E. coli* O157: H7 and (b) signals for blank (i.e., Cy5™ anti-*E. coli* O157: H7 only) captured on different membrane filters. Each plot is the average of two trials, which typically differed by ±2%.

Figure 3. Pseudo color fluorescence images of Cy5™ anti-*E. coli* O157: H7 labeled *E. coli* O157:H7 samples before (a) and after (b) filtration through a Membra-Fil® membrane filter (pore size 0.45 μm). The concentration of labeled *E. coli* O157:H7 in the test sample was 6×10^6 cells/mL.

Figure 4. (a) Kubelka–Munk responses for the same number of *E. coli* O157:H7 (3×10^7 cells) labeled with different amounts of Cy5™ anti-*E. coli* O157: H7. (b) Kubelka–Munk responses for blank samples (i.e., only Cy5™ anti-*E. coli* O157: H7). All experiments used a Membra-Fil® membrane filter. Each plot is the average of two trials, which typically differed by ±2%.

Figure 5. Kubelka–Munk responses for different concentration of *E. coli* O157:H7 labeled with same amount of Cy5™ anti-*E. coli* O157: H7 captured on Membra-Fil® membrane filter.

Figure 6. Calibration plot for *E. coli* O157:H7 measured by diffuse reflectance spectrometer (n=3 trials).

Figure 7. (a) Signals at entire wave length range and (b) signals at 660 nm for the same number of *E. coli* O157:H7 (1.2×10^7 cells) in different sample media labeled with same amount of Cy5™ anti-*E. coli* O157: H7 captured on Membra-Fil® membrane filter.

Figure 8. (a) Signals at entire wave length range and (b) signals at 660 nm for the *E. coli* O157:H7 (6.4×10^6 cells) and also mixture of same number of *E. coli* O157:H7 with other pathogenic bacteria labeled with same amount of Cy5™ anti-E. coli O157:H7 captured on Membra-Fil® membrane filter.

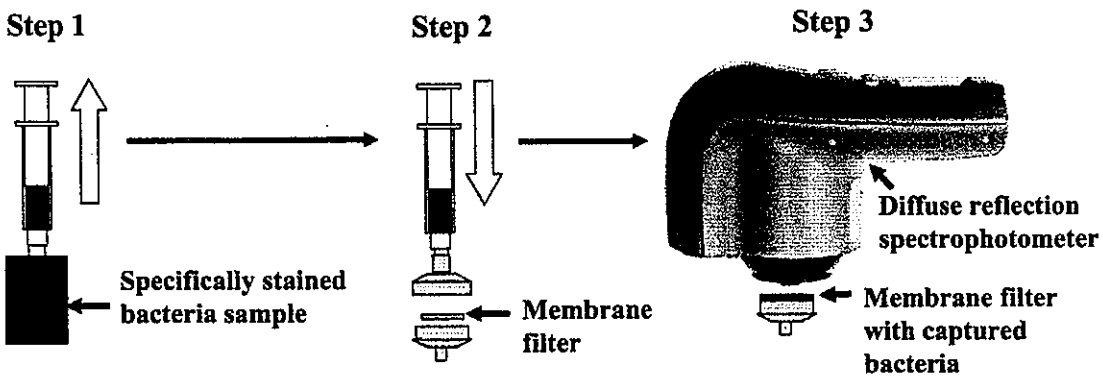
Step 1
Step 2
Step 3
Specifically stained bacteria sample
Membrane filter
Diffuse reflection spectrophotometer
Membrane filter with captured bacteria

Figure 1

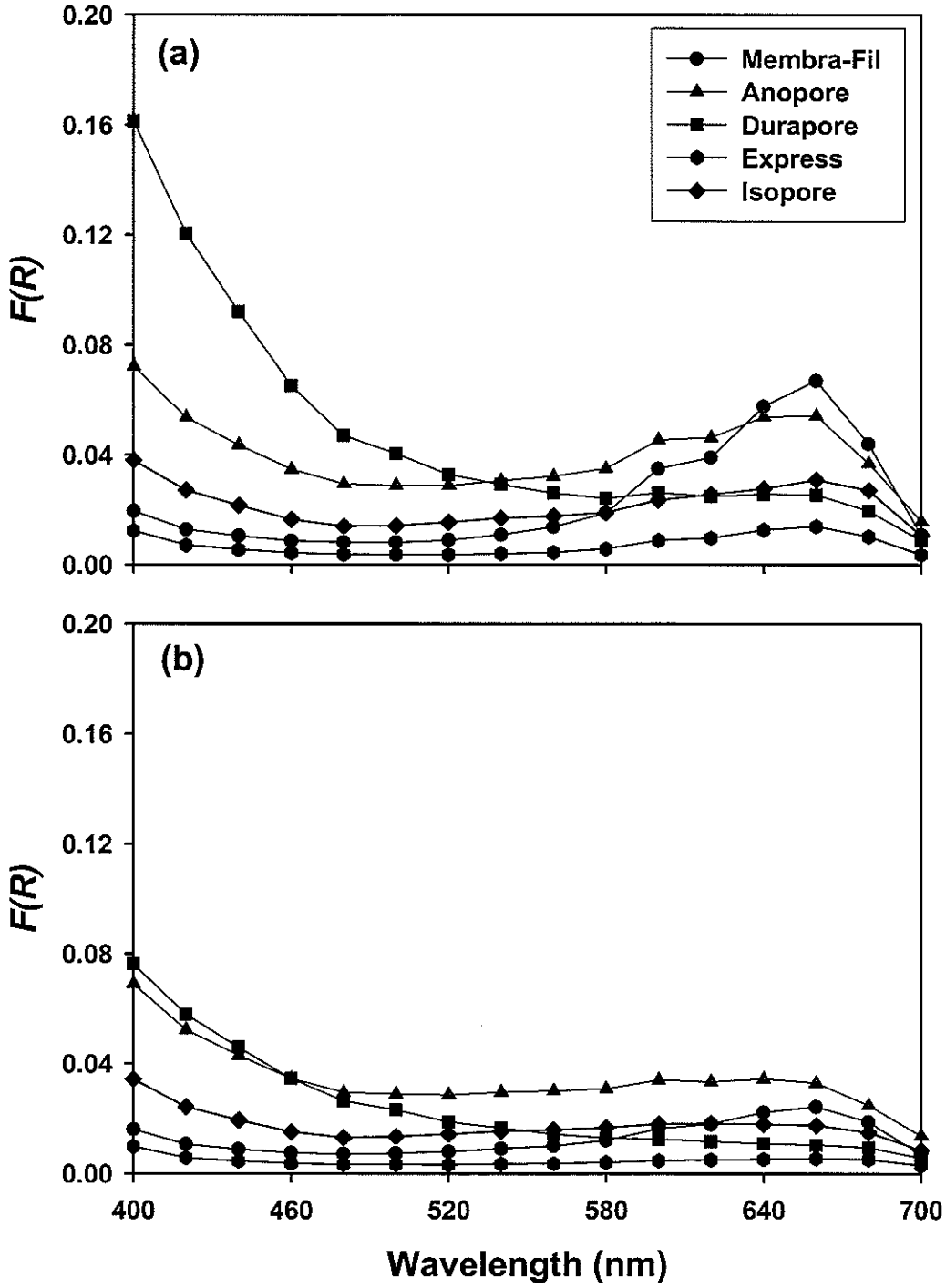
(a)
(b)
Membra-Fil
Anopore
Durapore
Express
Isopore
F(R)
0.20
0.16
0.12
0.08
0.04
0.00
400
460
520
580
640
700
Wavelength (nm)

Figure 2

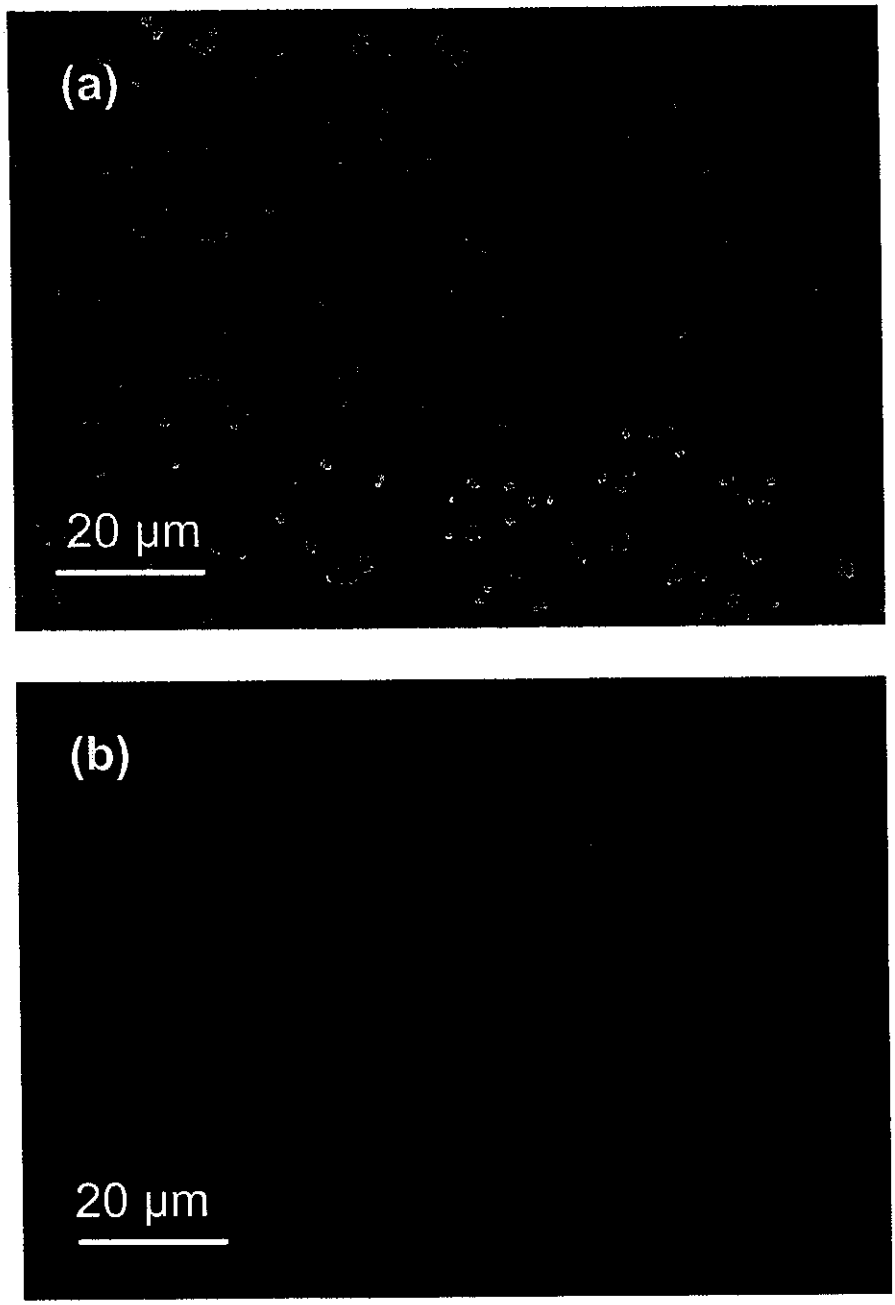

Figure 3

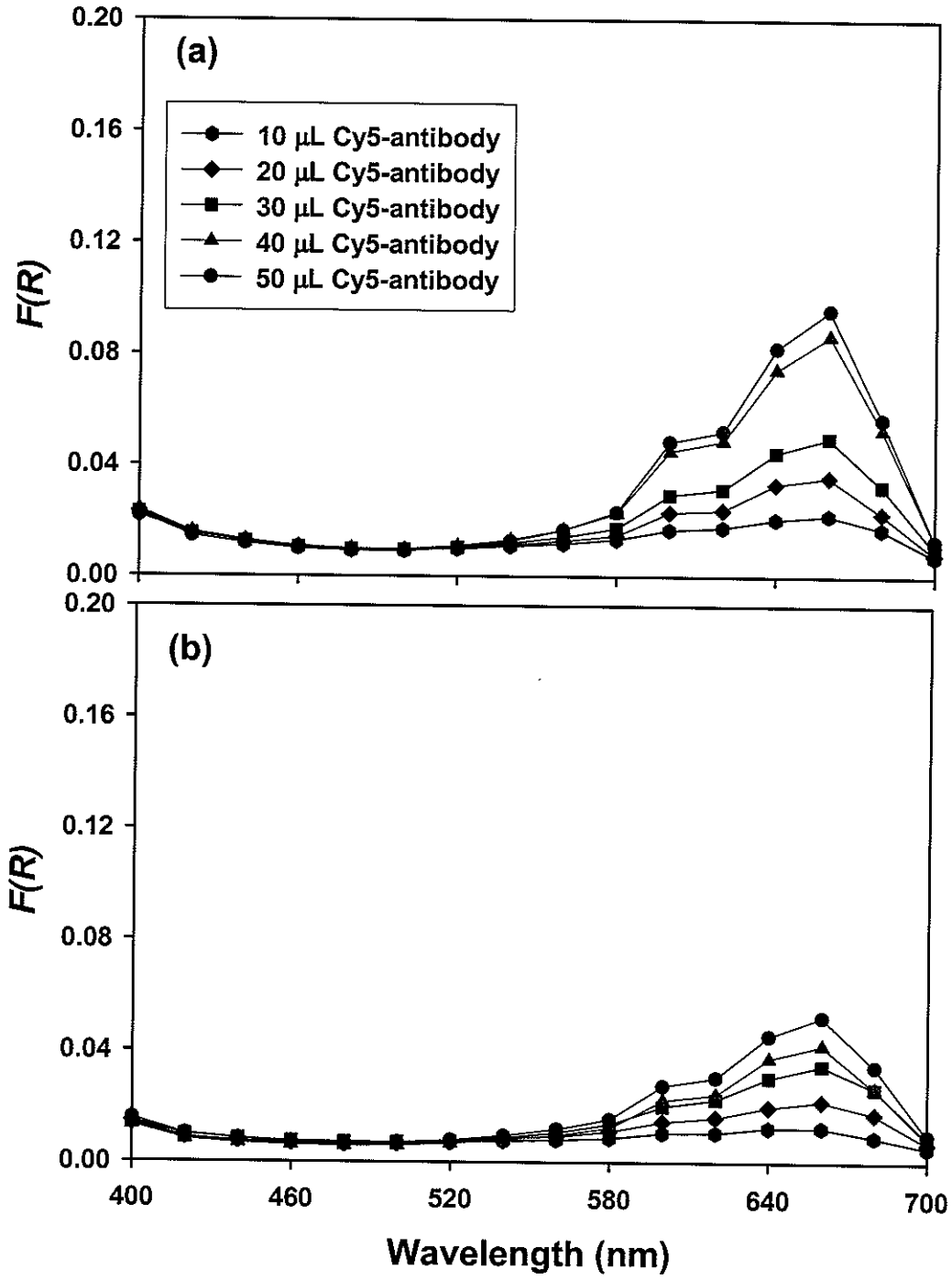
(a)
10 µL Cy5-antibody
20 µL Cy5-antibody
30 µL Cy5-antibody
40 µL Cy5-antibody
50 µL Cy5-antibody
F(R)
0.20
0.16
0.12
0.08
0.04
0.00
(b)
F(R)
0.20
0.16
0.12
0.08
0.04
0.00
400
460
520
580
640
700
Wavelength (nm)

Figure 4

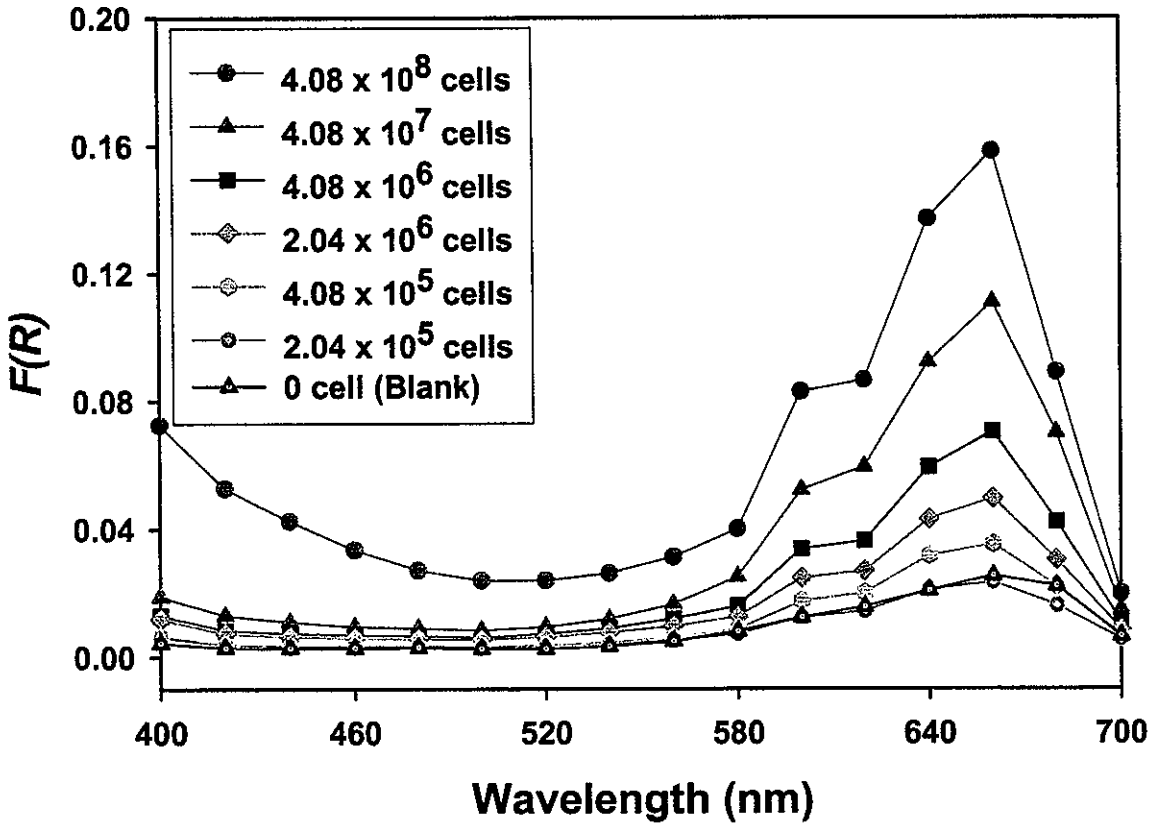
0.20
0.16
0.12
0.08
0.04
0.00
F(R)
4.08 x 10^8 cells
4.08 x 10^7 cells
4.08 x 10^6 cells
2.04 x 10^6 cells
4.08 x 10^5 cells
2.04 x 10^5 cells
0 cell (Blank)
400
460
520
580
640
700
Wavelength (nm)

Figure 5

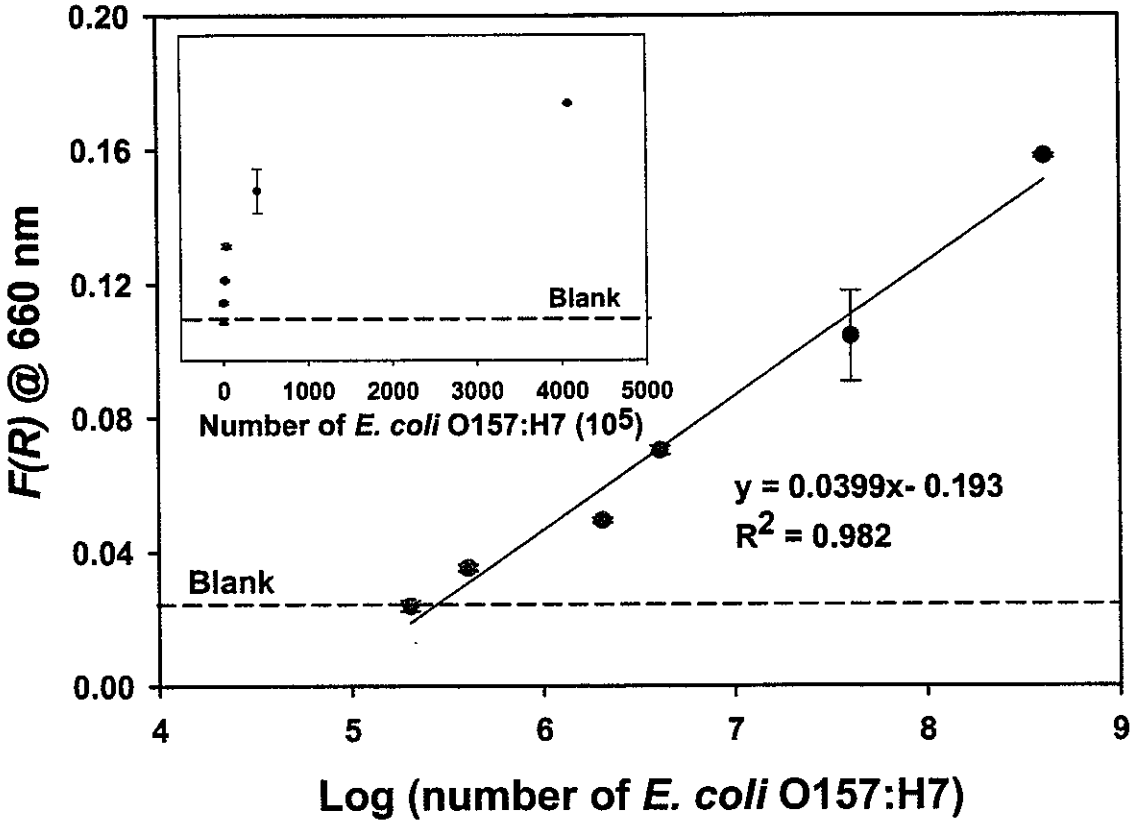
0.20
0.16
0.12
0.08
0.04
0.00
F(R) @ 660 nm
Blank
0
1000
2000
3000
4000
5000
Number of E. coli O157:H7 (10^5)
y = 0.0399x- 0.193
R^2 = 0.982
Blank
4
5
6
7
8
9
Log (number of E. coli O157:H7)

Figure 6

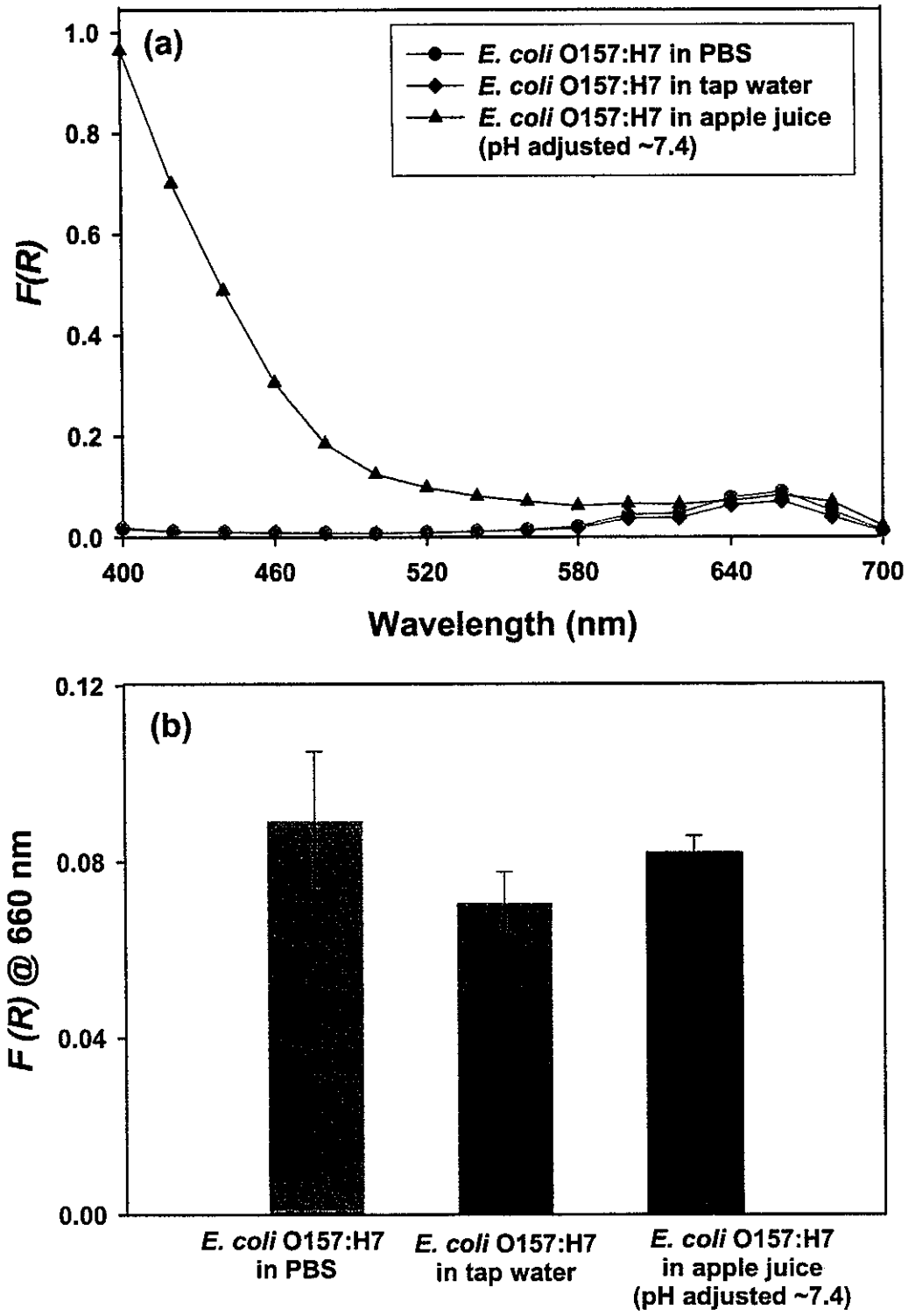
(a)
E. coli O157:H7 in PBS
E. coli O157:H7 in tap water
E. coli O157:H7 in apple juice (pH adjusted ~7.4)
F(R)
1.0
0.8
0.6
0.4
0.2
0.0
400
460
520
580
640
700
Wavelength (nm)
(b)
F (R) @ 660 nm
0.12
0.08
0.04
0.00
E. coli O157:H7 in PBS
E. coli O157:H7 in tap water
E. coli O157:H7 in apple juice (pH adjusted ~7.4)

Figure 7

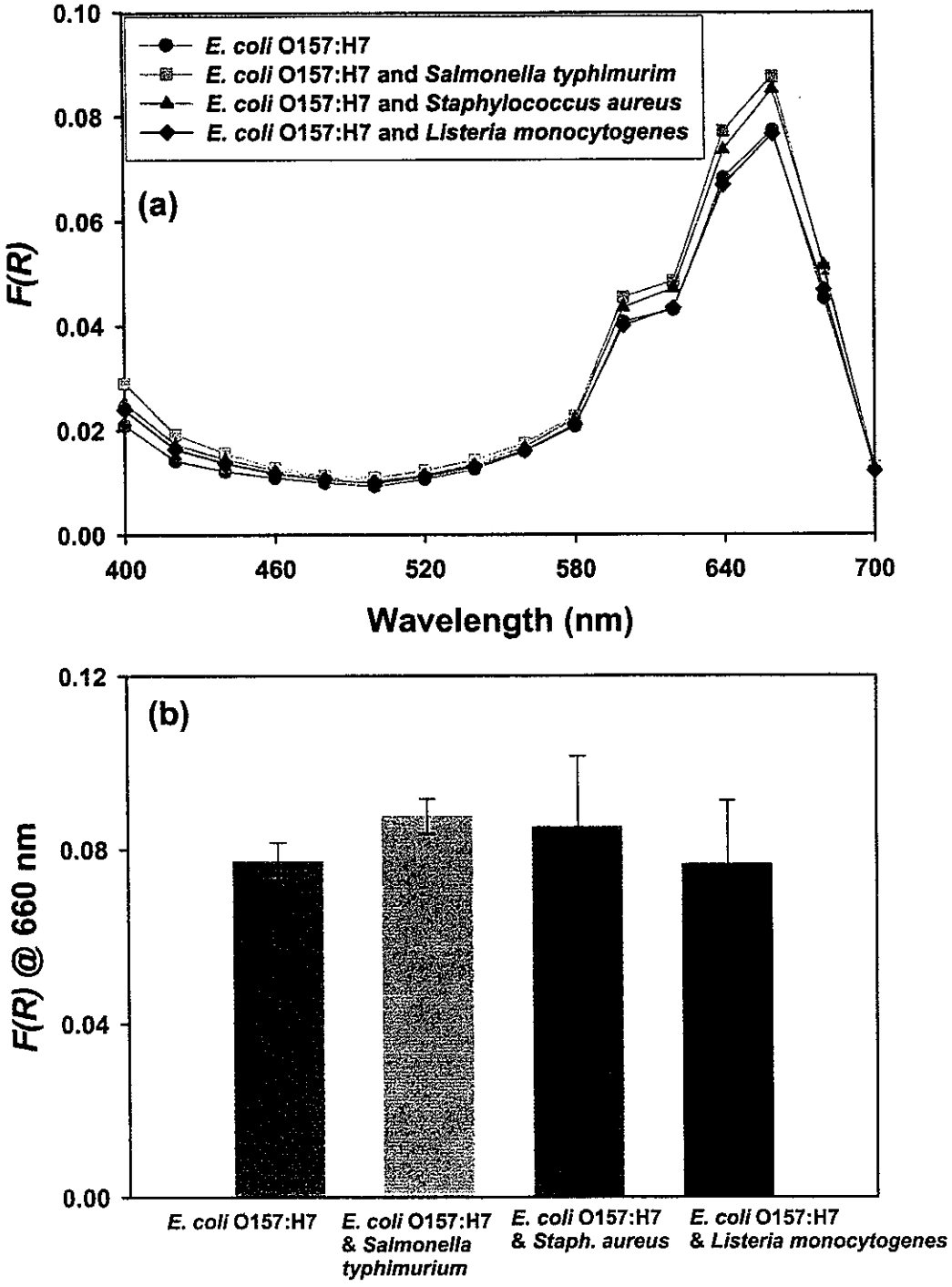
0.10
0.08
0.06
0.04
0.02
0.00
F(R)
E. coli O157:H7
E. coli O157:H7 and Salmonella typhimurim
E. coli O157:H7 and Staphylococcus aureus
E. coli O157:H7 and Listeria monocytogenes
(a)
400
460
520
580
640
700
Wavelength (nm)
0.12
0.08
0.04
0.00
F(R) @ 660 nm
(b)
E. coli O157:H7
E. coli O157:H7 & Salmonella typhimurium
E. coli O157:H7 & Staph. aureus
E. coli O157:H7 & Listeria monocytogenes

Figure 8

CHAPTER 4: STAINING STRATEGIES, CONSTRUCTION, AND EVALUATION (CHARACTERIZATION) OF RAPID CELL DETECTOR AND ENUMERATOR FOR FOOD BORNE PATHOGENS

A paper in preparation for submission to *Flow cytometry B*

Salma Rahman, Robert J. Lipert, and Marc D. Porter *

Institute of Combinatorial Discovery, Ames laboratory-USDOE, and Department of Chemistry and of Chemical and Biological Engineering, Iowa State University, Ames, IA 50011 USA

Abstract

The feasibility of the co-localization as well as dual staining concepts for the positive identification of target bacteria and elimination of problems associated with false positive counting due to antibody aggregation has been demonstrated utilizing fluorescence microscopy. For this, fluorescently labeled antibodies and DNA-bound fluorescent dye were selected. A positive bacterial cell count is recorded only when there is coincidence detection of both dyes in the target cell. This approach was then coupled with a novel prototype flow cytometer constructed specifically for the rapid detection and enumeration of pathogenic bacteria labeled by co-localization. This paper describes the instrument and some of its performance characteristics. The results show that the dual staining coupled with flow cytometry has promise for distinguishing target bacteria from non-target bacteria and for eliminating problems associated with false positive counting due to antibody aggregation. Other potential applications of this concept are being described.

* Corresponding Author

Introduction

Outbreaks of food borne illnesses caused by pathogenic microorganisms in undercooked meats and poultry and in unpasteurized juice have centered food safety as a national imperative.[1] A major part of the problem rests with the challenges in developing cost-effective analytical methods that have the requisite capabilities for the rapid and reliable identification and enumeration of such pathogens. This limitation not only has an impact on implementation of regulatory control protocols,[2] but also on the technical ability to respond rapidly in the event of an outbreak by identifying the source of contamination and controlling its spread. The traditional plate-culture approaches used for these purposes require 2-4 day enrichment and may underestimate the contaminant level due to physiological factors (e.g., sublethal injury) that may limit culturability.[3,4] In the past few years, a wide range of strategies has been explored in response to this critical problem.[5-9] Only a few, however, show real promise.[10-13] Selective binding scenarios have been adapted for use with a wide range of interfacial detection schemes based, for example, on acoustic wave propagation,[14] surface plasmon resonance (SPR),[15] and surface enhanced infrared spectroscopy.[16] These approaches, while having the advantage of not requiring a label, have only marginal levels of detection (e.g., 10^5 cells/mL for a bulk acoustic wave device[17] and 5×10^7 cells/mL for SPR).[15] A need therefore remains for the development of a system for the rapid, reliable, and low-level detection of food borne pathogens. This system would also find extensive use in environmental, biological warfare, clinical, and pharmaceutical assay applications.

Flow cytometry shows great promise in a wide range of micoorganism investigations because of breakthroughs in detector sensitivity, electronics, laser light sources, and intense fluorescent labels that began to appear in the late 1970's.[18-24] The technique is versatile, has

the potential for high sample throughput, and has already been adapted for use in label co-localization efforts to probe specific cell properties. Co-localization, based on dual labeling concepts, has been used by some researchers for other purposes like cell identity, cell viability, and assessment of physiological activities.[25-29] For example, Barnett et al. used cell size and a fluoresecently-labeled specific antibody to distinguish between two bacterial species.[21] Van Dilla et al. was able to determine by flow cytometry the ratio of bacterial-DNA base pairs using two different dyes, each of which bound to a different combination of DNA base pairs.[20] The idea of using two dyes to verify the identity of an organism found use in the detection of *Legionella* spp. during the 1980's. Tyndall et al. used a fluorescein-labeled anti-*Legionella* antiserum and propidium iodide (i.e., a nucleic acid stain) to positively identify *Legionella* in water that was collected from industrial and air-conditioning water towers.[25] Co-localization of two dyes was also used by Hoff to eliminate false positive readings.[26] More recently, cell identity and physiological status were determined using a combination of fluorescently labeled antibodies, DNA staining dyes, and viability dyes.[30, 31] A similar approach was developed for the effective identification and enumeration of *E. coli* O157:H7 in inoculated meat and water using a solid-phase laser cytometer, further demonstrating the discrimination provided by co-localization.[13] That study, however, focused primarily on issues related to recovery efficiencies when using immunomagnetic separations and did not pursue a clear assessment of detection capabilities.

In this paper, heat killed *E. coli* O157:H7 was selected as a model microorganism and a simple one-step labeling process was tested, in which a fluorescently-tagged antibody selectively binds to the antigenic determinants on the surface of the target bacteria. An automated fluorescence based cell counting system based on flow cytometry was used for

counting bacteria. Unfortunately, large numbers of false positive counts were recorded. Epifluorescence microscopy imaging revealed the false positive count was due to aggregation of fluorescently-tagged antibody. These large aggregations were incorrectly registered as bacteria cells by flow cytometry. Different sample preparation approaches were tested to minimize the false counts due to aggregation, but none of them showed real promise. This led to a co-localization strategy to minimize the false positive counting caused by fluorescently-tagged antibody aggregation.

We verified the feasibility of the co-localization concept using fluorescence microscopy for bacteria identification and examination. One label was a fluorescently-tagged antibody that is specific for *E. coli* O157:H7 (i.e., Cy5™-anti-*E. coli* O157:H7) and the other label was a global stain (i.e., a low molecular weight cell permeable fluorescent dye, 4'-6-diamidine-2-phenylindole dichloride (DAPI) that binds to the DNA of the cells). These two dyes have well separated fluorescence wavelengths (Em_{max}: 667 nm and 461 nm for Cy5™ dye and DAPI respectively). A positive count was recorded only when there was coincidence-detection of both dyes for the target bacteria cell. False positive counts from aggregations of antibodies have been eliminated because those lack signal from the global stain. Additionally, non-target bacteria in the sample were not counted because of the absence of the fluorescently-tagged antibody.

To implement the co-localization/dual staining concept and expand it to include the simultaneous detection and enumeration of multiple bacteria types, a novel flow cytometer was designed. It utilizes dyes that absorb and fluoresce at red wavelengths to minimize interference from sample native fluorescence, which therefore enhances detection sensitivity. The pair of dyes been used for the co-localization identification of bacteria was Cy5.5™ and

SYTO 61™. The maximum fluorescence intensity of Cy5.5™ is 694 nm and its absorption maximum is 675 nm; this dye can be conveniently coupled to antibodies for immunorecognition-based bacterial identification. SYTO 61™ has an absorption maximum at 628 nm, a fluorescence maximum at 645 nm, and is a cell permeant, DNA stain. The co-localization of these two dyes on an organism provides a high level of confidence in identification of the pathogen.

At present, flow cytometers use a single assay format, a situation that strongly limits sample throughput. Our flow cytometer design has the potential to address this analysis limitation by using a fluorescence detector, consisting of an array of 16 independent, miniature photomultiplier tubes (PMTs) that can be configured to simultaneously monitor for 8 dual-stain dye pairs. Instrument development has focused on the successful measurement of one bacterium, *E. coli* O157:H7, using a single set of dyes and one flow cell. For this purpose, half of the PMTs were covered with a filter that transmits fluorescence from the antibody stain (Cy5.5™) and the other half were covered with a filter that transmits DNA stain (SYTO 61™) fluorescence. In this paper, the instrument and some of its performance characteristics are described.

Experimental Section

Materials and reagents. Heat killed *Escherichia coli* O157:H7 was kindly provided by Dr. Cornick of the department of Veterinary Microbiology and Preventive Medicine of the Iowa State University. Affinity purified goat anti-*E. coli* O157:H7 was acquired from Kirkegaard and Perry Laboratories. The antibody was conjugated with Cy5™ and Cy5.5™ bisfunctional dyes (*N*-hydroxysuccinimide ester linker) using FluoroLink-Ab-Cy5 and Cy5.5 labeling kits

(Amersham Pharmacia Biotechnology). The DNA stains, DAPI and SYTO 61™, were obtained from Molecular Probes. Bovine serum albumin (BSA) and Tween 20 were purchased from Sigma.

Instrumentation. (i) Flow Cytometry. The commercial instrument used for initial bacteria counting is an automated fluorescence based cell counting system based on flow cytometry (RBD 2000, Advanced Analytical Technology Inc.). Sheath and sample core solution carry the fluorescently tagged target cells through a quartz flow cell where hydrodynamic focusing[32] results in single file cell flow through the detection region. Each target cell is associated with many fluorescently tagged antibodies and should produce a much higher signal compared to free fluorescently tagged antibody present in the solution. A 250 μL sample loop was used for all tests.

(ii) Construction of rapid cell detector and enumerator. Figure 1 shows a diagram of the flow cytometry based bacteria counter that has been constructed to detect, identify, and count cells. A photograph of the instrument is shown in Figure 2. Fluorescence excitation light from the diode laser is focused to the flow cell. Fluorescence signals from spectrally-distinct emitters (i.e., the DNA staining dye and a fluorescent dye on the primary antibodies used for microorganism identification) are collected by an objective lens and transmitted to a multianode photomultiplier tube (PMT) after passing through appropriate narrow bandpass filters. The multianode PMT selectively detects the fluorescence of the individual co-localized stains because sections of the array are covered with appropriate band pass filters. Signals from the multianode PMT are processed by a custom-designed circuit board.

Basic components of the system, including the flow cell and fluid handling system, optical layout, and components are described below.

The sheath-flow sample cell (4.25 x 4.25 x 20 mm) consists of a 250-μm, square-bore quartz cell (NSG Precision Cells: Type 526), with single-file flow of pathogens obtained using hydrodynamic focusing.[32] Square-shaped flow cells are preferred over the more conventional cylindrical-bore cells because the flat surfaces of the square cells reduce problems associated with scattered light from the excitation source. A precision syringe pump (Cavro Scientific Instruments) drives the core solution (18 mΩ, Millipore de-ionized water) and a 2-position, 6-port valve (Valco Instruments Co.) with a 0.5-mL sample loop is used to introduce an exact amount of sample into the core flow stream. The sheath fluid (18 mΩ, Millipore de-ionized water) is delivered pneumatically, i.e., the flow rate, which is monitored with a flow sensor (Omega, model # FLR1007), is adjusted by varying the pressure in a reservoir using compressed air.

A 635-nm, 15-mW diode laser [Power Technology, model # PM (LD1338)] that produced a collimated elliptical beam and was packaged with an integrated drive circuit is used for fluorescence excitation. A bandpass filter (Omega® Optical, 635NB4) is used to remove background emission from the laser beam. This laser was chosen because of its small size, low cost, ease of use, durability, and because this wavelength greatly reduces the excitation of native fluorescence of biological samples, which could interfere with the measurements.

Fluorescence is collected with a 20x microscope objective (Edmund Optics) and directed to the PMT array detector. An edge filter (643 nm, Omega® Optical) and holographic notch filter (635 nm, Kaiser Optical Systems) are used to block scattered laser light. At the detector, bandpass filters (650 nm, 20-nm bandwidth for SYTO 61™ dye and

700 nm, 20-nm bandwidth for Cy5.5™ dye, both from Omega® Optical) select the color of light that falls on each half of the PMT array.

The detector (Hamamatsu [R5900-L16]) is comprised of a linear array of sixteen multialkali photocathodes that have a sensitivity range from 350 to 850 nm (gain = 10^6 @ -800 V), and 0.5-ns rise time, and 1.7-ns fall time. Sections of the array are covered with band pass filters that selectively transmit the fluorescence of the individual co-localized stains.

Signals from the multianode PMT are processed by a custom-designed circuit board. The signals from two sets of eight PMTs are combined and processed in parallel by two identical circuits. The circuits amplify the pulsed PMT output and generate a digital output pulse if the magnitude of the signal exceeds a selectable threshold. The digital pulses from the two channels are sent to an AND gate, which generates an output signal only when two input pulses are present concurrently. This condition is met only when a dual-stained cell passed through the detection region. The output pulses of the AND gate are counted by a counter/timer board (National Instruments NI 6602) to determine the number of bacteria in the sample. Pulses from the individual channels are also counted for diagnostic purposes. Software for controlling the instrument has been written using the LabVIEW™ programming language.

(iii) Epifluorescence microscopy. A Nikon Eclipse TE200 inverted microscope equipped with a Prairie Technologies epifluorescent system that consisted of a uniblitz shutter, a mercury light source with a Prairie Technologies filter wheel, and a Hamamatsu C4742-95 CCD camera (6.7 x 6.7 μm pixels in a 1280 x 1024 pixel format) was used for imaging samples. The microscope also has a Prairie Technologies NeD microscope attachment for

simultaneous imaging at multiple wavelengths. Appropriate filter cubes (XF110/E/XC102 for Cy5 and XF06/E/XC102 for DAPI, both from Omega® Optical) to match the dye fluorescence wavelengths were used. Metaview imaging system (MetaMorph) from Universal Imaging Corporation was used for analyzing the images.

Method development. (i) Labeling antibodies with Cy5™ or Cy5.5™ dye. Anti-*E. coli* O157:H7 (1 mL, 1 mg/mL) was conjugated with Cy5™ or Cy5.5™ dye by following the vendor specified protocol which is designed for labeling the amine groups of 1 mg of protein. The average dye/protein molar ratio was estimated from the absorbance values obtained by transmission spectrophotometry of the Cy5™ dye and antibody at 650 nm and 280 nm, respectively, using the following expression: [Cy5™ dye]/[Antibody] = $([A_{650}/250000\ M^{-1}\ cm^{-1}]/[A_{280}\ (0.05 \cdot A_{650})]/170000\ M^{-1}cm^{-1})$.[33] This procedure yielded a dye/protein molar ratio between 4 and 12, with the molar ratio estimated for each new batch of labels.

(ii) *E. coli* O157:H7 staining with Cy5™ or Cy5.5™-labeled anti-*E. coli* O157:H7. *E. coli* O157:H7 (50 μL, $1x10^9$ cells/mL) was diluted with 900 μL phosphate buffered saline (PBS) containing 0.05 % Tween 20. Cy5™ or Cy5.5™-labeled anti-*E. coli* O157:H7 (50 μL) was added and the solution was incubated at 37 °C for 1 h with mild rotation (85 rpm) in a rotary incubator shaker. Further dilution was done with PBS containing 0.05% Tween 20.

(iii) *E. coli* O157:H7 staining with nucleic acid stain. DAPI staining: Stock *E. coli* O157:H7 (50 μL, $1x10^9$ cells/mL) was diluted with 950 μL PBS with 0.5% BSA. DAPI (0.1 μL of 10 mM) and Triton X-100 (1 μL) were added to the solution and incubated at room temperature for 30 min.

SYTO 61™ staining: Stock *E. coli* O157:H7 (50 μL, $1x10^9$ cells/mL) was diluted with 920 μL PBS containing 0.05% Tween 20. Stock SYTO 61™ dye solution was diluted (50x) with deionized water and 30 μL of diluted dye was added to *E. coli* O157:H7. The solution was incubated at room temperature for 30 min. Further dilution was done with PBS containing 0.05% Tween 20.

(iv) Dual staining of *E. coli* O157:H7. Cy5™-anti-*E. coli* O157:H7 and DAPI staining. Cy5™ labeled anti-*E. coli* O157:H7 (50 μL) was added to 50 μL 1:1 (volume) mixture of *E. coli* O157:H7 ($1.2x10^9$ cells/mL) and *Staphylococcus epidermidis* ($7.7x10^8$ cells/mL), and the solution was incubated at 37 °C for 1 h. The incubated sample was diluted by adding 900 μL PBS with 0.5% BSA. DAPI (0.1 μL of 10 mM) and Triton X-100 (1 μL) were added to the solution and incubated at room temperature for 30 min. Incubated sample (3 μL) was immobilized on a poly-L- lysine coated coverslip, which was then sealed on a glass slide. The slide was examined by using epifluorescence microscopy with an oil immersion 100x objective lens (Omega Optical®) and appropriate filter cubes. Both Cy5™ and DAPI fluorescence images were taken sequentially for the same sample and in the same field of view.

Cy5.5 anti-*E. coli* O157:H7 and SYTO 61™ staining. Stock *E. coli* O157:H7 (50 μL, $1x10^9$ cells/mL) was diluted with 870 μL PBS containing 0.05% Tween 20. Cy5.5™-labeled anti-*E. coli* O157:H7 (50 μL) was added and the solution was incubated at 37 °C for 1 h with mild rotation (85 rpm). Stock SYTO 61™ dye solution was 50x diluted with deionized water and 30 μL of the diluted dye was added. The solution was then incubated at room temperature for 30 min. Further dilution was done with PBS containing 0.05% Tween 20.

(v) Sample preparation in single staining process to minimize false positive counting. Different sample preparation approaches (e.g., immediate injection of sample to the bacteria counter after incubation, filtration of sample, dilution of labeled antibody) were tested (Table 1) to minimize the false positive counting due to aggregation of fluorescent antibody, keeping the same incubation temperature (37 °C) and time (1 h) in all the approaches. In one approach, 50 μL (5 μg/mL) of Cy5™-labeled anti-*E. coli* O157:H7 was added to 50 μL of *E. coli* O157:H7 ($1x10^5$ cells/mL). The solution was incubated and diluted with 1 mL PBS containing 1% BSA. In the second approach, 16 μL (0.23 mg/mL) Cy5™ anti-*E. coli* O157:H7 was added to 1 mL of *E. coli* O157:H77 ($1x10^4$ cells/mL) and incubated. Incubated samples were filtered through 0.22 μm cellulose acetate filter (Costar Corporation) pretreated with 1 mL 0.1% Tween 20 and washed (3x) and back flushed with PBS containing 0.5% BSA to original volume (1 mL). In the third approach, Cy5™ anti-*E. coli* O157:H7 (0.23 mg/mL) was serially diluted with PBS containing 0.5% BSA to 2.3×10^{-2}, 2.3×10^{-3}, 2.3×10^{-4}, and 2.3×10^{-5} mg/mL, respectively. The labeled antibodies were then added to bacteria samples by adding 16 μL of antibody to the 1 mL of *E. coli* O157:H7 ($1x10^4$ cells/mL) and incubated. In all the approaches, the same procedures were followed for the controls except PBS solution was used instead of *E. coli* O157:H7.

(vi) Optimum Assay Parameters for rapid cell detector and enumerator

Sample loop: 500 μL

Sheath flow rate: 5-6 mL/min @ 3 psig air pressure

Syringe dispensation or core flow rate: 0.498 mL/min

Syringe push volume for each test: 2 mL

Time required for each test: ~4 min

Sheath/Core flow ratio ~10-12

Calculated core diameter[34]: ~70 μm

Voltage applied to PMT: -900 V

Threshold voltage for SYTO 61™ channel: + 0.375 V and Cy5.5™ channel: + 0.365 V

Results and Discussion

Single staining of target bacteria. Table 1 presents results that summarize the ineffectiveness of the single staining methodology for the accurate enumeration of *E. coli* O157:H7. Especially significant are the high count levels in the control samples (i.e., samples prepared without the pathogen present). This result suggests that the tagged antibody can cluster into aggregates of sufficient size to be interpreted as labeled bacteria when using fluorescence-threshold detection and single-staining. This situation was also documented by epifluorescence imaging (Figure 3). The sample has only Cy5™-labeled anti-*E. coli* O157:H7 that are 150 nm in diameter, which is much smaller than each bacteria cell. Figure 3 shows micron-sized fluorescent objects that look very similar to labeled bacteria (1-3 μm) and can cause false positive results. These objects are probably aggregated antibodies.

Different sample preparation approaches (Table 1) were examined to minimize the extent of antibody aggregation. For example, the incubated sample was immediately injected to the RBD 2000 counter to minimize the time for antibody aggregation. The incubated sample was also filtered (pore size 0.2 μm) to remove antibody aggregates and in another approach the antibody solution was diluted at different ratios to minimize the affect of

antibody aggregation. However, none of the approaches helped to minimize false positive counting. As is evident, standard sample preparations (e.g., filtration[35] and centrifugation[36, 37]) are grossly inadequate, even when using an innocuous medium like PBS. These data illustrate the well-recognized difficulties in the analysis of food borne pathogens.[5, 6]

Dual staining of target bacteria with Cy5™-labeled antibody and DAPI.

Epifluorescence microscopy was used to demonstrate the dual staining approach for identifying target bacteria in the presence of non-target bacteria and antibody aggregates. The two stains were Cy5™-labeled anti-*E. coli* O157:H7 antibody and DAPI, a DNA specific dye. Affinity purified Cy5™-labeled anti- *E. coli* O157:H7 specifically interacts with O antigens of highly complex lipopolysaccharides located on the outer membrane of *E. coli* O157:H7.[38] DAPI is a DNA-specific probe that forms a fluorescent complex by attaching in the minor groove of A-T rich sequences of DNA. The fluorescence quantum yield of the free dye is very low with a maximum of emission at 453 nm; when bound to DNA, there is a bathochromic shift of excitation and a hypsochromic shift of emission, and the fluorescence quantum yield increases more than 20 fold.[39]

Figure 4a is an image of a sample containing *E. coli* O157:H7 and *Staphylococcus epidermidis* that have been treated with both stains and viewed through a Cy5™ fluorescence transmitting filter. This image represents *E. coli* O157:H7 stained with Cy5™-labeled anti-*E. coli* O157:H7. Based on the flow cytometry results and the results in Figure 3, some features in the image may represent aggregated antibodies. The DAPI fluorescence image (Figure 4b) represents both *E. coli* O157:H7 and *Staphylococcus epidermidis* stained with the DNA dye. Because DAPI binds to DNA nonselectively, it is difficult to distinguish between *E. coli* O157:H7 cells from any other cell.

Figure 4c represents a co-localized pseudocolor image of Cy5™ and DAPI fluorescence. Yellow areas indicate the presence of *E. coli* O157:H7 cells that are specifically labeled with many Cy5™-labeled anti-*E. coli* O157:H7 antibodies and also stained with DAPI. Non co-localized dyes retain their original color, thus the red color corresponds Cy5™-labeled anti-*E. coli* O157:H7 antibody aggregation and green color indicates other cells, which are not *E. coli* O157:H7. These data demonstrate that co-localization can potentially eliminate problems associated with false positive counting due to aggregation of fluorescent-labeled antibodies or non-target microorganisms.

Evaluation of rapid cell detector and enumerator. (i) Sensitivity. The sensitivity of the flow cytometer built in house, in terms of the level of fluorescence that can be measured, was evaluated using 2.5 μm-diameter calibration beads containing a fluorescent dye (absorption maximum at 633 nm, emission maximum at 660 nm, Molecular Probes). The relative intensity of the beads ranged from 100% (saturated with dye) to 0.04%. It was found (Table 2) that signals from 100%, 20%, and 4% intensity beads were observed with the expected levels of particle enumeration (recovery >98%). Counts were lower than expected in case of 0.8% intensity beads. No signals were observed for 0.2% and 0.04% intensity beads.

(ii) Accuracy and precision. The accuracy of the system was assessed by measuring the number of counts given by 4% relative intensity calibration bead solutions and comparing the results to the known bead concentrations (Table 3). The 4% relative intensity beads were chosen because their fluorescence intensity is approximately the same as the fluorescence from stained *E. coli* O157:H7. It was found that the number of counts corresponds very well to the number of beads in the solutions. Recoveries are 96% or better for concentrations up

to 100000 beads/mL. The recovery is expected to decrease at higher concentrations because the probability of more than one bead being in the observation volume at one time increases. The precision of the measurements is also very good (≤1.4% relative standard deviation).

(iii) Effects of threshold voltage on counts. The threshold voltage is used to discriminate against background noise, i.e., a signal level must exceed the threshold voltage level before it is considered to be an actual signal and not a noise fluctuation. When properly set, a sample without fluorescent beads or bacteria should give no, or very few, counts. On the other hand, setting the threshold too high will cause weak but legitimate counts to be missed. During testing to establish the proper setting for the threshold voltage, noise from the pulse detection circuitry was revealed. This noise interferes with the detection of weak signal levels. Currently, threshold settings of greater than ~300 mV are required to prevent false counts from this noise (Table 4).

Serial dilution of dual stained *E. coli* O157:H7. Because of the noise issue noted above, the number of counts registered for bacteria samples was typically much lower than expected. This situation is because the fluorescence intensity from bacterium to bacterium can vary widely due, for example, to variability of size, number of epitopes, and the amount of inter cellular DNA. The flow cytometry histogram for DNA stained *E. coli* O157:H7, measured by the Iowa State University Cell and Hybridoma Facility, documents this variability (data not shown). Cells with the lowest fluorescence are not detected in our instrument at present because their signal level falls below the threshold level necessary to discriminate against instrument noise. In spite of this, an experiment was performed to determine if the instrument could accurately measure the relative concentration of bacteria samples. For this, a series of measurement were made of samples that were serially diluted

from the stock (1 x 10^6 cells/mL) sample. The number of counts in serially diluted bacteria samples followed the dilution factor quite well, though the observed counts were much lower than expected (Table 5).

Demonstration of the co-localization concept. To demonstrate the co-localization concept, *E. coli* O157:H7 was selected as target bacteria and as non-target bacteria was *Staphylococcus epidermidis* selected. Counts in the SYTO 61™ channel represent the total number of bacteria stained with the DNA stain SYTO 61™, whereas counts in the Cy5.5™ channel represent the number of both Cy5.5™ labeled *E. coli* O157:H7 and aggregates of anti-*E. coli* O157:H7 (Table 6). It is seen that false antibody aggregate counts have been minimized in the AND gate channel in the dual stained sample. A few unexpected counts in each channel have been observed, which is probably due to overlapping of SYTO 61™ fluorescence with the Cy5.5™ detection filter band pass and vice vesa as both are red fluorescent dyes. *Staphylococcus epidermidis* was also single and dual stained to characterize the level of cross reactivity of anti- *E. coli* O157:H7. Counts in the case of Cy5.5™ stained *Staphylococcus epidermidis* in the Cy5.5™ channel were similar to the Cy5.5™ staining control (data not shown), which is due to aggregates of Cy5.5™ anti-*E. coli* O157:H7. No significant AND gate counts were observed, indicating minimum cross reactivity of anti-*E.coli* O157 antibody with non-target bacteria.

Mixing and dual staining of different amounts of target (*E. coli* O157:H7) and non-target (*Staphylococcus epidermidis*) bacteria is another way to demonstrate the effectiveness of the co-localization approach to detecting and counting only target bacteria. In this experiment (Table 7), the counts in the SYTO 61™ channel represent the total number of bacteria (target and nontarget) whereas the Cy5.5™ channel counts represent the number of

target bacteria and aggregated antibodies. Thus, neither channel represents the number of any specific bacteria. On the other hand, AND gate counts will appear only when there are signals in both SYTO 61™ and Cy5.5™ channels, i.e., when co-localization occurs, which is possible only in case of the target bacteria.

In this experiment, the number of target bacteria was kept constant while the number of non-target bacteria varied. The responses showed that the number of counts in the SYTO 61™ channel increased as the total number of bacteria (target and non target bacteria) increased, whereas the number of counts remained roughly constant in the Cy5.5™ channel (target bacteria and aggregated antibody). The number of target bacteria alone is represented by the AND gate counts, which were found to be a little lower than the Cy5.5™ channel counts. This finding is expected if antibody aggregation is present. The non-target bacteria number was obtained by subtraction of the AND gate counts from SYTO 61™ channel counts. This number approximately doubled when the number of *Staphylococcus epidermidis* was doubled, while the AND gate counts showed only a small increase. In both experiments, the number of counts registered for bacteria samples was typically much lower than expected because of the noise issue noted earlier as well as the variation of bacterial fluorescent intensity in the sample. However, these findings demonstrate that the co-localization approach enables the selective counting of target bacteria in the presence of a large number of non-target bacteria and antibody aggregates.

Conclusions and Future Work

Dual staining coupled with flow cytometry shows promise for distinguishing target bacteria from non-target bacteria and eliminating problems associated with false positive counting due to aggregation of fluorescent-labeled antibodies.

A prototype flow cytometer that can simultaneously detect one global label and one antibody label has been constructed and is in testing stage. In this prototype instrument, fluorescence is collected and imaged on a multichannel detector with different channels detecting light in different wavelengths bands, which correspond to fluorescence of the different labels. Fluorescent calibration beads have been counted by this instrument with high accuracy and precision. A specific example using fluorescence detection of co-localized indicator dyes to positively identify and enumerate specific types of bacteria (*E. coli* O157:H7) is presented. The number of counts for bacteria was typically lower than expected which is probably due to the noise issue noted earlier as well as the variability of fluorescent intensity among bacterial population. Thus fluorescently stained bacteria with signal below threshold settings cannot be registered as count. Currently threshold settings higher than ~300 mV are required to prevent false counts from pulse detection circuitry noise. Further modification in the circuit board needs to be done to minimize this noise so that threshold settings can be lowered, which should improve the sensitivity of bacterial detection.

Other detection methods that can be applied with this scheme include Raman spectroscopy, absorption spectroscopy, light scattering, electrochemical, and magnetic particle detection. High sample throughput as well as simultaneous microorganism detection can be accomplished by using additional combination of dye sets and an array of flow cells

that can be coupled to a variety of multiple labeling/detection platforms. Also, further versions of the instrument should take advantage of the flexibility and ease of alignment of a bifurcated fiber optic bundle, specifically designed for fluorescence measurements to collect and transmit the fluorescence signal, simplifying the optical alignment. The ultimate version of the instrument hopefully will address the need for a rapid and reliable approach to the selective and sensitive detection and enumeration of several food borne pathogens.

Acknowledgments

The authors express appreciation and thank to CIRAS of Iowa State University for helping in constructing the flow cytometry instrument, Ames laboratory's Engineering Services Group in making the circuit board of the instrument, and also to Dr. Nancy Cornick of VMPM department of Iowa State University for providing *E. coli* O157:H7. Funding for this work was provided by the United State Department of Agriculture Cooperative State Research, Education, and Extention Service (UDSA CSREES award number 20002-35201-12659), the Roy J. Carver Charitable Trust through a University Exploratory Research Program, and the Institute of Combinatorial Discovery of Iowa State University through the Roy J. Carver Laboratory for Ultra High Resolution Biological Microscopy. The Ames Laboratory is operated for the U.S. Department of Energy by Iowa State University under Contract W-7405-Eng-82.

References

(1) Foegeding, P.; Roberts, T., "Foodborne Pathogens: Risks and Consequences," Task Force Report , No. 122, **1994**.

(2) U.S. Department of Agriculture, F. S. a. I. S., "Pathogen Reduction; Hazard Analysis, and Critical Control Points (HACCP) Systems: Final Rule," Supplement-Final Regulatory Impact Assessment for Docket No. 93-016F, **1996**.

(3) Smith, J. J.; Howington, J. P.; McFeters, G. A. *Appl. Environ. Microbiol.* **1994**, *60*, 2977-2984.

(4) Mossell, D. A. A.; Corry, J. E. L.; Struikj, C. B.; Baird, R. M. In *Essentials of the Microbiology of Foods: A Textbook for Advanced Studies*; John Wiley & Sons: Chichester, 1995, pp 96-106.

(5) Bilitewski, U. *Anal. Chem.* **2000**, *72*, 692A-701A.

(6) Vives-Rego, J.; Lebaron, P.; Nebe-von Caron, G. *FEMS Microbiol. Rev.* **2000**, *24*, 429-448.

(7) Hage, D. S. *Anal. Chem.* **1999**, *71*, 294 R-304 R.

(8) Hennion, M.-C.; Barcelo, D. *Anal. Chim. Acta* **1998**, *362*, 3-34.

(9) Ivnitski, D.; Abdel-Hamid, I.; Atanasov, P.; Wilkins, E. *Biosens. Bioelectron.* **1999**, *14*, 599-624.

(10) Wadkins, R. M.; Golden, J. P.; Pritsiolas, L. M.; Ligler, F. S. *Biosens. Bioelectron.* **1998**, *13*, 407-415.

(11) Brewster, J. D.; Gehring, A. G.; Mazenko, R. S.; Van Houten, L. J.; Crawford, C. J. *Anal. Chem.* **1996**, *68*, 4153-4159.

(12) Belgrader, P.; Benett, W.; Hadley, D.; Richards, J.; Stratton, P.; Mariella, R., Jr.; Milanovich, F. *Science* **1999**, *284*, 449-450.

(13) Pyle, B. H.; Broadaway, S. C.; McFeters, G. A. *Appl. Environ. Microbiol.* **1999**, *65*, 1966-1972.

(14) O'Sullivan, C. K.; Vaughan, R.; Guilbault, G. G. In *Anal. Lett.*, 1999; Vol. 32, pp 2353-2377.

(15) Fratamico, P. M.; Strobaugh, T. P.; Medina, M. B.; Gehring, A. G. In *Biotechnology Technique*, 1998; Vol. 12, pp 571-576.

(16) Brown, C. W.; Li, Y.; Seelenbinder, J. A.; Pivarnik, P.; Rand, A. G.; Letcher, S. V.; Gregory, O. J.; Platek, M. J. *Anal. Chem.* **1998**, *70*, 2991-2996.

(17) Guilbault, G. G.; Luong, J. H. T. In *Food Science and Technology*, 1994; Vol. 60, pp 151-172.

(18) Hutter, K. J.; Eipel, H. E. *J. Gen. Microbiol.* **1979**, *113*, 369-375.

(19) Boye, E.; Steen, H. B.; Skarstad, K. *J. Gen. Microbiol.* **1983**, *129*, 973-980.

(20) Van Dilla, M. A.; Langlois, R. G.; Pinkel, D.; Yajko, D.; Hadley, W. K. *Science* **1983**, *220*, 620-622.

(21) Barnett, J. M.; Cuchens, M. A.; Buchanan, W. *J. Dent. Res.* **1984**, *63*, 1040-1042.

(22) Seo, K. H.; Brackett, R. E.; Frank, J. F. *Intl. J. Food Microbiol.* **1998**, *44*, 115-123.

(23) Seo, K. H.; Brackett, R. E.; Frank, J. F.; Hilliard, S. *J. Food Prot.* **1998**, *61*, 812-816.

(24) Kim, Y.; Jett, J. H.; Larson, E. J.; Penttila, J. R.; Marrone, B. L.; Keller, R. A. *Cytometry* **1999**, *36*, 324-332.

(25) Tyndall, R. L.; Hand, R. E., Jr.; Mann, R. C.; Evans, C.; Jernigan, R. *Appl. Environ. Microbiol.* **1985**, *49*, 852-857.

(26) Hoff, K. A. *Appl. Environ. Microbiol.* **1988**, *54*, 2949-2952.

(27) Pyle, B. H.; Broadaway, S. C.; Mcfeters, G. A. *Appl. Environ. Microbiol.* **1995**, *61*, 2614-2619.

(28) Yu, F. P.; Mcfeters, G. A. *J. Microbiol. Methods* **1994**, *20*, 1-10.

(29) Mcfeters, G. A.; Singh, A.; Byun, S.; Callis, P. R.; Williams, S. *J. Microbiol. Methods* **1991**, *13*, 87-97.

(30) Hewitt, C. J.; Nebe-Von Caron, G.; Nienow, A. W.; McFarlane, C. M. *Biotechnol. Bioeng.* **1999**, *63*, 705-711.

(31) Barbesti, S.; Citterio, S.; Labra, M.; Baroni, M. D.; Neri, M. G.; Sgorbati, S. *Cytometry* **2000**, *40*, 214-218.

(32) Shapiro, H. M. *Practical Flow Cytometry*; Wiley- Liss: New York, 1995.

(33) Mujumdar, R. B.; Ernst, L. A.; Mujumdar, S. R.; Lewis, C. J.; Waggoner, A. S. *Bioconjugate Chem.* **1993**, *4*, 105-111.

(34) Lioyd, D. *Flow Cytometry in Microbiology*; Springer-Verlag London Ltd.: London, 1993.

(35) Entis, P.; Brodsky, M. H.; Sharpe, A. N. *J. Food Prot.* **1982**, *45*, 8-11.

(36) Stannard, C. J.; Wood, J. M. *J. Appl. Bacteriol.* **1983**, *55*, 429-438.

(37) Sharpe, A. N. In *Rapid Methods and Automation in Microbiology and Immunology*; Spencer, R. C., Wright, E. P., Newsom, S. W. B., Eds.; Intercept: Andover, 1994, pp 97-105.

(38) Garret, R. H., Grisham, C. M. *Biochemistry*; Saunders College Publishing, 1999.

(39) Kapuscinski, J. *Biotech. Histochem.* **1995**, *70*, 220-233.

Figure Captions

Figure 1. Flow diagram of flow cytometry based bacteria counter.

Figure 2. Photograph of flow cytometry based bacteria counter.

Figure 3. Pseudocolor fluorescence image of aggregations of Cy5™-labeled anti-*E. coli* O157:H7.

Figure 4. Pseudocolor fluorescence image of *E. coli* O157:H7 and some antibody aggregates in a mixture of *E. coli* O157:H7 and *Staphylococcus epidermidis* dual stained with Cy5™-labeled anti-*E. coli* O157:H7 and DNA dye DAPI. Image obtained using Cy5™ filter cube (a), DAPI filter cube (b), and overlay image (c) of figure (4a) and (4b) with co-localized dyes in yellow identifying the target bacteria (*E. coli* O157:H7) from the non target one (*Staphylococcus epidermidis*).

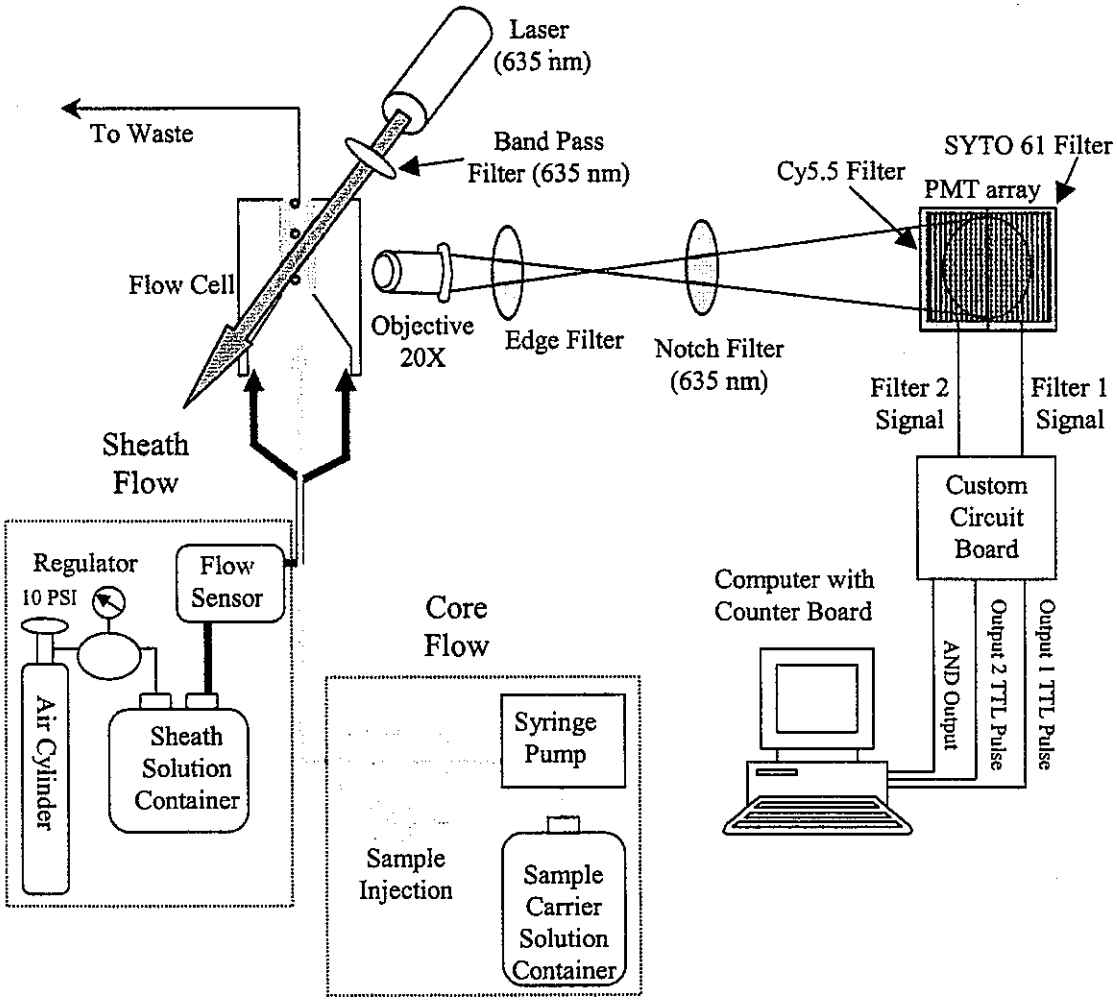
Laser
(635 nm)
To Waste
Band Pass
Filter (635 nm)
SYTO 61 Filter
Cy5.5 Filter
PMT array
Flow Cell
Objective
20X
Edge Filter
Notch Filter
(635 nm)
Filter 2
Signal
Filter 1
Signal
Sheath
Flow
Custom
Circuit
Board
Regulator
10 PSI
Flow
Sensor
Computer with
Counter Board
Core
Flow
Air Cylinder
Sheath
Solution
Container
Syringe
Pump
Sample
Injection
Sample
Carrier
Solution
Container
AND Output
Output 2 TTL Pulse
Output 1 TTL Pulse

Figure 1

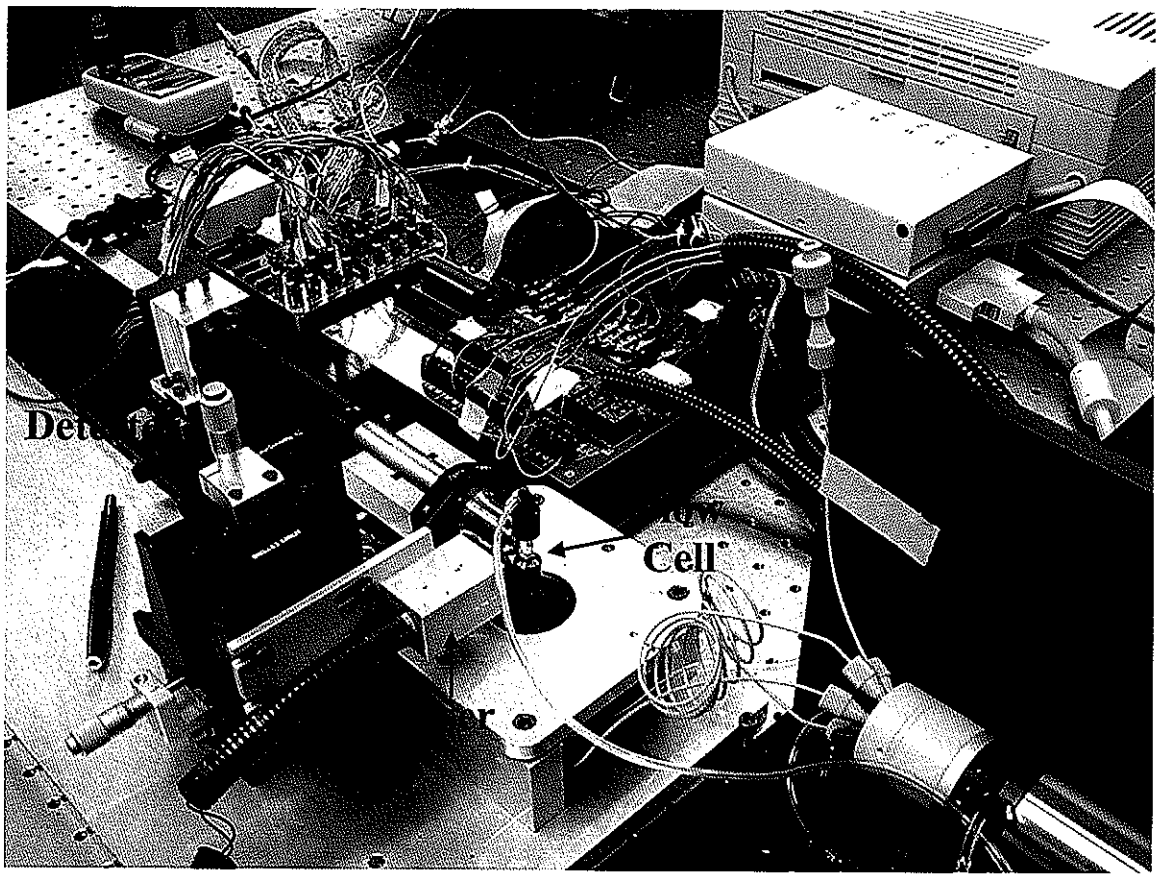

Figure 2

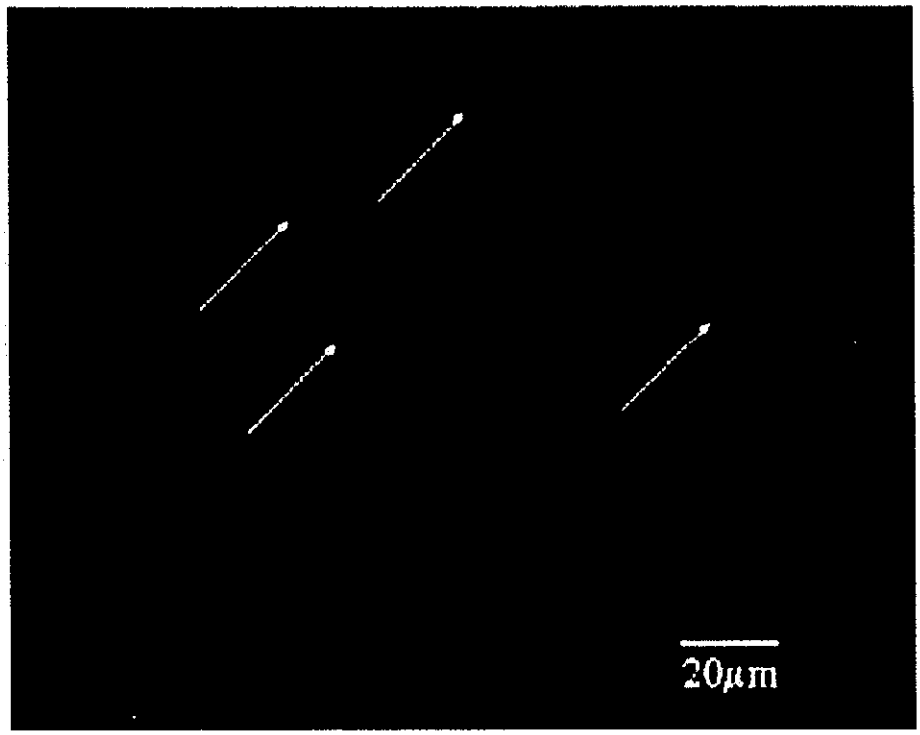

Figure 3

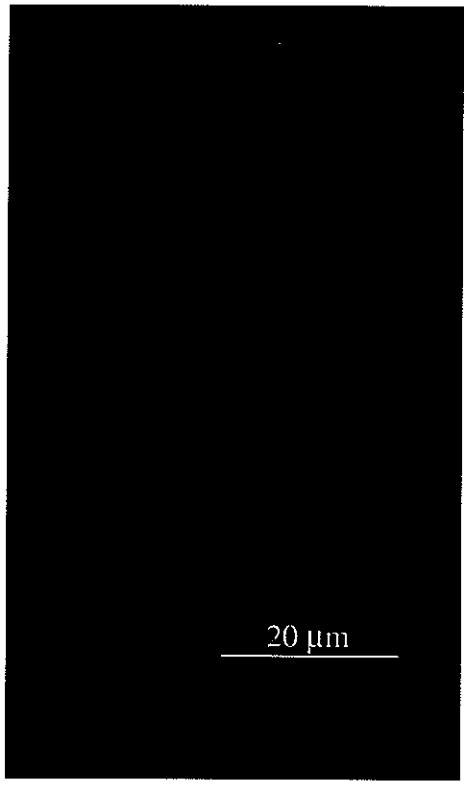

Figure 4a

Figure 4b

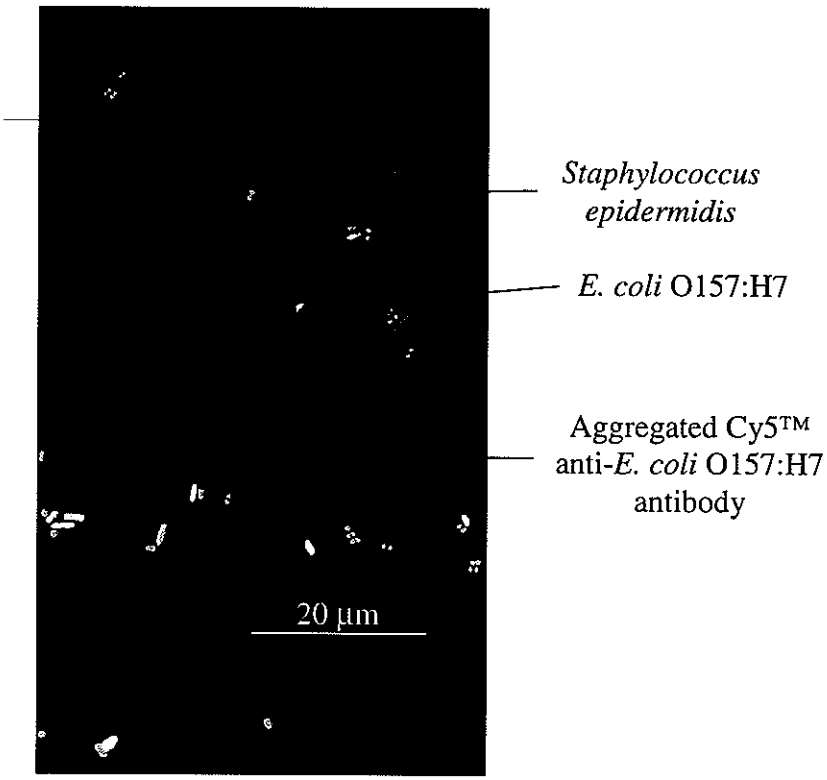

Figure 4c